LOW ENERGY, LARGE ANGLE ELECTRON IMPACT SPECTROSCOPY

Ph. D. Thesis

by

Andrew Barrie

September 1971

University of Stirling,

Scotland.

ProQuest LLC.
789 East Eisenhower Parkway
P.O. Box 1346
Ann Arbor, MI 48106 – 1346

To Eleanor, Samantha, Louise and Lulu.

LOW ENERGY, LARGE ANGLE ELECTRON IMPACT SPECTROSCOPY by Andrew Barrie

ABSTRACT

Previous theoretical and experimental work has indicated that at low incident energies, singlet-triplet transitions may take place via a spin exchange mechanism and that cross-sections for these processes decrease more slowly with angle than do those for allowed transitions. Low incident energies and large scattering angles are therefore indicated when studying optically forbidden transitions.

Consideration of the signal available at large angles suggests the use of an analyser capable of accepting 2π in azimuth and this approach was pioneered by Kuppermann and Raff(1963) who used a retarding field energy analyser(R.F.E.A.) with cylindrical grids. In the present work, a study of the factors affecting resolution and peak shape in a R.F.E.A. leads to the choice of spherical grids while a split scattered electron collector is used to determine the angular dependence of relative cross-sections. Improvements in the electron optics and the use of a clean U.H.V. environment free from magnetic fields leads to a spectrometer capable of operating at incident energies of 10 to 50 eV over the angular range 15° to 165° with a resolution of about 400 to 500 meV. Spectra may be obtained simultaneously on three collectors using a data logging system with automatic scanning.

Spectra obtained for N_2, CO and C_2H_4 show that at incident energies close to threshold, and large scattering angles, singlet-triplet transitions can, in favourable cases, be more strongly excited than singlet-singlet transitions. It is found, in general, that the intensity ratio for a triplet state relative to a reference singlet state increases rapidly with increasing scattering angle at a fixed impact energy and this may serve as a test for a triplet state. This ratio is not, however, so dependent on incident energy in the 20 to 50 eV range

and, in general, only increases noticably when the incident energy is within 10 eV of threshold.

As regards the controversy arising from the discrepancy between the results of Kuppermann and Raff(1963) and Simpson and Mielczarek(1963) for ethylene, the present work gives results consistent with electron trap spectra and large angle, energy loss spectra using dispersion analysers, showing only peaks at 4.4 eV, 8 eV and 9.5 eV with no indication of the so-called "mystery band" at 6.5 eV.

CONTENTS

1.1 General

In the interaction of electrons with atoms and molecules, various processes may occur which are of interest to the fields of physics, chemistry, engineering and biology. Such processes include elastic scattering, in which internal states of the target are not affected, inelastic and superelastic scattering, in which internal states are respectively excited or de-excited, ionisation, negative ion formation, electron exchange, molecular dissociation or fragmentation, or a combination of several of these processes. For any particular scattering process, the probability of its occurrence is expressed in terms of a quantity known as the collision cross-section. For example, the probability, p_i, that an electron of specified energy will experience a particular type of collision, i, in passing through a distance, x, of a gas of number density, N, is

$$p_i = NQ_ix \qquad (1.0)$$

where Q_i is the cross-section for the process, i, and has the dimensions of area.

However, atoms and molecules are not rigid spheres with defined boundaries and the force between a target atom and an electron will fall off continuously with distance so that the cross-section cannot be taken as a true measure of the cross-sectional area of the target atom or molecule. Also, as a result of the gradual decrease of scattering field with interparticle distance, we would expect the cross-section to vary with electron energy. For any scattering process in which an electron collides with a stationary target and is scattered into a given direction (defined by spherical polar angles $\Theta,\emptyset$) we may specify a differential cross-section, $I(\Omega)$, which is defined as the cross-section per unit solid angle. The total cross-section is the integral of the differential cross-section over the whole range of solid angle. If we define the coordinate system so that the incident beam passes along the z-axis, Θ is the polar scattering angle and $\emptyset$ is the azimuthal angle, then for randomly oriented target particles, the differential cross-section will be independent of $\emptyset$.

One application of low energy electron-molecule collision studies is in the field of health physics. When ionising radiation interacts with matter, a considerable number of low energy ($\lesssim 15$eV) electrons are

ultimately produced and these are then free to interact further(1). The ability of polyatomic molecules to capture low energy electrons and thus form temporary or stable negative ions is believed to play an important role in the biological action of molecules, such as the cancer inducing ability of chemical carcinogens(2). In space science, laboratory studies of electron excitation mechanisms and cross-sections can be used to explain various aspects of planetary atmospheres, such as the auroral emmisions from molecular nitrogen which are compatible with excitation mechanisms involving electrons with energies less than 25eV(3).

An important development in the last decade has been the application of electron-molecule collision studies as a spectroscopic tool and it is with this application that the present work is concerned. The selection rules for the excitation of electronic energy levels of atoms and molecules by electron impact depend very strongly on the particular experimental conditions used. At high incident electron energies the selection rules for photon impact are obeyed while at low energies practically all electronic transitions are allowed (4). This along with the facility of readily extending measurements into the region of the spectrum equivalent to the vacuum ultraviolet (above 11eV) makes electron impact a useful spectroscopic tool. Spin-forbidden transitions are made possible at low electron energies due to the possibility of the slowly moving electron being captured into an excited orbital of the molecule while a molecular electron is ejected. Hence although the spin of the molecule has changed, the total spin of the system of molecule + electron is conserved and the transition may take place. The theory of Ochkur (5) suggests that the cross-sections for singlet-triplet transitions, occuring via the spin-exchange mechanism, decrease more slowly with momentum change(and hence angle) than do those for allowed transitions. This has been verified experimentally by Rice et.al. (6) who find that at large scattering angles spectra are obtained in which singlet-triplet transitions are as prominent as optically allowed ones.

Electron impact spectroscopy thus provides a means of determining the energy levels of triplet states in atoms and molecules. Since the lowest triplet state is usually also the first excited state, it is quite likely to be involved as an intermediate in chemical reactions(1,

7,8). A well known example is the cis-trans isomerisation about the ethylenic bond. Other examples occur in biological systems where, because the available energy quanta are small compared with energies of activation, the reaction will tend to go via the path of lowest activation energy. A knowledge of the possible triplet levels is therefore important if detailed reaction mechanisms are to be established for such cases.

1.2 Electron Impact Spectroscopy

At high incident electron energies, the target molecule experiences the electron as a transient electrical perturbation and the electron is likely to suffer only a small deflection from its initial path. Consequently, a perturbation theory, Born's approximation, is found to be applicable at high energy. In the energy range 25 keV to 50 keV, Boersch, Geiger et.al. (9_{a-c}) have obtained energy loss spectra which show only optically allowed transitions. In their experiments both monochromator and analyser are of the Wien filter type which employs crossed electrostatic and magnetic fields. This technique has given half-widths of better than 14 meV and provides the highest resolution achieved in electron impact spectroscopy. The scattering angle is fixed at 0° but this is no great disadvantage as the cross-sections are strongly peaked in the forward direction. Spectra have been obtained for N_2, A, He, H_2, O_2, and C_2H_4 using this technique.

Early work by Lassettre and co-workers (10a-j) using incident energies of 200 - 600 eV and scattering angles of 0°- 15° produced spectra which were similar to the optical spectra. The gases studied were He, N_2, H_2, CO, O_2, CH_4, C_2H_6, C_2H_4 and H_2O. Some of this work involved an oxide cathode electron gun and a parallel plate electrostatic analyser (10d) while later work employed a 127° analyser (10a). Both arrangements employed electron multiplier detection and a variable scattering angle. They were able to show that as the scattering angle increased for an energy of 500 eV, the intensity of the helium 1'S - 2'P transition fell off sharply while the angular momentum forbidden transition 1'S - 2'S slowly gained intensity relative to the 1'S - 2'P transition. They also found that the 2'S transition gained intensity as the incident energy

was lowered from 350 eV to 250 eV at 0° scattering angle. Later development resulted in a high resolution spectrometer (11) employing a hemispherical deflector type monochromator and an identical analyser both with a mean radius of 5". Real slits are used at the entrance and exit of each deflector and in a later version (12) additional lenses were added to correct for chromatic aberation and thus allow direct comparison of spectral peak heights. Spectra have been obtained for a large range of molecules using incident energies between 30 and 100 eV. In N_2 and CO these workers have reported singlet-triplet transitions (13) but the intensities are very low, the $C\,^3\pi_u$ transition in N_2 for example being only 0.4% of the optically allowed $b\,^1\pi_u$ for an incident energy of 48 eV and 12° scattering angle. Also a survey of sixteen polyatomic molecules (12) at incident energies between 33 and 100 eV failed to reveal any singlet-triplet transitions. As singlet-triplet transitions in this energy range do not occur by the spin exchange mechanism but principally by spin-orbit coupling (14) these authors have suggested that incident energies closer to threshold might be necessary to excite such states in polyatomic molecules at small scattering angles. The 30 - 100 eV range in forward scattering experiments is not a favourable one for detection of singlet-triplet transitions because they tend to be obscured not only by optically allowed transitions but by electric quadrupole transitions as well.

Forward scattering using incident energies closer to threshold has been studied by Simpson, Kuyatt et.al. using the high resolution apparatus developed by Simpson (15). The spectrometer employs concentric hemispherical deflectors of mean radius 1" in both monochromator and analyser and in a later version the scattering angle may be varied from -30° to $+90^{\circ}$. No physical apertures are used in the focal planes of the deflectors, "virtual apertures" being provided by the images of real apertures placed in higher voltage elements of an electrostatic lens system. The advantages of this method have been discussed by Kuyatt and Simpson (16); and it is necessary when operation at very low impact energies is contemplated. Energy loss spectra obtained using impact energies close to threshold and 0° scattering angle have shown significant singlet-triplet excitation in contrast with spectra at 35 eV which agree

with those of Lassettre et.al.. As an example, a spectrum of N_2 at 15.7 eV impact energy (17) shows peaks of equal magnitude for the $C^3\pi_u$ and $b^1\pi_u$ states while at 35 eV the triplet C state is not detectable and the optically allowed b state at 12.9 eV is the strongest feature in the spectrum in agreement with Lassettre et.al..

Electron impact at energies within a few tenths of a volt above threshold was first studied by Schulz (18) using the trapped electron technique. A magnetically collimated , pseudo-monoenergetic electron beam produced by a R.P.D. gun is used to excite a sample gas in a collision chamber which is operated as an electron trap of variable well depth by means of field penetration from a biased collector placed outside the gridded walls of the collision region. At small well depths an effectively threshold electron impact spectrum is obtained. Bowman and Miller (19) claim that the geometric collection efficiency is around 90% and so the electron trap has a high sensitivity due to collection of electrons over a wide angular range. Unfortunately the necessity for a magnetic field (100 gauss) means that the scattering angle cannot be defined. In general, singlet-triplet transitions are found to predominate in spectra obtained by this method. In Bowman and Miller's work, the helium 2^3S transition at 19.82 eV was so pronounced that they used this peak to calibrate the energy scale. Brongersma and Oosterhoff (20) have recently developed a high resolution (100 meV) electron trap in which they claim to have increased the sensitivity by a factor of 500 with respect to that of Bowman and Miller. In addition, the whole apparatus can be operated at temperatures of 50° to $150^\circ C$ permitting the use of certain liquid and solid samples. Vibrational structure is observed in the $X - a^3\Pi$ transition of CO and in the $X - B^3\pi_g$ transition of N_2. Spectra have been obtained for olefins in which low-lying triplet states and temporary negative ion resonances leading to vibrational excitation in ground state are observed (21). Hall et.al. (21a) have very recently reported an electron trap in which parallel plates are used to produce the potential well. They have obtained a spectrum of N_2 at 70 meV (F.W.H.M) resolution in which a new state at 9.75 eV is observed.

A new approach to the study of threshold electron impact spectra has been demonstrated by Curran (22) who used sulphur hexafluoride mixed with sample gas to scavenge the zero energy electrons ejected at

excitation thresholds. The advantage of SF_6 as an electron scavenger is that it has a very high cross-section for electron attachment ($10^{15} cm^2$) and the resonance is positioned very close to zero energy with a width of less than 20 meV (23). Consequently the resolution is dependent only on the energy spread of the incident electron beam. Curran used a conventional mass spectrometer with a R.P.D. gun and obtained a threshold electron impact spectrum for N_2 by recording the SF_6^- ion current as a function of incident electron energy in a mixture of N_2 and SF_6. Compton et.al.(24) have extended this method to the measurement of threshold spectra for HCl, H_2O, D_2O and a number of aromatic molecules, using a time-of-flight mass spectrometer employing a R.P.D.gun, while Jennings and O'Malley (25) have obtained spectra for some unsaturated organic molecules using an ion cyclotron resonance mass spectrometer. In principle, SF_6^- threshold spectra may be obtained in any conveniently available mass spectrometer but for high resolution it is necessary to design special apparatus. Brion and co-workers (26a-c) have used a 127^o electron monochromator in conjunction with a monopole mass spectrometer for SF_6^- detection and resolution of 30 - 50 meV F.W.H.M. is possible. The highest resolution obtained in this approach is in work by Stamatovic in which 20 meV F.W.H.M. was generally obtained (23) and 10 meV at best (27), using a trochoidal electron monochromator and a quadrupole mass spectrometer. Due to the sharply resonant SF_6^- electron capture peak, this technique is a very powerful one for the detection of energy levels in molecules but it must be recognised that it gives no information about either the energy dependence of the cross-section above threshold or of the angular dependence, both quantities which are useful for the identification of states.

Relatively few energy loss spectra have been obtained at large scattering angles due to angular distributions being generally forward peaked. Kupperman and Raff used retarding field analysis to obtain spectra over angles of 22^o to 112^o with scattering at 90^o being preferred by the cylindrical geometry of the analyser. Spectra (28,29) obtained at energies of 25 - 75 eV showed peaks of approximately equal magnitude for elastic, allowed inelastic and forbidden inelastic processes. Gases studied were He, A, H_2, and C_2H_4. In C_2H_4 , two new transitions

were observed at 4.6 and 6.5 eV. Simpson and Mielczarek (30) were however unable to reproduce these results in high resolution studies at 50 eV and 0° scattering angle. These differences may be explained either by impurities or instrumental effects in the Kupperman and Raff spectrometer or by a rapid fall off in the intensity of optically allowed transitions with increasing scattering angle while the spin-forbidden transition have a more nearly uniform angular distribution(31). As the use of magnetic materials and oil diffusion pumps in the Kuppermann and Raff spectrometer may have been responsible for instrumental effects, Read and Ferguson built a replica (32) of the original instrument constructed of non-magnetic materials and housed in a bakeable, mercury-pumped vacuum chamber. They found that the He and A results could be reproduced but only with great difficulty, the data processing being very subjective. In order to examine the relative intensities of optically forbidden and optically allowed transitions at large scattering angles, Doering (33) used an apparatus in which electrons from a directly heated thoriated iridium filament were accelerated into a gas-filled collision chamber from which electrons scattered at a fixed angle of 90° were analysed by a 127° electrostatic analyser. Electron beam currents of around 100 micro-amps and gas pressures of 10 millitorr were typical and the energy spread was 1.2 eV at best. The spectra obtained for ethylene resembled those of Simpson and Mielczarek rather than Kuppermann and Raff's with the exception of a weak transition at 4.7 eV which occured in the 50 eV and 35 eV spectra and was assigned to a singlet-triplet transition. No peak was however observed at 6.5 eV.

An improved apparatus was later developed by Doering and Williams(34) using a 180° hemispherical monochromator which gave a beam of 0.5 micro-amps at energies of 10 - 40 eV with an energy spread of 200 meV and the 127° analyser at a fixed scattering angle of 90°. This instrument was used to obtain energy loss spectra of He, N_2, ethylene and benzene. In N_2 singlet-triplet transitions were found to dominate the spectrum below 20eV and in ethylene, the triplet was observed at 4.4 eV but no transition was observed at 6.5 eV for incident energies as low as 10.9eV.

A modified version of the Kuppermann and Raff spectrometer using

non-magnetic materials and employing a direction selecting baffle to restrict detection of scattering to $90^{\circ} \pm 6^{\circ}$ was put into operation by Wei and Kuppermann (35). Spectra were obtained for a number of molecules despite some instrumental problems(36) which restricted measurements to above 30 eV incident energy. Spectra obtained for ethylene agreed very well with those of Doering showing only the transitions at 4.4 and 7.8 eV and with similar relative intensities.

A versatile instrument for the study of large angle inelastic scattering has been constructed by Trajmar, Rice and Kuppermann (37). It employs hemispherical deflectors for monochromator and analyser and the lens systems are similar to those in Simpson's early apparatus giving beam energies of 25 - 60 eV with resolution variable between 40 and 150 meV and the gas cell consists of a bellows which permits the scattering angle to be varied in the range -30° - $+80^{\circ}$. Detection of the very small signals available at large scattering angles is made possible by the use of an electron multiplier and a sophisticated multi-channel analyser. Spectra have been obtained for He, N_2, CO, H_2, acetylene and ethylene(38, 6) and a set of empirical rules for the identification of triplet states has been drawn up (39).

A similar instrument employing the latest Simpson-Kuyatt optics(40) has been constructed by Williams and Doering(41) which is capable of operation at energies of 6 - 100 eV with a variable resolution of 30 - 200 meV and a range of -2° - $+100^{\circ}$ scattering angle. Electron multiplier detection is used in conjunction with a 128 channel multi-scaler. This instrument has been used to make an extensive study of inelastic scattering from nitrogen at energies between 9 and 50 eV (41,3)and to obtain energy loss spectra of benzene at 13.6 eV and 20 eV incident energies.(42) Spectra obtained show triplet peaks to gain intensity relative to singlet peaks as the scattering angle is increased, in agreement with the work of Trajmar, Rice and Kuppermann.

Favourable experimental conditions for the observation of triplet states would therefore appear to be low incident energy and large scattering angle, while identification of triplet states requires measurements to be made at a number of different scattering angles. These considerations must be borne in mind when designing the instrument.

2.1 General Considerations

As scattering cross-sections for electron molecule collisions in general fall off rapidly with increasing scattering angle, the signal at a detector of small incoming solid angle, such as a deflection analyser of the 127° or 180° type will fall to the noise level at large angles necessitating inconveniently long accumulation times with signal averaging equipment. One solution to this problem is to use an analyser capable of accepting 2π in azimuth and such a device is a retarding field energy analyser (R.F.E.A.) where the retarding field is generated by a cylindrical grid concentric with the scattering region. Such a device was first applied to electron impact spectroscopy by Raff(28). The electron trap developed by Schulz also has this large solid angle of acceptance but the impact energy is fixed at effectively threshold and the presence of the magnetic field renders the concept of scattering angle meaningless. As we require an apparatus for the detection and identification of singlet-triplet excitation, variable impact energy and defined scattering angles are desirable. A consideration of the factors affecting the resolution of a R.F.E.A. leads to the choice of a spherical retarding field concentric with the scattering centre and the split spherical collector system used by Ramsauer and Kollath(43) for total cross-section measurements suggests a method of determining the angular dependence of excitation cross-sections. A spherical R.F.E.A. with a split collector is thus used for energy analysis of the scattered electrons

As the optically forbidden excitation processes in which we are interested have their cross-section maxima at low energies, we require an electron beam in the energy range 10 - 100 eV. The beam should have a small cross-section and a low convergence angle at the scattering region to optimise the analyser resolution and to avoid a large background signal due to reflected and secondary electrons resulting from collisions of electrons with metal surfaces.

Consideration of the effect of fluctuations in pressure and beam current shows that this type of instrument is particularly susceptible to these and that normalisation of the scattered currents to constant pressure and beam current may be necessary. This suggests the use of a data logging system for data collection.

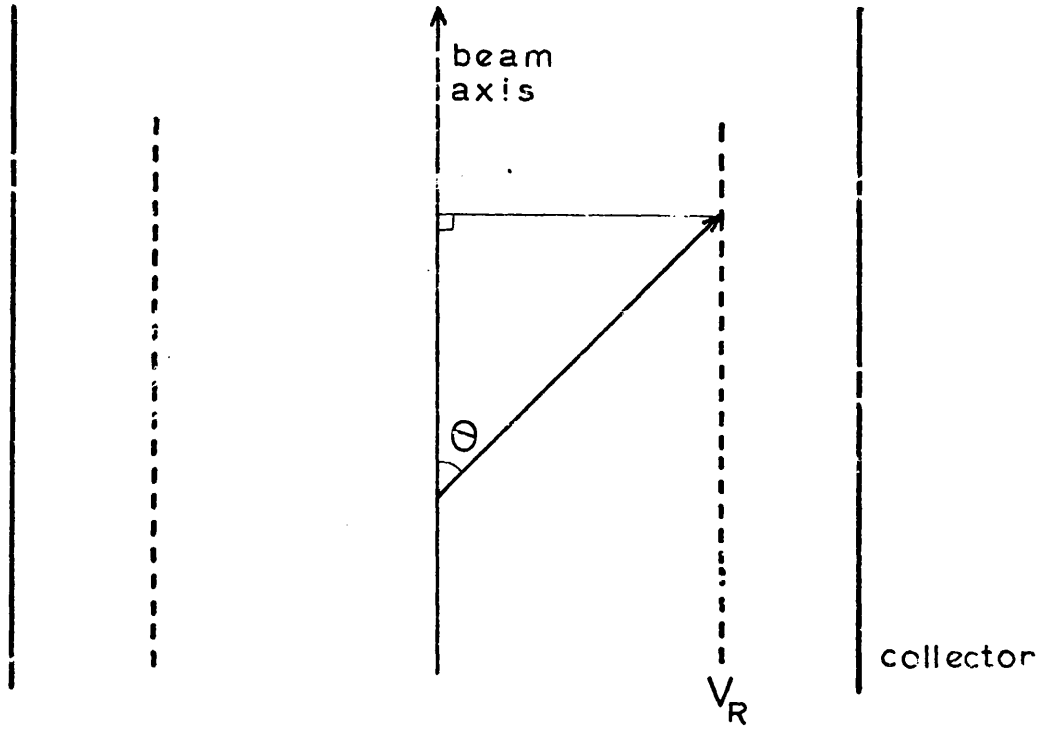

Fig. 2.0(a) Cylindrical R.F.E.A.

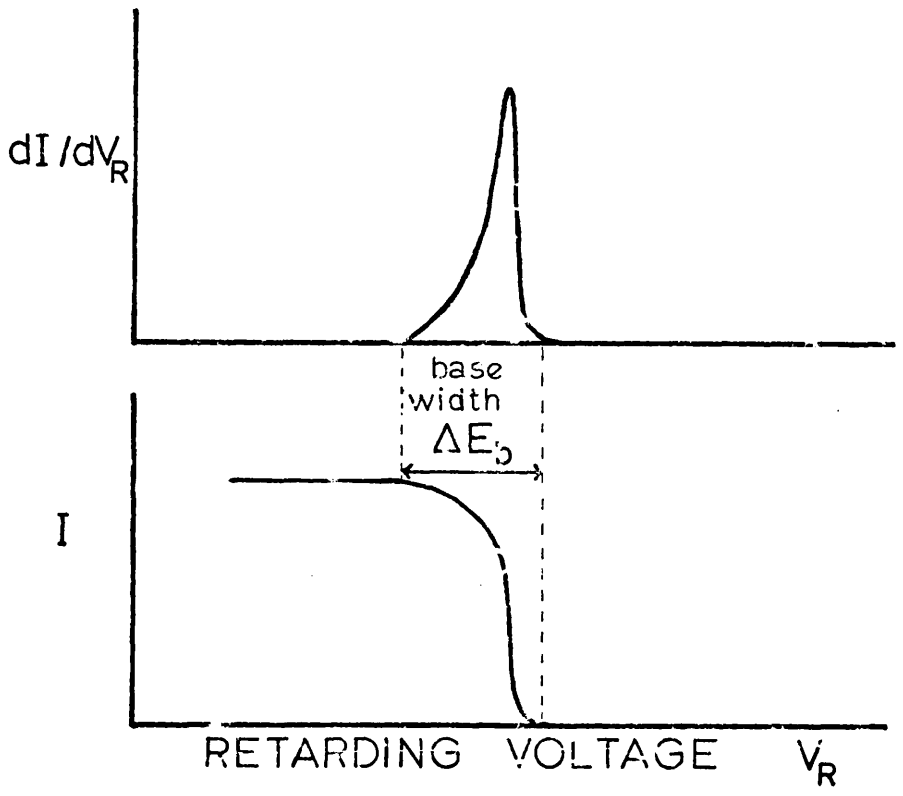

Fig. 2.0(b) Typical characteristics for a R.F.E.A.

2.2 Retarding Field Energy Analyser (R.F.E.A.)

A retarding field analyser acts as a high pass energy filter in which the kinetic energy(K.E.) of the electrons is deduced from the height of the potential barrier that they must surmount as opposed to conventional dispersion analysers which pass an energy band(44). Unfortunately, the height of this barrier is not a measure of the total K.E. but of the momentum in a direction perpendicular to the equipotential lines. As we require a measurement of the total K.E., the difference between "total" and "normal" K.E. may be considered as an energy aberation which limits the obtainable resolution. In designing an analyser of this type , it is necessary to be able to estimate the magnitude of this aberation and its dependence on various parameters of the instrument. In many applications, such as the present work, the energy distribution of the electrons is of interest and a drawback of this type of analyser is that its response is the integral of the energy distribution. It is thus necessary to differentiate the collected current with respect to retarding voltage to obtain the energy distribution of the electrons concerned.

2.2.1 Geometrical Factors Determining Resolution

Cylindrical Analyser

We shall consider first an analyser consisting of a cylindrical retarding grid and a cylindrical collector concentric about an axial scattering region [fig.(2.0a)]. This is the analyser used by Kuppermann and Raff(29) and Ferguson(32).The total K.E. of a scattered electron is

$$E = \tfrac{1}{2}mv^2 \qquad (2.0)$$

and the velocity component normal to the grid is

$$v_n = v \sin\theta \qquad (2.1)$$

Since only the normal component of the momentum of the electron is effective in overcoming the retarding potential V_r, the electron will just be stopped when the retarding potential reaches a value

$$V_r = \tfrac{1}{2}m v_n^2 = \tfrac{1}{2} m v^2 \sin^2\theta = E \sin^2\theta \qquad (2.2)$$

The energy aberation is then

$$\Delta E = E - E \sin^2\theta = E (1 - \sin^2\theta) = E \cos^2\theta \qquad (2.3)$$

This energy aberation will be greatest when the electron approaches the retarding grid at a glancing angle and least when $\theta \simeq 90^\circ$. Calculation of ΔE by eqn.(2.3) for the most glancing angle allowed by the particular

geometrical arrangement used thus gives an estimate of the base width to be expected when the cut-off curve is differentiated [fig.2.0b]. The base width defines the extent of the high-energy "tail" which is characteristic of retarding field analysers. From eqn.(2.3) we see that if direction selecting baffles are fitted between the scattering region and the retarding grid restricting the acceptance of the analyser to electrons scattered within a small range around 90°, then the resolution should be much improved at the expense of restricting the measurements to this angle alone. This is the approach recently taken by Kuppermann and Wei (36).

Spherical Analyser

In this case the analyser consists of a spherical retarding grid and a spherical collector concentric about a small scattering region of defined path length, l, and negligible thickness as shown in the inset of fig.2.2. Since only the radial component of the momentum will be effective in overcoming the retarding potential, Vr, the largest energy aberation will occur when an electron is scattered from either end of the scattering region at 90° to the electron beam axis[fig. 2.1]. The retarding potential will just stop such an electron when

$$V_r = \tfrac{1}{2} m v_r^2 = \tfrac{1}{2} m v^2 \cos^2\alpha = E \cos^2\alpha \qquad (2.4)$$

where v_r is the radial velocity component. The base width is therefore

$$\Delta E_b = E (1 - \cos^2\alpha) = E \sin^2\alpha \qquad (2.5)$$

We must now express sin α in terms of known geometric parameters such as the path length, l, and the retarding grid radius, R.

In triangles ABC, AOC and AOB of fig.2.1 we see that

$$\sin\alpha = a/k \; ; \; \cos\alpha = b/k \qquad (2.6)$$

$$k^2 = R^2 - l^2/4 \qquad (2.7)$$

$$\cos\alpha = 2a/l \; ; \; \sin\alpha = 2(R-b)/l \qquad (2.8)$$

Combining eqns. 2.6 and 2.8,

$$Rb = a^2 + b^2 \qquad (2.9)$$

In triangle ABC,

$$k^2 = a^2 + b^2 \qquad (2.10)$$

Combining eqns. 2.9 and 2.10 and substituting for k in eqn.2.7,

$$b = R - l^2/4R \qquad (2.11)$$

Substituting for b in eqn. 2.8 we obtain

$$\sin\alpha = l/2R \qquad (2.12)$$

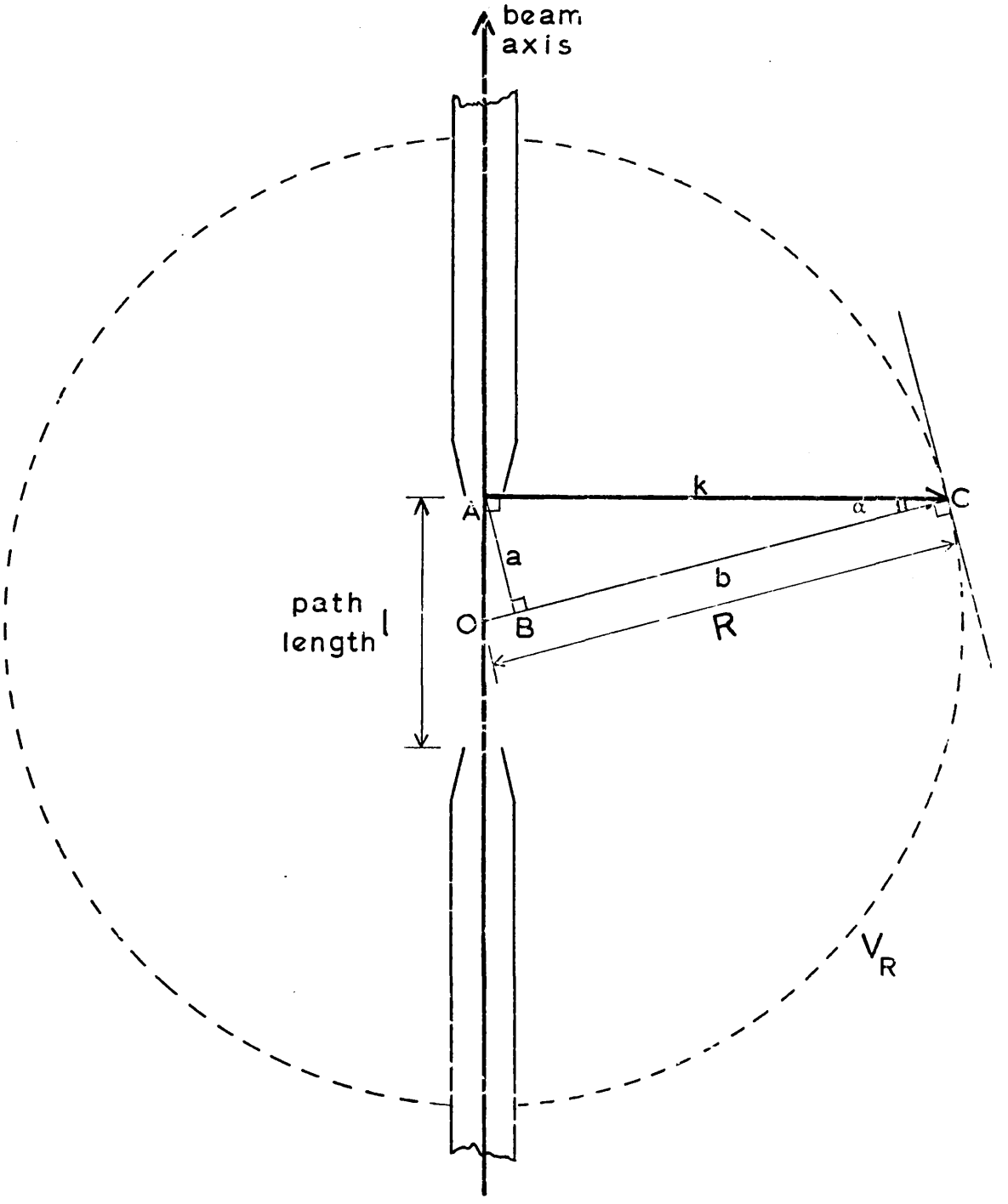

Fig. 2.1 Condition for limiting resolution of a spherical R.F.E.A.

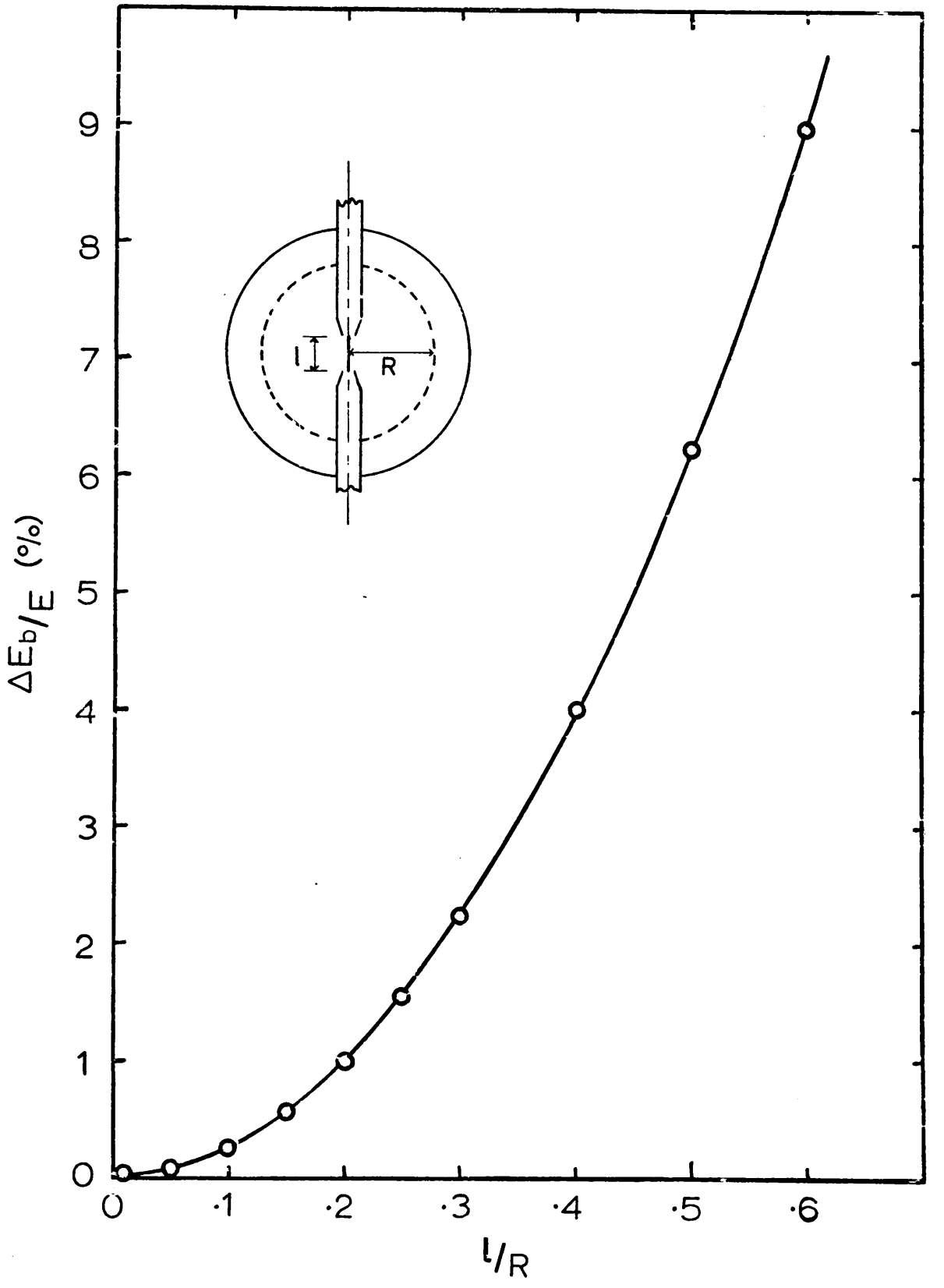

Fig. 2.2 Dependence of the limiting resolution on path length, l, and retarding grid radius, R, for a spherical R.F.E.A.

Consequently, we see by eqn. 2.5 that the base width, ΔE_b, for a spherical analyser is related to the path length, l, and the retarding grid radius, R, by the expression

$$\Delta E_b/E = l^2/4R^2 \qquad (2.13)$$

This calculation assumes that the diameter of the incident electron beam is negligible compared with the path length through the scattering region. It also neglects any lens effect at the holes of the gauze, but for a gauze of large mesh number (i.e. wires per inch) this effect is expected to be small. We can derive a correction for the finite radius, r of the incident beam and the expression obtained by a similar method to that above is

$$(\Delta E/E)_{corr.} = r^2/R^2 \qquad (2.14)$$

However for a typical example where the radius of the beam is 5% of the path length, the correction required by eqn. 2.14 would only amount to 1% of the value for $\Delta E_b/E$ obtained by eqn. 2.13.

Some base widths calculated using the expressions derived in this section for various analysers are given in Table 2.0 and the dependence of the limiting resolution, $\Delta E_b/E$, on path length and retarding grid radius for a spherical R.F.E.A. is shown in fig. 2.2.

Analyser Functions

Although a calculation of the base width for an analyser of given dimensions is useful in determining suitable dimensions for a desired resolution, a knowledge of the expected peak shape will be useful in comparing a R.F.E.A. with dispersion analysers for which the calculated energy aberation normally quoted is the full width at half maximum(F.W.H.M) of the analyser function(i.e. the transmission of the analyser as a function of electron energy.).

If we consider an analyser of the type shown in fig. 2.3 where the grids are in the form of a pair of cones and a cylinder or a similar version where these are replaced by spherical grids and if we define a spherical polar coordinate system where the electron beam passes along the z-axis, then the current scattered into the solid angle, $d\Omega$, which reaches the collector will be given by an eqn. of the form

$$d^2I = \sum_i AQ_i g_i(\theta,\phi) t^3(\theta)\, d\Omega \qquad (2.15)$$

where A is a normalisation factor taking account of gas pressure, beam

TABLE 2.0 : Calculated base widths for various R.F.E.A.'s.

Investigator	Analyser Type	Limiting Resolution $\Delta E_b/E$	Base Width for electron energy of 1 eV	5 eV	10 eV	30 eV
Kupperman & Raff (29)	cylindrical R = 22 m.m. $\theta_{min} = 22^o$	0.86	.86 V	4.3 V	8.6 V	25.7 V
Ferguson (32)	as above					
Wei & Kupperman (36)	cylindrical R = 27 m.m. $\theta_{min} = 84^o$	.011	11mV	55mV	110mV	330mV
present	centre cylindrical section of analyser	.20	.20 V	1.0 V	2.0 V	6.0 V
Vroom et.al.(48)	spherical l = 6 m.m. R =19 m.m.	.028	28mV	140mV	280mV	840mV
Vroom et.al.(49)	spherical l = 10 m.m. R = 95 m.m.	.0028	2.8mV	14mV	28mV	84mV
present	spherical l = 7.5 m.m. R = 23 m.m.	.026	26mV	130mV	260mV	780mV

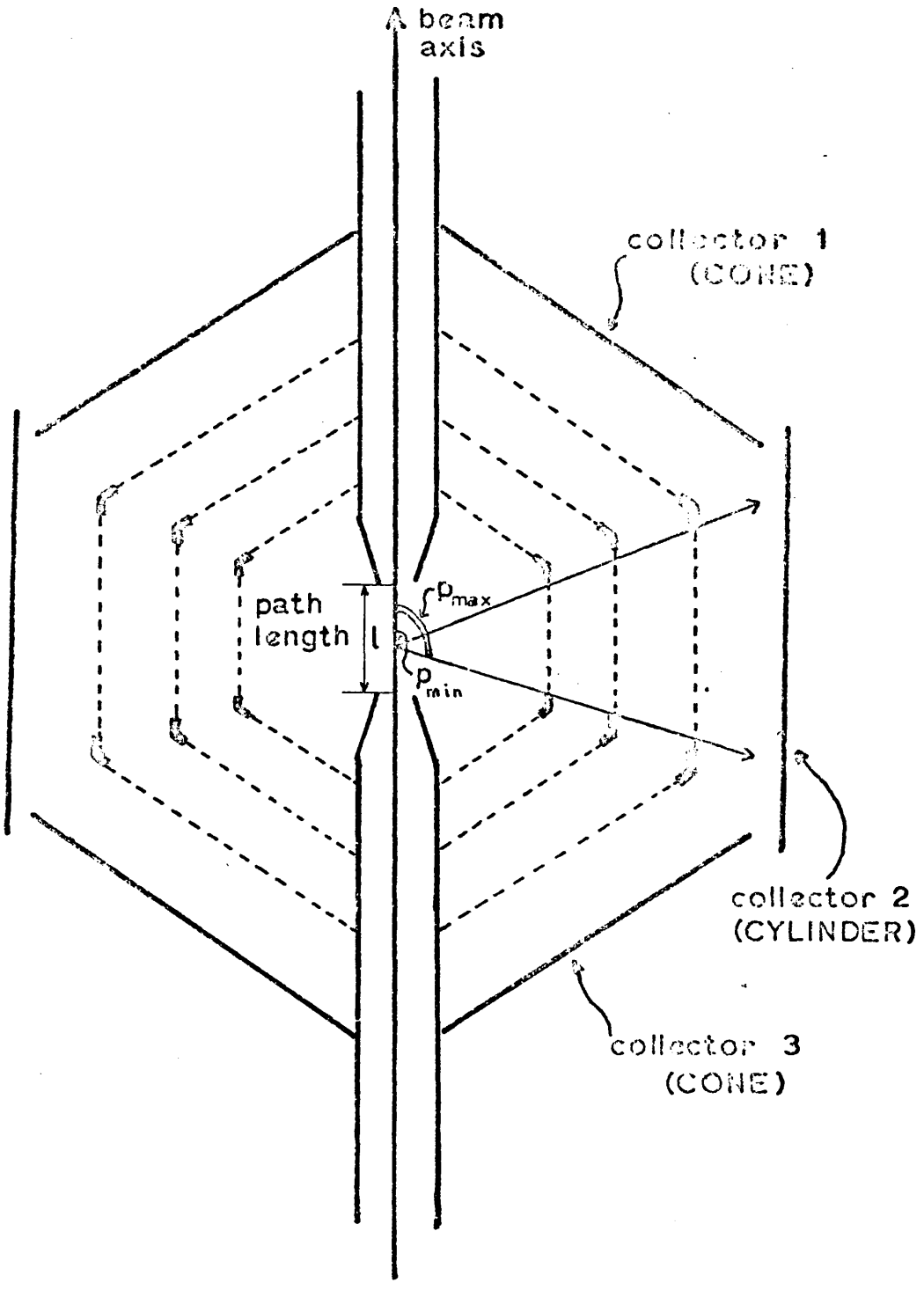

Fig. 2.3 Schematic diagram of the "pseudo-spherical" R.F.E.A. showing geometric limiting angles, p_{min} and p_{max}, for the cylindrical section of the analyser and an arbitrary point along the path length.

current and path length, Q_i and $g_i(\theta,\phi)$ are the total cross-section and angular distribution for any given process, i, and $t(\theta)$ is a transmission function which allows for the variation of transmission through the grids with scattering angle. The transmission function is cubed as the electrons pass through three grids in a R.F.E.A. used for electron impact spectroscopy(29). As scattering is expected to be isotropic in azimuth(45,39), we can integrate over 2π in ϕ, giving

$$dI = 2\pi A \sum_i Q_i g_i(\theta) t^3(\theta) \sin\theta . d\theta \qquad (2.16)$$

since $d\Omega = \sin\theta . d\theta . d\phi$

In the actual experimental arrangement, electrons may be scattered from various points along the path length, l, and through a range of angles limited only by certain obstructios, such as the tubes by which the electron beam enters and leaves the scattering region and the support rings for the grid structures. The limiting angles defined by these obstructions will be referred to as <u>geometric</u> limiting angles, p_{min} and p_{max}. There is however another parameter in the experiment which limits the angular range over which electrons may pass through the retarding grid and be collected and that is the ratio of retarding voltage to electron energy, V/E. From eqn.2.2, we see that, for a cylindrical analyser, the minimum angle through which an electron can be scattered and still reach the collector is

$$T_{min} = \arcsin (V/E)^{\frac{1}{2}} \qquad (2.17)$$

while the corresponding maximum angle is

$$T_{max} = \pi - T_{min} \qquad (2.18)$$

Similar expressions can be obtained for analysers of other geometries and T_{min} and T_{max} will be defined as <u>physical</u> limiting angles since they are determined by the physics of the experiment.

Hence, for any given value of V/E, the current reaching the collector will be

$$I_{(V/E)} = 2\pi B \sum_i Q_i \int_0^l \int_{\theta_{min}}^{\theta_{max}} g_i(\theta) t^3(\theta) \sin\theta . dz . d\theta \qquad (2.19)$$

where B is a constant and θ_{min} and θ_{max} are the <u>overall</u> limiting angles at this value of V/E. For a single collision process, j, this will reduce to

$$I_{(V/E)} = C_j \int_0^1 \int_{\theta_{min}}^{\theta_{max}} g_j(\theta) t^3(\theta) \sin\theta . dz . d\theta \qquad (2.20)$$

where C_j is a constant for the process j.

Hence, knowing the transmission function, $t(\theta)$, for a given geometry and choosing a particular angular distribution, $g(\theta)$, we can calculate the expected collector current over a range of values of V/E. This enables us to plot $I_{(V/E)}$ against V/E and thus obtain the analyser function by differentiation of this curve. The derivation of the transmission functions and the geometric and physical scattering angles for the various analyser geometries is dealt with in appendix A but a typical flow diagram for the computer program used in the calculation of $I_{(V/E)}$ is shown in fig. 2.4. The integrations over path length and scattering angle were approximated by summations, and increments of 0.5mm in path length and 0.5° in angle were found to be adequate while calculation of $I_{(V/E)}$ at intervals of 0.005 in V/E was sufficient to give a reasonable description of the analyser function when $I_{(V/E)}$ was differentiated using the method of Rutledge(46). The squares of the first three Legendre polynomials in cos θ were chosen as angular distribution functions because of the use of these functions in electron-atom scattering theory(47). These functions are shown as insets in fig. 2.5 which shows the calculated analyser functions for the various grid geometries and these angular distributions.

These calculations indicate that the F.W.H.M. is not significantly affected by the geometry of the retarding grid although the base width is. The F.W.H.M. of all the analysers is predicted to be in the region of 100 meV for a 10 eV electron which is less than the energy spread of the electron beam and therefore adequate for the present purposes.

An anomalous analyser function is obtained for the cylindrical section of the "pseudospherical" analyser when the second Legendre polynomial is used. For this angular distribution, no electrons are scattered at 90° and so when V/E is close to unity and only electrons scattered at 90° can be passed, none are available and no signal is obtained. As V/E decreases, the angular range available increases according to eqns. 2.17 and 2.18 and the current passed by the retarding grid is determined by the shape of the angular distribution function.

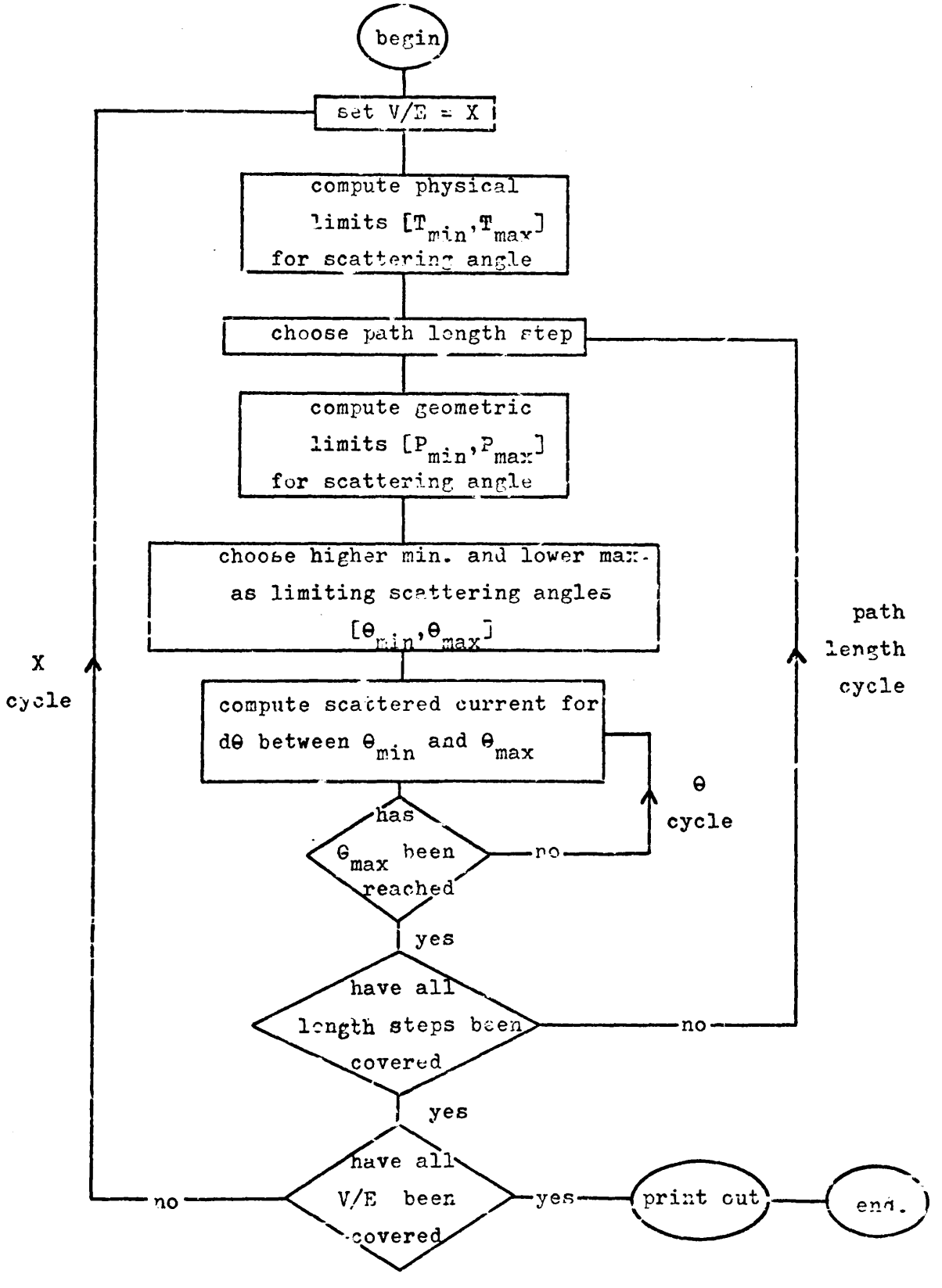

Fig. 2.4 Typical flow chart for a program to compute scattered current as a function of V/E .

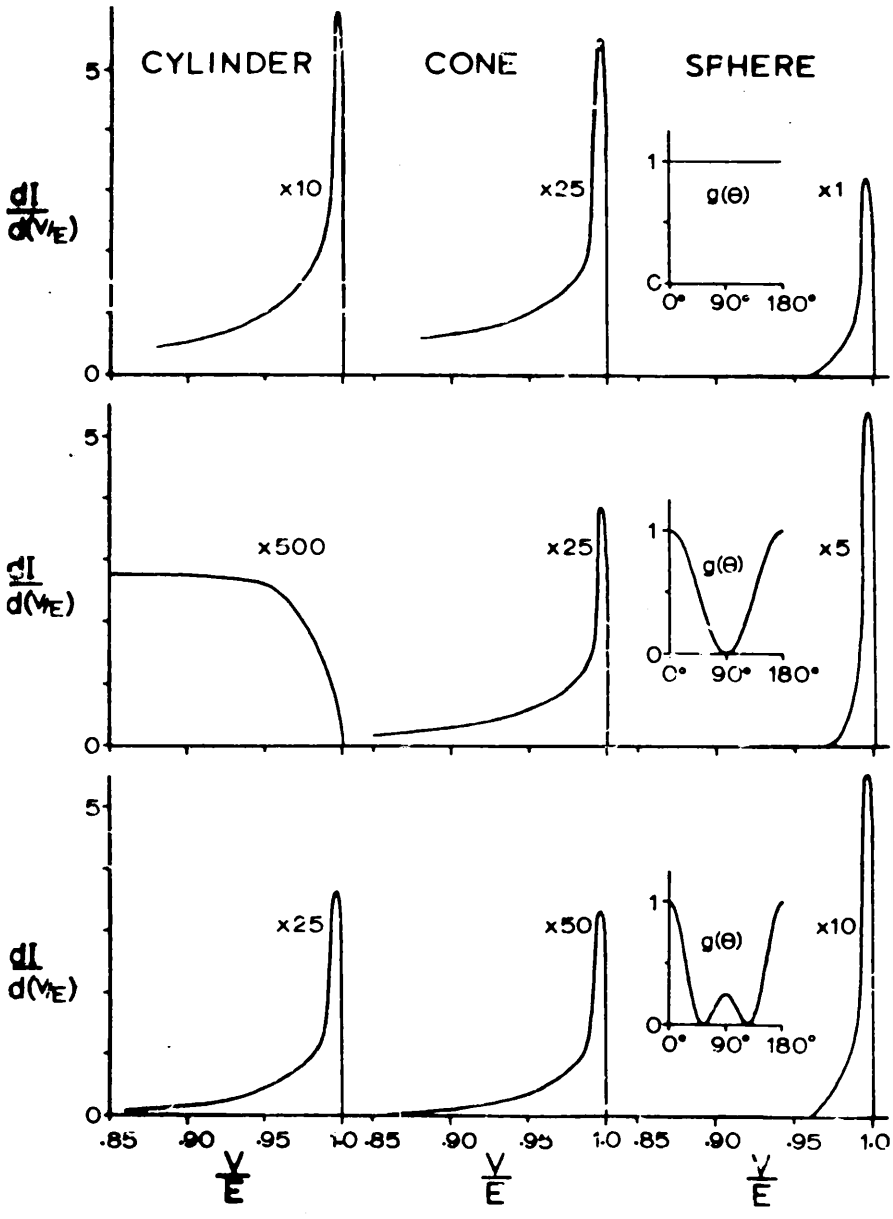

Fig. 2.5 Calculated analyser functions for the various grid geometries and the angular distribution functions shown.

2.2.2 Other Factors Affecting Resolution

In the previous section, it was assumed that electrons leaving the scattering region travel in straight lines paths on their way to the retarding grid. Any effects which deflect the electrons from such paths will decrease resolution and must be minimised or, if possible, eliminated.

The presence of insulating films on the grids is to be avoided and the choice of mercury diffusion pumps rather than oil ones should help in this respect.

The effect of significant magnetic fields in the analyser would be that any electron initially approaching the retarding grid at normal incidence would be deviated from its path and would subsequently intersect the grid at other than normal incidence. A 1 eV electron travelling perpendicularly to the Earth's magnetic field of 0.6 gauss would describe a circular orbit of 5.6 cm radius, which is of the order of the dimensions of the apparatus. Reduction of the field to 10 milli-gauss would increase this radius to 337 cm and the effect on the base width of a 1 eV electron would then be less than 1 meV. Magnetic field cancellation is therefore essential.

Another factor which can result in loss of resolution in an R.F.E.A. is the nature and number of grids used. In thermionic valve design, it is found that the plate-current/plate-voltage characteristic is sharpened as the number of grids is reduced(51a) or if two grids are accurately aligned. The loss of resolution which occurs when a number of grids are present is due to an increase in the transverse velocity components of the electrons caused by scattering from grids and by deflection of electron paths by electrostatic lens action at the grid holes(51b). Scattering from grids may be minimised by using a high transparency gauze composed of small diameter wires and by using the minimum number of grids which the experiment will allow(52). The deflection of electrons by the lens action at the grid holes is directly related to the strength of the lens formed and consequently, for highest resolution, parameters should be chosen such as to weaken the lens. Qualitative application of the principles described by Spangenberg(51c) suggests that in a R.F.E.A. used for electron impact spectroscopy, there will be a very weak convergent action at the first grid, a weak divergent action at the

second (+ve ion repeller) grid and a strong convergent action at the third (retarding) grid.

The lens effect at the retarding grid is the most important and for a spherical R.F.E.A. employing a point source the resolution is determined almost entirely by this factor(50). The resolution can therefore be improved by increasing the mesh number of the gauze and increasing the inter-grid spacing as both of these measures will result in a weakening of the lens, the latter by reducing potential gradients. Huchital and Rigden(50) have recently developed a spherical R.F.E.A. for use in X-ray photoelectron spectroscopy in which the photoelectrons are assumed to emanate from a point source. In their design, they have found lens theory insufficiently accurate and they rely on computer calculations of electron trajectories. Their preliminary calculations(53) indicate that the lens effect limit to the resolving power($E/\Delta E_{\frac{1}{2}}$) is approximately $5D/d$ where d is the diameter of a mesh hole and D is the spacing between the grid at the scattering region potential and the retarding grid for their two grid analyser. This suggests that if the analyser of fig. 3.1 , fitted with the spherical grids was operated with a point source and a gauze of 100 mesh and .0016" dia. wires was used, then the resolution at half height ,$\Delta E_{\frac{1}{2}}/E$, would be in the region of 0.6%.

Although, in the present application, where there is an extended source, the geometric factors mainly limit the resolution, the scattering and lens effects may be minimised by using high transparency gauze of large mesh number, composed of small diameter wires and large inter-grid spacings. Limitations will be structural rigidity, commercial availability of suitable gauze and the internal dimensions of the vacuum tank. Slight distortions in the inner two grids should be tolerable if this permits an increase in transparency but the retarding grid should be made distortion-free, if necessary at the expense of reduced transparency.

Although the electron energy (E) cannot strictly be said to affect the resolution ($\Delta E/E$), it does affect the peak widths (ΔE) because in a R.F.E.A. it is necessary to energy analyse the scattered electrons at the energy with which they present themselves at the retarding grid. This situation is conveniently avoided in an electron impadt spectrometer of type developed by Simpson and Kuyatt(40) by decelerating the electrons to a low energy before analysis in the 180° deflector. Consequently, sharper peaks will be obtained in a R.F.E.A. when the scattered electron

energy is low and this will require operation with incident beam energies close to threshold.

2.2.3 Signal-to-Noise Ratio

The main sources of noise in this instrument are fluctuations in gas pressure and beam current. Under single collision conditions, the scattered electron current, I_s, may be approximated by

$$I_s = kpQl\, I_b \qquad (2.21)$$

where p is the gas pressure, Q the total cross-section, l the path length, and I_b is the current at the beam collector. This current may be further subdivided into components from elastic and inelastic processes and experimentally this is measured by energy analysis of the scattered electrons. From eqn.2.21, we see that a steady signal requires stabilisation of gas pressure and beam current and this requirement is more stringent in the case of the R.F.E.A. than for an electrostatic deflection analyser. Typical signals for the two types of experiment are shown in fig. 2.6 where the elastic scattering and one inelastic process are considered.

For the R.F.E.A., the signal of interest is the current difference $I_2 - I_1$ as this is proportional to the inelastic cross-section Q_1.

$$I_2 - I_1 = k\, l\, I_b\, p\, Q_1 \qquad (2.22)$$

Now if a pressure fluctuation, Δp, occurs, this will induce a current fluctuation

$$\Delta I_p = k\, l\, I_b . \Delta p\, (Q_{el} + Q_1) \qquad (2.23)$$

and as electron impact inelastic cross-sections are typically 1 - 10 % of the elastic cross-section, this reduces to

$$\Delta I_p \simeq R\, (k.l.I_b)\, \Delta p\, Q_1 \qquad (2.24)$$

where $R = Q_{el}/Q_1$.

Combination of eqns. 2.22 and 2.24 gives the signal-to-noise ratio

$$(I_2 - I_1)/\Delta I_p \simeq R\, (p/\Delta p) \qquad (2.25)$$

For an electrostatic analyser the signal I_2 is proportional to the inelastic cross-section, Q_1.

$$I_2 = k\, l\, I_b\, Q_1\, p \qquad (2.26)$$

and the amplitude of the noise produced by the pressure fluctuation is

$$\Delta I_p = k\, l\, I_b\, Q_1 . \Delta p \qquad (2.27)$$

Hence the signal-to-noise ratio is

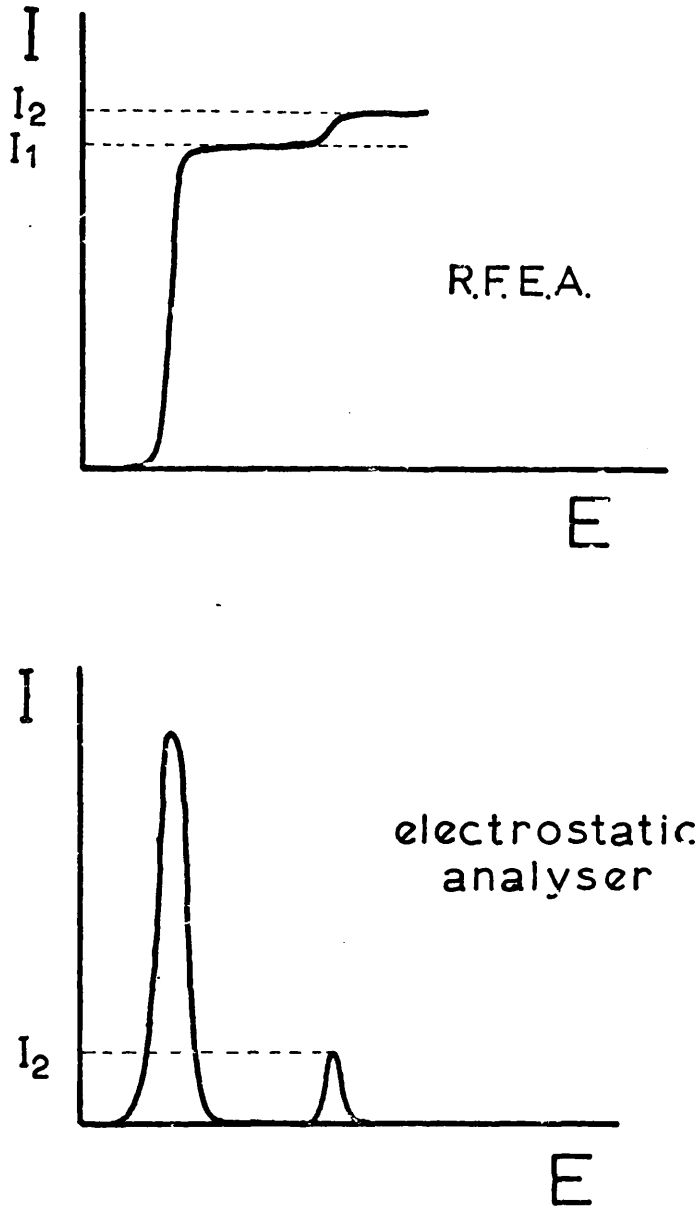

Fig. 2.6 Comparison of the signals cbtained from the two types of analyser.

$$I_2/\Delta I_p = p/\Delta p \qquad (2.28)$$

Expressions similar to eqns. 2.25 and 2.28 may be derived to cover fluctuations in beam current. From these eqns. we see that the signal-to-noise ratio in an electron impact spectrometer employing a R.F.E.A. may be 10 - 100 times poorer than for an instrument with electrostatic deflection analysis .

On the basis of signal-to-noise, the R.F.E.A. is more suited to applications such as photoelectron spectroscopy where the cross-sections are of the same order of magnitude. For the purposes of the present application, a need for stabilisation of pressure and beam current is indicated combined with the use of data logging for normalisation of the scattered currents to constant pressure and beam current and for averaging of a number of scans. This problem may also be partly alleviated by the fact that Q_{el}/Q_1 (R of eqn.2.25) tends to decrease with increasing scattering angle in electron impact spectroscopy.

2.3 Electron Gun

Previous instruments of this type(29,32,36) have used guns consisting of a parallel plate diode followed closely by three apertured plates which serve both as a lens and as a means of collimating the beam. The lens is operated as a Einzel lens with the outer elements at the same potential while the potential on the centre element is varied to minimise the ratio of scattered current to current reaching the beam collector with no gas in the collision chamber. Unfortunately, the electron beams produced by these guns rapidly increase in angular divergence as the electron energy is lowered, giving rise to large background currents which have so far restricted measurements by this technique to impact energies above 25 eV(29). The adoption of a spherical geometry for the R.F.E.A. in the present design necessitates the use of an electron gun capable of producing a narrow beam of small convergence angle because of the mechanical requirement of transporting the beam along a tube into the scattering region at the centre of the spheres. Such a beam would be expected to have the additional advantages of minimising background scattering off metal surfaces in the collision region and of providing a sharply defined source for the analyser.

An ideal beam would be one which has high current density and low angular divergence, however there are fundamental electron optical laws which place a limitation on these parameters.

The law of Helmholtz and Lagrange states that along any beam path, whether or not images are formed, and where current is conserved, the energy, E, differential solid angle, $d\Omega$, and differential area, dA, at any two planes, 1 and 2, are related by

$$E_1 . d\Omega_1 . dA_1 = E_2 . d\Omega_2 . dA_2 \qquad (2.29)$$

This law expresses the conservation of electron "brightness" or Richtstrahlwert, defined as

$$R = dI/dA . d\Omega \qquad (2.30)$$

where dI is the current through the differential area dA and differential solid angle $d\Omega$. Combination of eqns. 2.29 and 2.30 when current is conserved, leads to

$$R_1/E_1 = R_2/E_2 \qquad (2.31)$$

Thus we see that Richtstrahlwert divided by energy is a conserved quantity and the practical effect of this is to reduce the Richtstrahlwert as the final energy of an electron beam is lowered.

Eqn. 2.29 applies to any system whether or not images are formed. However, if this is applied to the case where planes 1 and 2 are conjugate object and image, the differential form may be integrated to give the Abbe-Helmholtz Sine Law

$$(E_1)^{\frac{1}{2}} . \sin \theta_1 = M (E_2)^{\frac{1}{2}} . \sin \theta_2 \qquad (2.32)$$

where M is the linear magnification from plane 1 to plane 2. Here we see another practical limitation on our ideal low energy beam; if a deceleration takes place between planes 1 and 2, the final convergence angle, θ_2 will be greater than the corresponding angle in the higher voltage element, θ_1.

The Abbe - Helmholtz Sine Law may be used to relate the maximum attainable current density in the final beam, $J_2(max)$, to that at the cathode. If plane 1 is the cathode and E_1 is expressed in terms of the cathode temperature and M as a ratio of current densities, the Langmuir equation

$$J_2(max) = J_c [1 + (E_2/kT)] . \sin^2 \theta_2 \qquad (2.33)$$

may be obtained where the subscript 2 refers to the final beam.

Space charge, set up by the mutual repulsion of electrons in the beam, places an upper limit on the current which can be passed through a given volume. For the case of a tube, or two apertures of diameter D separated by a distance L, the maximum current is

$$I_{max} = 38.5\ E^{\frac{3}{2}}\ (D^2/L^2) \qquad (2.34)$$

where I is in micro-amps and E in eV and this current may only be achieved if the electron beam enters the volume such that in the absence of space charge it would be focussed to a point at the centre of the the volume.If this relation is required in terms of the convergence half-angle, α, then D/L may be replaced by tan α.

Considering these limitations, Simpson and Kuyatt(54) have shown that it is impossible to force the maximum permissible (saturation) current through any given space below a certain critical voltage which depends on the half - angle of the space. A general technique used by these authors to circumvent this difficulty is to use multi-stage guns (55) in which the beam is initially formed at a higher energy and then decelerated to the required low energy. The design may thus be considered in two parts; the extraction stage and the deceleration stage. Using a Soa triode gun as the extraction stage and a double- aperture lens as the deceleration stage, Simpson and Kuyatt produced a multi - stage gun which performed well for final energies down to 30 eV.

As discussed by Harting and Burrows(56), the Soa gun is unsuitable at energies below this because of both inconvenient dimensions and its inability to filter out from the beam electrons with large radial velocity components. This angle sorting is necessary because at low energies the thermal emission velocities are significant in comparison with the beam velocity leading to severe chromatic aberations. A more suitable extraction stage is the Pierce diode in which a parallel electron flow takes place up to the anode aperture after which the beam diverges at a calculable angle and electrons emitted with zero transverse velocity appear to emanate from an axial virtual point behind the cathode surface.

A lens system is required to place the desired image at the scattering centre and to provide the deceleration to the desired energy. As we require a fixed image at various beam energies, the use of a

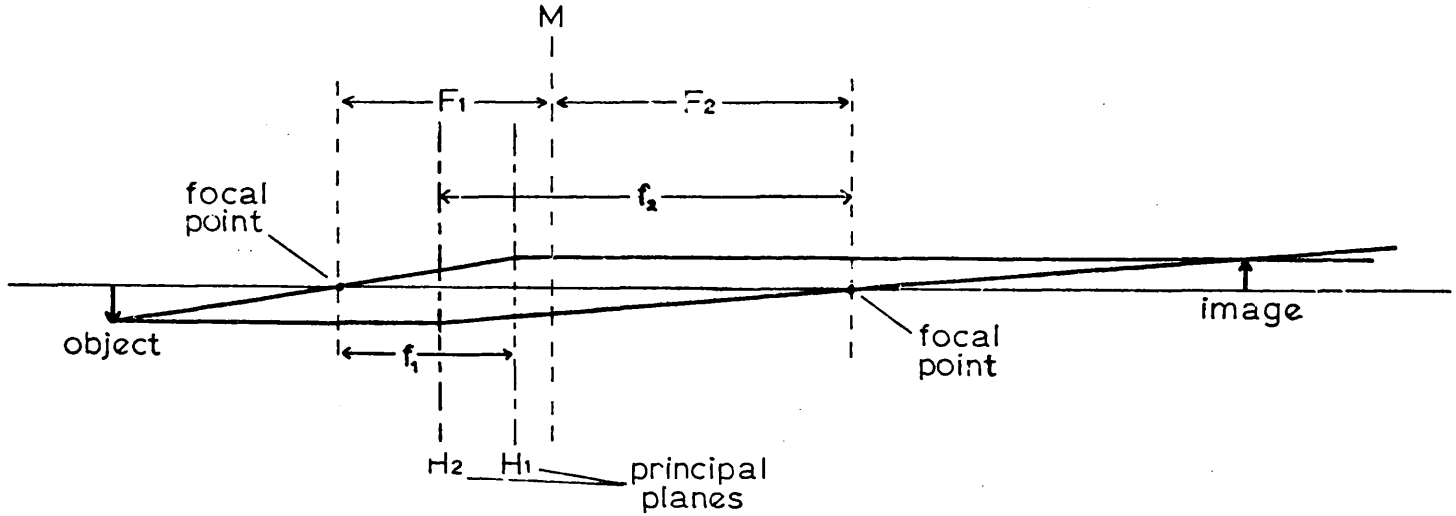

Fig. 2.7(a) Thick Lens Notation.

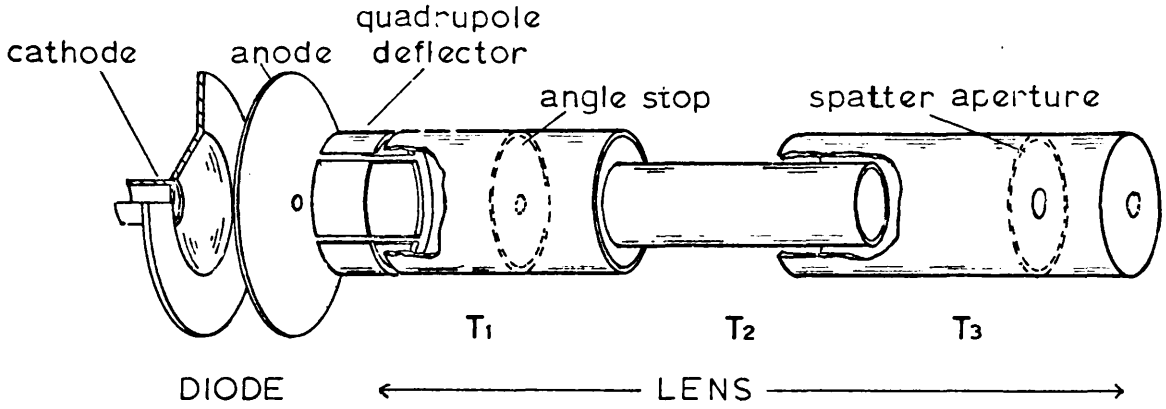

Fig. 2.7(b) Schematic representation of the electron gun.

variable - ratio lens is indicated and as large angle scattering is to be detected, the overall diameter of the lens must be small, suggesting the use of tube lenses.

2.3.1 Extraction Stage

As discussed above, the parallel flow Pierce diode is a suitable source for a low energy electron gun and this is the source used here. The space-charge-limited current density, J, may be calculated from the anode voltage, V_a, and the cathode-anode spacing, d.

$$J = 2.33\, V_a^{3/2}/d^2 \qquad (2.35)$$

If the anode aperture has a radius, a, then we can also find the total current leaving the diode

$$I_{(tot)} = J\pi a^2 = 7.32\, V_a^{3/2}.a^2/d^2 \qquad (2.36)$$

As an electron emmitted parallel to the cathode with thermal energy at emmision, V_k, has a slope

$$\gamma = (V_k/V_a)^{\frac{1}{2}} \qquad (2.37)$$

when it reaches the anode hole, the Richtstrahlwert at the anode is given by

$$R/V_a = (2.33\, V_a^{3/2}d^2)/(\pi\gamma^2 V_a)$$

$$\text{i.e. } R/V_a = .74\, V_a^{3/2}/(V_k.d^2) \qquad (2.38)$$

where $V_k = T(^\circ K)/11600$ eV

The anode aperture may be considered as a Calbick(or single-aperture) lens and the virtual point object has a focal length which may be calculated as -4d, -3d, or -2.7d depending on whether we assume uniform field in the diode, a space-charge-limited diode, or a space-charge-limited diode to which an empirical correction(57) is applied to account for field distortion near the aperture. As there is some doubt on this matter, in the present design the anode aperture itself is chosen as the object for the lens system since its position may be accurately defined subject only to mechanical tolerances.

Parallel electron flow in the diode is achieved by shaping the electrodes to suit the appropriate equipotentials as given by Pierce(58). The cathode mounting plate should have a conical recess making an angle of $67\frac{1}{2}^\circ$ with the beam axis as shown in fig. 2.7(b). The correct anode shapes for different ratios of diode spacing to cathode radius are given by Pierce and as this ratio increases, the optimum anode shape approaches more and more closely a flat plate. However, as we see from eqns. 2.36

and 2.38, increasing the spacing, d, decreases the current and Richtstrahlwert at the anode aperture. Too large a spacing may also result in the need for an excessively large anode voltage during activation of the dispenser cathode, although it does have the advantage of reducing the angular divergence of the beam at the anode aperture. For a diode spacing of 5mm, a flat anode is a good approximation to the correct equipotential up to about 3mm out from the axis and as the cathode in use has a radius of 1.5mm, this spacing is satisfactory. If space-charge-limited operation is assumed, then the beam divergence angle at the anode aperture is

$$\theta_b = a/3d \qquad (2.39)$$

and for this spacing and an anode aperture of .46mm dia. the divergence of the beam leaving the diode will be .0154 rad. ($\sim 1^o$).

Once the diode dimensions have been determined, an estimate of appropriate anode voltages can be made using the Helmholtz - Lagrange Law in the form of eqn. 2.31 if the Richtstrahlwert in the final beam is known. If we assume that the final beam is space-charge-limited with energy V (in eV), convergence half angle α (in rad.), and that its radius in the absence of space charge is estimated to be r (in cm), then the Richtstrahlwert is given by

$$R/V = [I/(\pi r^2 \pi \alpha^2)]/V$$

by eqn. 2.34

$$R/V = (38.5\, V^{3/2}\alpha^2)/(V\pi^2 . r^2 . \alpha^2)$$

i.e.

$$\underline{R/V = 3.9\, V^{\frac{1}{2}}/r^2} \qquad (2.40)$$

Eqns. 2.38 and 2.40 may thus be used to obtain an estimate of the required anode voltage for different final beam energies and thus enables the choice of a suitable power supply to be made.

For final beam energies between 10 and 50 eV and assuming non-space-charge beam diameters of 0.5 to 1 mm, the anode voltages required are calculated to be in the range 100 to 150 volts. Also for an anode aperture of 0.46 mm diameter, the current leaving the diode is calculated from eqn. 2.36 to be a few tenths of a micro-amp at the calculated anode voltages.

2.3.2 Variable-Ratio Lens

The electrons leaving the diode must be focussed into the scattering

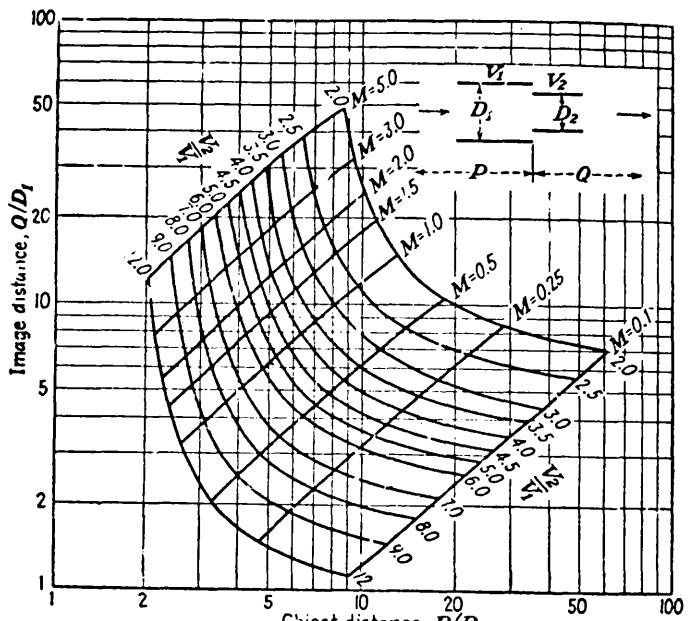

Fig. 2.8(a) P-Q curves of a two-cylinder lens, $D_2/D_1 = 2/3$.

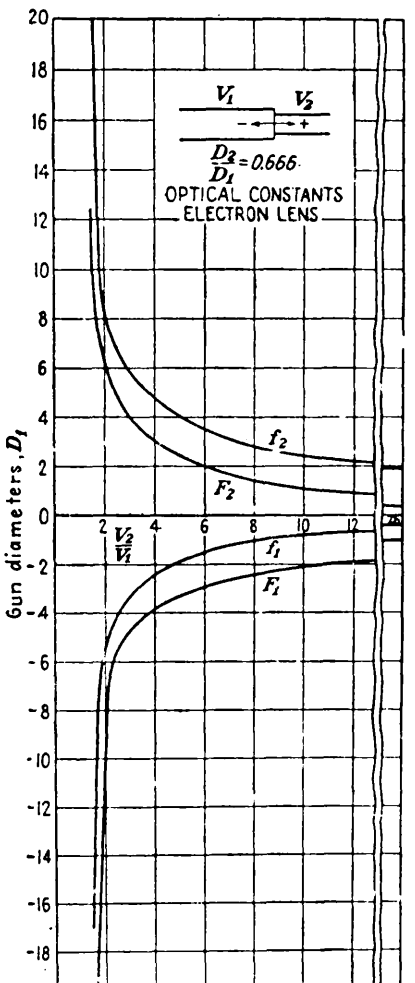

Fig. 2.8(b) Optical characteristics of a two-cylinder lens, $D_2/D_1 = 2/3$.

region where they are required to have a variable energy in the range 10 to 50 eV and an image at the scattering centre. Such an application requires the voltage ratio between object and image planes to vary over a wide range and this precludes the use of a two - element lens since its focal properties will be uniquely determined by the voltage ratio. A three-element lens may be used as a variable ratio lens because its focal properties depend on two voltage ratios and for a given final beam energy the potential on the middle element may be adjusted to place the image in the desired position.(59,60,61)

Mechanical considerations resulting from the analyser design suggest the use of tube lenses and that the junction of the first two tubes should be approximately 45 mm from the scattering centre. The beam entrance tube of the analyser is 4 mm i.d. as a result of the requirement of observing large angle scattering given a vacuum tank of 4" i.d.. A convenient object - image distance is around 65 mm and if as a rough initial approximation we assume that the double lens has the same property as a single lens, i.e. that

$$M = 0.8\ Q/P \qquad (2.41)$$

then, for unit magnification, the object and image distances (P and Q) will be 29 mm and 36 mm respectively. Consideration of Spangenberg's P - Q curves(51d), such as that reproduced in fig. 2.8(a) suggests that for unit magnification and a large tube diameter of 4 mm, the lens for which $D_2 = (2/3)\ D_1$ should be suitable. This is convenient as it means the centre lens element is a tube of 2.65 mm i.d. which can be placed inside the beam entrance tube of the analyser[see fig.3.1] thus enabling the lens centre to be moved closer to the scattering centre.

Kuyatt(60) has shown that for a combination of two simple lenses, the focal parameters are, referring to figs. 2.9 and 2.7(a),

$$f_1^* = f_1.f_1'/(F_1' + F_2 - S) \qquad (2.42)$$

$$f_2^* = f_2.f_2'/(F_1' + F_2 - S) \qquad (2.43)$$

$$F_1^* = F_1 - [(f_1.f_2)/(F_1' + F_2 - S)] + S/2 \qquad (2.44)$$

$$F_2^* = F_2' - [(f_1'.f_2')/(F_1' + F_2 - S)] + S/2 \qquad (2.45)$$

where the unmarked symbols refer to the first lens, the primed letters to the second lens and the starred letters to the combined lens.

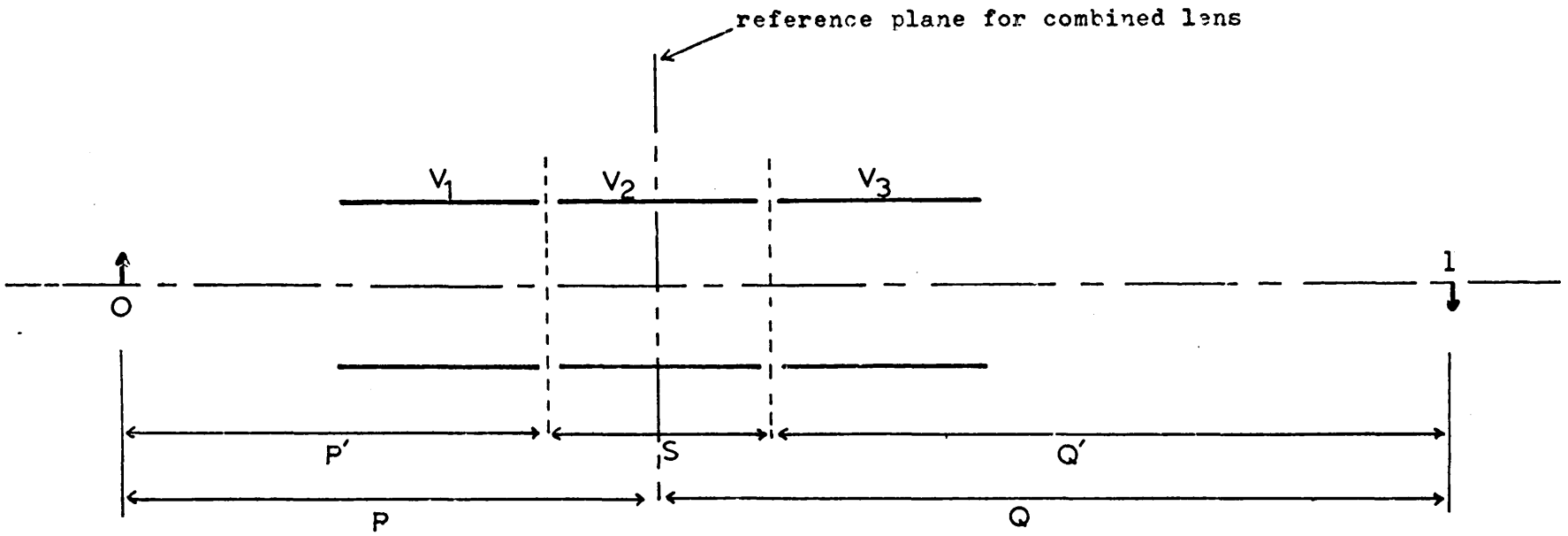

$$P' = P - S/2 \; ; \quad Q' = Q - S/2 \; .$$

Fig. 2.9. Combination of two simple lenses

Trial and error calculations were carried out using eqns.2.42 to 2.45. S, V_1 and V_3 were chosen and V_2 varied, the optical characteristics measured by Spangenberg(51e) and shown in fig. 2.8(b) being used in the calculation. For the second (decelerating) lens the values of f_1 and f_2 etc. are interchanged since the curves given by Spangenberg are for accelerating lenses. As the use of batteries for supplying the electrode potentials was being considered, large voltage ratios were undesirable. A calculation with S = 18 mm, V_1 = 25 volts and V_3 at 25, 30, 40 and 50 volts suggested that suitable focussing should occur for the ratio V_2/V_3 close to 2.0 and that this ratio would be expected to decrease slightly as V_3 is increased from 25 to 50 volts. This calculation also showed the position of the first focal point, F_1^*, to be very nearly constant at around 14.5 mm for the chosen values of V_1, V_2, and V_3.

If the anode were to be operated at a higher potential than V_1, then on the assumption of a Calbick lens at the anode hole we would expect the focal length of the virtual object to be decreased, thus increasing the divergence of the beam at the anode aperture.

An aperture of 0.6 mm dia. located at the first focal point of the combined lens will limit the angular divergence of the beam, reduce collisions of electrons with the walls of the small diameter tube and reduce spherical aberation by reducing the beam diameter relative to the tube diameter(51f). Stray electrons produced by collisions at walls may be filtered out by a "spatter" aperture of 1.2 mm dia. placed in T3 at 14 mm from the scattering centre. A final aperture of 0.9 mm dia. is dimensioned to clear the beam and is included for the purpose of providing differential pumping. A quadrupole deflector with its mean potential maintained equal to V_1 will align the beam between the anode aperture and the angle stop.

2.3.3 Beam Collector

It is the purpose of the beam collector to collect the unscattered beam efficiently and without interfering with the scattered electrons. To enable scattering to be studied over as large an angle as possible, the use of a long tube closed at one end and fitted inside a tube similar to the beam entrance tube seems convenient. This has the

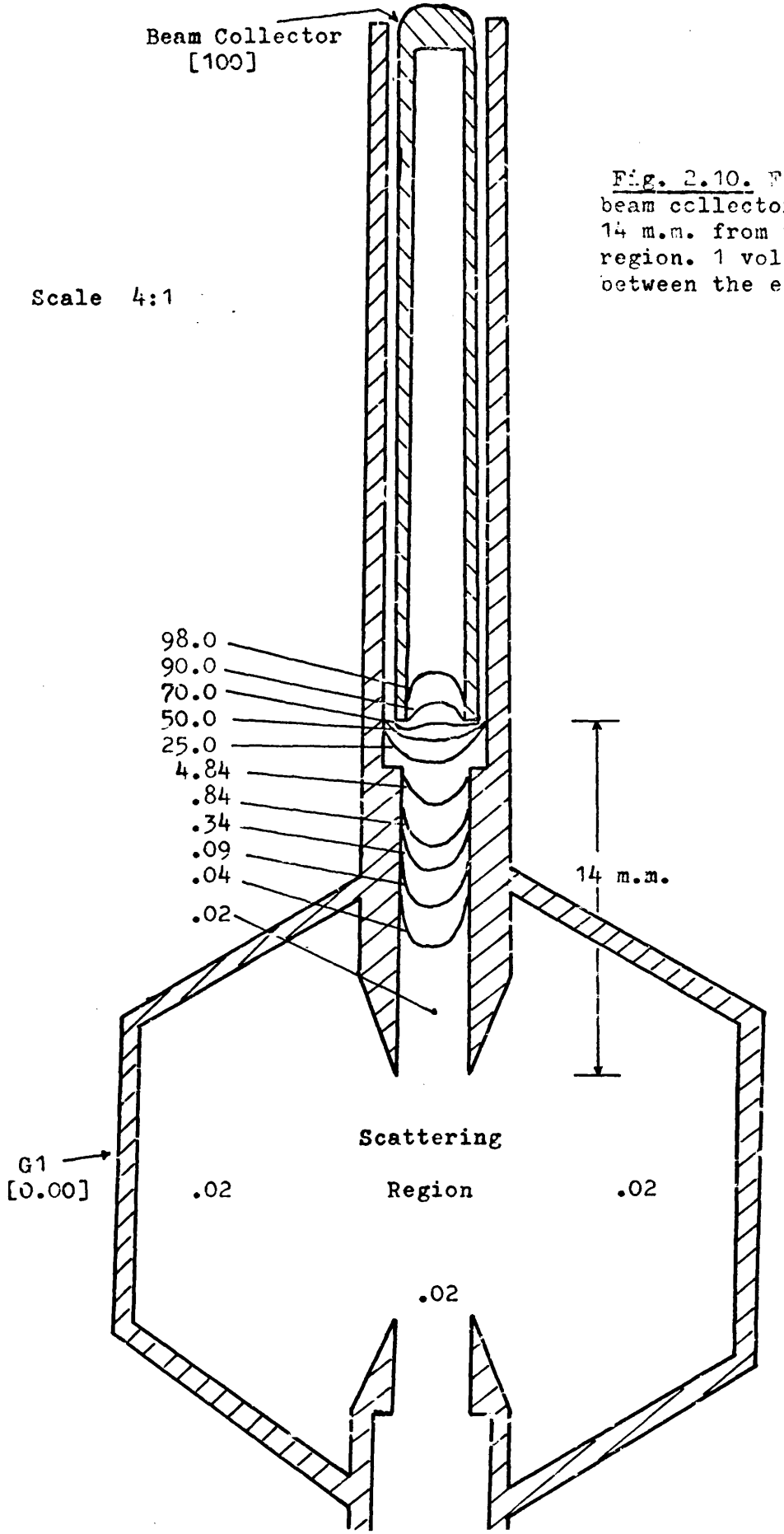

Fig. 2.10. Field plot for beam collector entrance at 14 m.m. from the scattering region. 1 volt was applied between the electrodes.

additional advantages of the collector being efficient due to the large length-to-diameter ratio and of its being shielded.

Efficient collection also requires the application of a holding voltage between the beam collector and the scattering region and it is important that this potential should not penetrate into the scattering region and affect the trajectories of the inelastically scattered electrons. To check this, field plots were made using resistance paper on which the electrode shapes had been painted with conducting paint. A digital voltmeter was used to determine the equipotential lines and plots were made for different positions of the beam collector in the beam exit tube. The plot for the collector in its final position is shown in fig. 2.10, which overestimates the penetration in the real situation, since the resistance paper technique only provides a two-dimensional representation of the field. The penetration from the beam collector may therefore be taken as negligible when the open end is positioned 14 mm from the scattering region.

Fig. 3.1 Typical cross-section through the experimental region.

(Unfold)

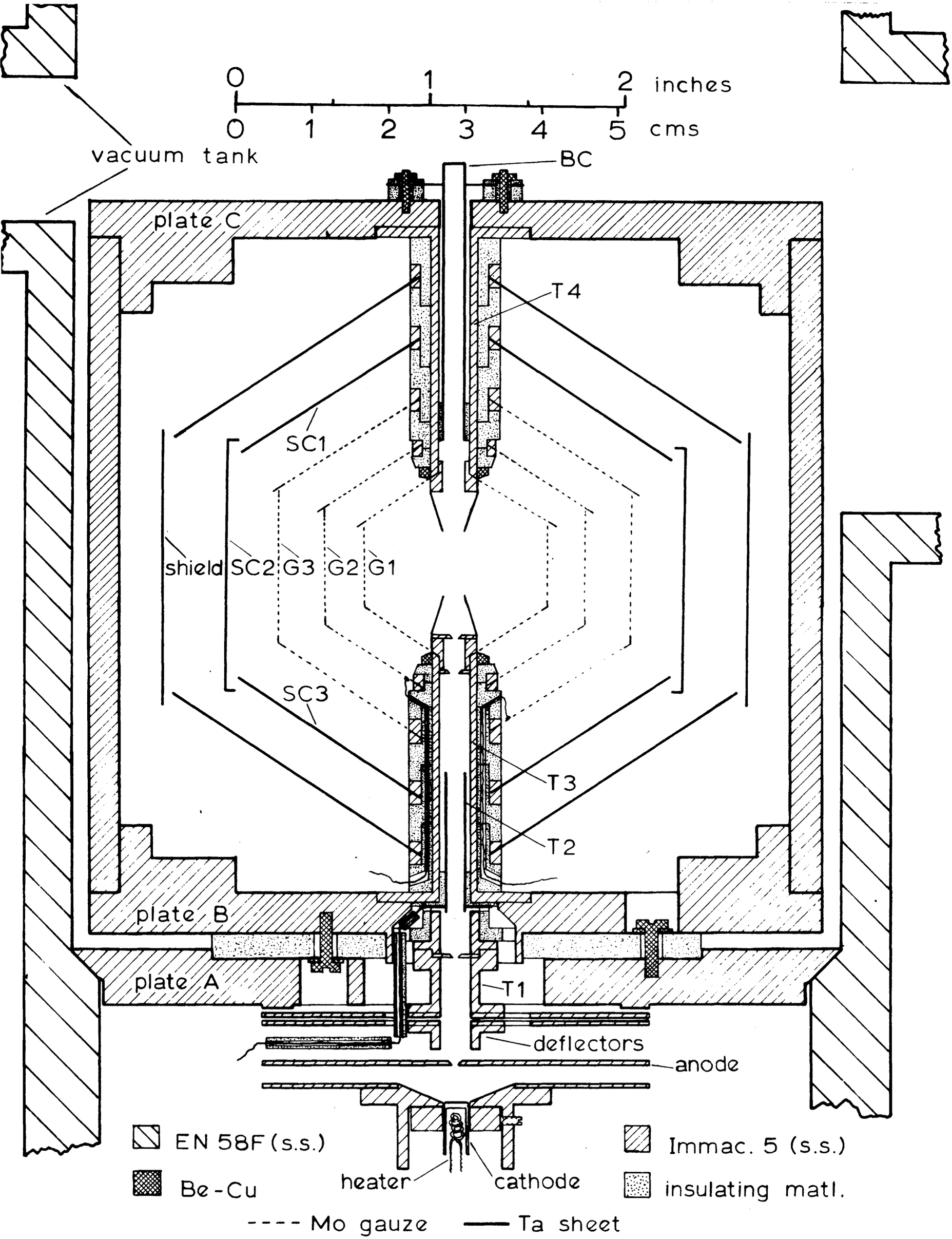
0 1 2 inches
0 1 2 3 4 5 cms
vacuum tank
BC
plate C
T4
SC1
shield
SC2
G3
G2
G1
SC3
T3
T2
plate B
plate A
T1
deflectors
anode
heater
cathode
EN 58F (s.s.)
Be-Cu
Immac. 5 (s.s.)
insulating matl.
---- Mo gauze
— Ta sheet

CHAPTER 3 APPARATUS

3.1 Electrode Assembly

The spectrometer electrode assembly is designed as a self - contained unit which can be lowered into position on the chamfered surface inside the vacuum tank. The connections to the electron gun elements and cathode heater are then taken to a multi-pin feedthrough on the side flange of the vacuum tank while the analyser connections are made to various feedthroughs on the top flange.

The materials used in the early development stages were all non - magnetic and capable of withstanding bake-out at 400°C but experience showed that such extreme temperatures were not necessary and in later development, small amounts of P.T.F.E. were used for convenience of manufacture. Components were cleaned by ultrasonic agitation in aromatic - free, Analar petroleum spirit and in some cases this was followed by vacuum furnacing at 1000°C.

A typical cross-section through the electrode assembly is shown in fig. 3.1 which is twice full scale. Because of the small size of the various apertures used in the electron gun, it is important that the gun elements be accurately aligned with respect to the beam axis. It is also important to avoid any of the gun elements being inclined to the axis as this can lead to a tadpole-shaped image(51g). The alignment was carried out as follows. Plates A and B were assembled loosely with the quartz disc between them. Tube T3 was then fitted loosely to plate B. These three components could be aligned about the axis by means of an accurately turned jig which consisted of a rod with three diameters corresponding to the i.d. of tube T3, the diameter of the recess on the base of plate B and the diameter of the central hole in plate A and the appropriate screws could then be tightened up and the jig removed.

A cylinder with large cut-outs in the side for manipulation of analyser components and to permit gas entry and pumping is used to connect plates B and C. Tube T4 may then be loosely assembled to plate C and once the latter is in position, a long accurate dowel may be passed down T4 into T3 to ensure alignment on the axis and the screws again tightened before removing the dowel. Small marks may then be engraved to facilitate subsequent assembly.

Most of the gun elements are mounted on 2" o.d. discs and these may be referenced to plate A by a cylindrical jig which fits over the disc stack and over a spigot on the base of plate A. The discs are separated from one another by quartz spacers slipped over Pyrex sheathed 8 B.A. studding which passes through clearance holes in the discs and secures the stack to plate A. Four studs were used and the spacers are selected to within 0.01 mm in sets of four. The positions of the apertures in T1 and the anode were both measured relative to their respective discs using a travelling microscope thus enabling small off - centre errors to be minimised by appropriate orientation of the discs with respect to each other.

Constructional materials and dimensions of the components may generally be obtained from fig. 3.1, however components which play a role in the functioning of the spectrometer will be dealt with in detail.

The cathode is a Phillips Metalonics BP1A dispenser cathode of nominal diameter 3 mm and operating temperature 1150°C. It is heated by a non-inductively wound ceramic-coated filament and mounted in a stainless steel block to maintain temperature stability. The block is then secured in the Pierce electrode by three stainless steel grub screws.

The anode is an Immaculate 5 disc, .025" thick and 2" o.d. with a spark eroded, knife-edged aperture of .46 mm diameter at its centre. Immaculate 5 stainless steel is used throughout the assembly because of the extreme insensitivity of its non-magnetic properties to mechanical treatment, and "stainless steel" should in this section be taken to mean this particular grade. Some small screws of 18/8 grade stainless steel are used in positions remote from the electron beam but these were first demagnetised by heating to 900°C [Curie point of iron 760°C] in a mu-metal can in a vacuum furnace.

The deflectors are for beam alignment between the anode and the angle defining aperture in T1 and consist of a tube of 4 mm bore spot-welded to one of the standard 2" o.d. discs which is then cut into four segments with a gap between each of 1 mm. Opposite pairs of these segments are then biased positively and negatively to provide the required deflection. Four holes of about 3 mm dia. are drilled in the disc on a P.C.D. of 16 mm to enable gas entering the gun chamber from

the collision chamber to be more readily pumped away. The overall length of the deflector section is 3.5 mm.

T1 is the first lens element of the variable - ratio lens and it consists of a demountable tube which carries a replaceable aperture, and which is spot-welded to a 2" o.d. stainless steel disc. The overall length is 14 mm and the only angle limiting aperture to be used was one of .60 mm dia.. Holes similar to those in the deflectors were drilled to increase the pumping speed in this region. T1 is insulated from plate B and T2 by a machineable ceramic spacer[Ceramtec] which has several slots cut in it to enable the region between the T1 aperture and the apertures in T3 to be pumped more efficiently.

T2 is the second element of the lens and is constructed from .005" thick tantalum sheet. It is a tube of length 18 mm and bore 2.65 mm spot welded to a disc of .010" tantalum sheet. The tube is made by rolling the tantalum around an aluminium rod turned to 2.65 mm dia., leaving a slight overlap which enables a spot-weld to be made when the tube is slid slightly off the rod at one end. A tweezer attachment on the spot welder enables welds to be made along the entire length of the tube. The disc is 10 mm o.d. and has a small lip on the edge of the central hole to facilitate spot-welding to the tube. This lip is formed by means of a punch and die, the dimensions of the pilot hole in the disc and the hole in the die being chosen to give a 0.5 mm lip. T2 is electrically insulated from T3 by Ceramtec insulators.

T3 serves both as the final element of the lens and as a support for the stack of interlocking quartz spacers which in turn support and insulate the analyser electrodes. It is threaded at the end nearest the scattering region and a copper nut is used to secure the spacer stack.

T4 acts as a support in the same way as T3 and serves the functions of shielding the beam collector from stray electrons and providing a field-free scattering region.

The cones fitted to T3 and T4 define the path length and are made from .005" tantalum sheet. They are initially developed from flat sheet to the approximate shape after which the final shape is determined by a punch and die to ensure symmetry about the axis and with respect to one another. These cones are mounted on plugs which are a tight fit in

the tubes. the plug in T3 also carries a 1.2 mm "spatter" aperture and a 0.9 mm aperture to restrict gas flow from the scattering region into the electron gun. The alignment of these apertures is checked with a travelling microscope before assembly.

The beam collector (BC) is contained within T4 and has a large length to diameter ratio (12:1) to ensure efficient collection of the unscattered electron beam. It consists of a tube of 3 mm i.d. made of .005" tantalum sheet spot-welded to a disc made of .010" Ta, the constructional techniques being the same as for T2, while the mounting disc is secured to plate C in the same way as the gun discs are secured to plate A. The tube is insulated from T4 by a piece of thin walled ($\simeq$.5 mm) quartz tubing.

G1 is the first grid encountered by a scattered electron and its purpose is to provide a field-free scattering region by being in electrical contact with T3. In the "pseudo-spherical" analyser it consists of two cones and a cylinder constructed of 100 mesh molybdenum gauze of 70% transparency composed of wires of .0016" dia.. Strengthening strips of .005" Ta sheet are used at the joins of adjacent sections. In the spherical analyser, G1 consists of two 12 mm radius hemispherical sections of the same gauze spot-welded onto two stainless steel support rings which are clamped together around the plugs in T3 and T4. The support rings are clamped 'longitudinally' so as not to introduce an assymmetry in the sensitivity with respect to scattering angle. When in position the width of the rings is 2 mm. The hemispherical grids are made by the following method. A former is made which consists of a hemisphere turned on the end of a copper rod with a slot cut along its length. The radius used is smaller than that of the support ring by the thickness of the gauze plus .002". The gauze is pressed over the former by hand and when the gauze has taken up the shape, the support ring is then pressed down over the gauze and the spot welder electrode introduced into the slot to make a tack weld. As molybdenum does not spot-weld well, a thin strip of tantalum is used inside the support ring to secure the molybdenum mesh to the stainless steel ring.

G2 is the grid used to prevent positive ions formed by electron impact from reaching the scattered collectors by the application of a small

positive potential which retards the ions. It is made of the 70% Mo gauze in the "pseudo-spherical" analyser and secured at the interlocking spacers by split support rings, the two halves of which are spot-welded together with the gauze in between. In the spherical analyser, a 85% transparency tungsten gauze of 100 mesh and .0008" dia. wires was used. The radius of the spherical grid is 17 mm.

G3 is the grid which provides the retarding field used for energy analysis of the scattered electrons. It is made of the 70% Mo gauze in both analysers. Construction is similar to that for G2 and G1 and the radius is 23 mm.

The grids used in the "pseudo-spherical" analyser were all cleaned by vacuum furnacing at 1000°C in a vacuum furnace pumped by a diffusion pump using Convalex-10 (polyphenyl ether) pump oil. This facility was not available when the spherical grids were being installed, so these were electropolished using a procedure described by Rosebury(62).

The scattered collectors (SC1, SC2, SC3) collect the electrons passed by the retarding grid and the resulting currents are amplified by the electrometers during an experiment. In the "pseudo-spherical" analyser, these electrodes are of the dimensions shown in fig. 3.1, are made from .005" Ta sheet, and SC1 and SC3 are supported on the interlocking spacers by the same means as the grids. SC2 is supported on four 4 mm dia. quartz rods which are each secured in a bush spot-welded to the collector and pass through slots in the shield to be secured in holes drilled in the main support cylinder which connects plates B and C. Also in this analyser, a shield made of .010" Ta sheet is installed to guard against stray electrons striking the SC's and producing erroneous signals. The radii of SC2 and the shield are 30 mm and 38 mm respectively.

In the later, spherical analyser no shield is used as tests showed this unnecessary but the SC's of fig. 3.1 are removed and the electrodes forming the shield are now used as SC1, SC2, and SC3. In addition, these electrodes are covered with "black gold" produced by evaporation of gold wire at a pressure of about 1 torr nitrogen. These modifications were carried out to improve collection efficiency and to minimise field penetration from the SC's through the mesh of the retarding grid.

3.2 Vacuum System

An organic-free, ultra-high vacuum system using mercury diffusion pumps and sorption pumps is employed to provide stable operation of the spectrometer. The vacuum tank is divided into two cylindrical chambers which are separately pumped and interconnected by a 0.9 mm dia. aperture through which the electron beam produced in the lower chamber enters the upper chamber which houses those electrodes necessary for energy analysis of the scattered electrons. Differential pumping of these chambers minimises cathode poisoning by the sample gas and provides stable emission. A best base pressure of 1.9×10^{-9} torr was achieved but pressures below 10^{-8} torr are normally obtainable after a mild overnight bake(100°C-150°C). A schematic diagram of the vacuum system is shown in fig. 3.2 .

Vacuum Tank

The vacuum tank is basically that inherited from Edinburgh University which was used by Ferguson and Read(32). The internal diameter is 4" and the wall thickness 1/4". A 45° chamfer is provided, upon which the electrode assembly may rest. For the present work, new top and side flanges were designed for the tank. These were made by Vacuum Generators Ltd. from EN58B stainless steel and each was fitted with two elbows in 3/4" nominal bore tube, terminated in 2.25" o.d. flat flanges to allow for the fitting of ionisation gauges and a capacitance manometer. The top flange contained four Leybold KM 12 very high insulation feedthroughs arranged to allow for direct mounting of the electrometer head amplifiers, and one Vacuum Generators EFT 5 eight-way feedthrough, while the side flange was fitted with two EFT 5 feedthroughs. To allow for unforeseen developments, more feedthroughs than strictly necessary were fitted.

Vacuum Pumps

Each chamber is pumped by an Edwards UHVM2 unitary construction trap/diffusion pump unit. The UHVM2 is a three-stage mercury diffusion pump with a throat diameter of 3" and a peak pumping speed at the inlet of 70 l/sec. for air. The trapping system consists of a lower chevron baffle, cooled by a water-cooled thermoelectric element, and an upper Z baffle in contact with an annular liquid nitrogen reservoir, kept filled by an automatic system.

The UHVM2 units are both backed by the same Edwards 2M4A four-stage 2" mercury diffusion pump, which has an unbaffled pumping speed of 70

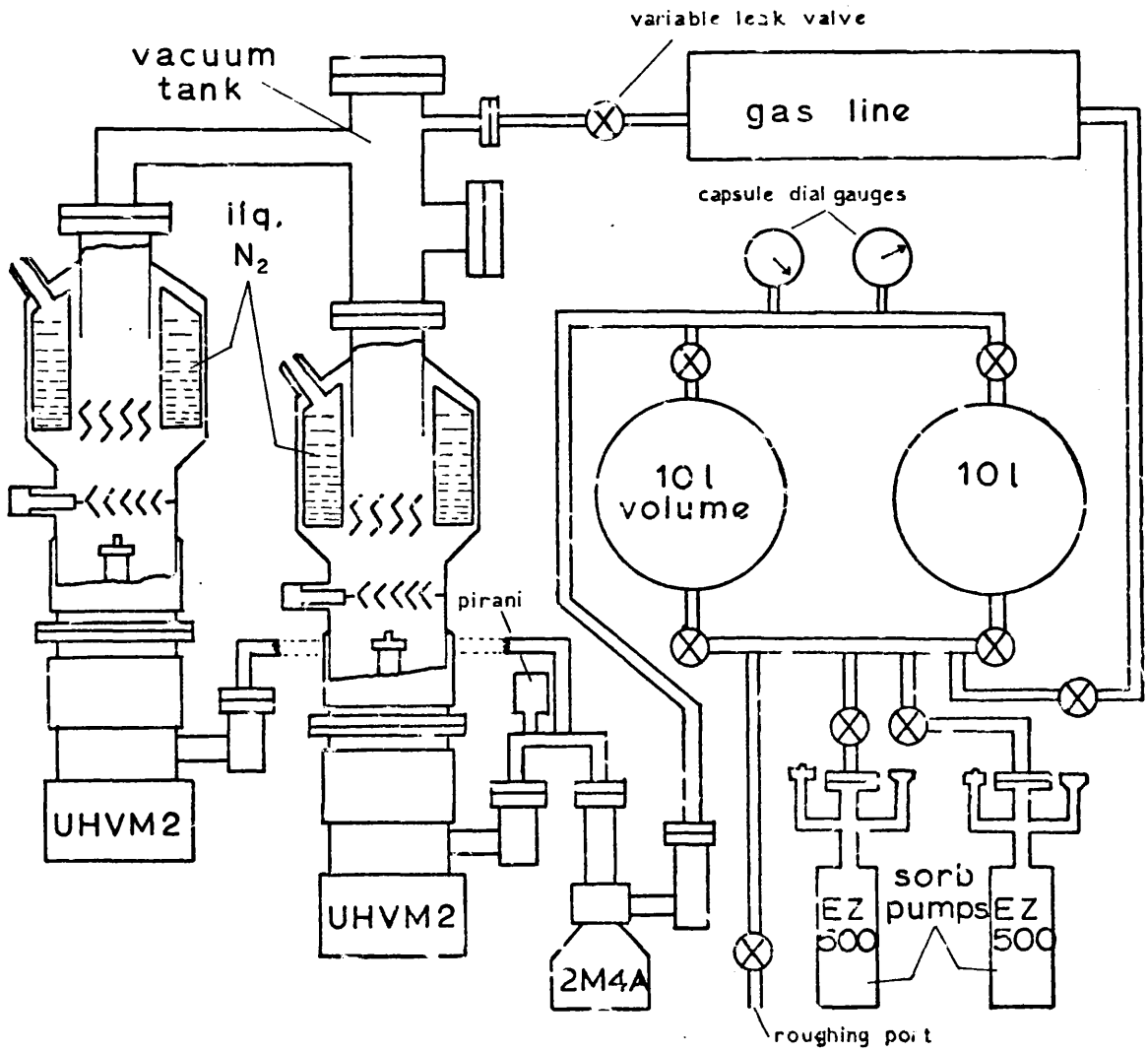

Fig. 3.2 The Vacuum System

l/sec and a critical backing pressure of 30 torr. The 2M4A can pump into either of two 10 litre volumes and consequently 300 litre-torr of gas can be pumped into one volume before it begins to stall. At this point, the first backing volume can be valved off and roughed while the 2M4A is valved into the second volume. If we allow for the conductance of the tube connecting the collision chamber to the UHVM2, then the pumping speed is reduced to about 30 l/sec.,so for a typical gas pressure of 5×10^{-4} torr during an experiment, we would have a throughput of 150×10^{-4} torr.l/sec.. Hence the time required for the pressure in a 10 l. volume to reach the 2M4A critical backing pressure of 30 torr is

$$(30 \times 10)/150 \quad \times 10^{4} \text{ seconds.}$$

Consequently the pumping system may be left unattended during an experiment for about five hours at which point the simple operation of switching volumes is all that is required to extend this period for a further five hours.

A pair of Edwards EZ 500 sorption pumps using 5A molecular sieve are normally used for roughing out the volumes and for roughing out the whole system during an initial pump down from atmosphere. Either of these pumps may be connected to either of the 10 l. volumes. During initial pump down the system is first roughed using an Edwards RCB2 oil-free carbon vane pump. This has a pumping speed of 1 l/sec and will pump the system down to 125 torr. This removes much of the water vapour in the system and thus prolongs the life of the molecular sieve.

The pumps desribed up to now provide a clean organic-free system. However, for certain gases such as He, Ne and H_2, sorption pumps are ineffective. For these gases, an NGN PSR2 rotary pump fitted with an activated alumina foreline is available to rough out the isolated backing volumes. As the rotary pump is never connected directly to the UHV system and as such a trap is claimed to remove 99% of backstreaming oil vapour, it is very unlikely that any contamination of the UHV chamber by volatile fractions of the pump oil will occur.

Gaskets and Connections

Most of the vacuum seals in the UHV part of the system are made by means of gold wire gaskets on flat flanges. The exceptions to this are the aluminium gaskets used in the Cajon UHV couplings fitted to the capacitance manometer and the 95% Al - 5% Si alloy gaskets used to

combat mercury attack in the lower parts of the UHVM2 pumps. The gold gaskets are made by annealing the appropriate length of .020" dia., 99.9% pure gold wire, forming it into shape and butt welding the ends together using a small gas-oxygen torch. The gaskets are re-annealed prior to use by heating to 400°C for half an hour in an oven.

On vertical flanges, .017" dia. indium wire has been used to secure the gasket in position while the mating flange is offered up but, on occasions, after bakeout, leaks have occured at the points of contact between the gold and indium and signs of alloying have been apparent. consequently, well-annealed .005" dia gold wire is now preferred for this purpose.

The 2M4A diffusion pump inlet flange is fitted with a Viton O-ring as are all couplings in front of it, while all unions and diaphragm valves further back are fitted with the appropriate neoprene components.

Vacuum plumbing in the UHV region is in stainless steel and argon arc or plasma - arc welding is used. In the backing line, plumbing is mainly in copper "Yorkshire" tubing and fittings (with solder removed) and these are brazed with Easy-Flo No.2. A few Edwards pipeline coupling components are also used in the backing line. All components are cleaned before assembly and no vacuum greases are used.

Bakeout

Because of the possibility of stray fields due to insulating films on surfaces and effects due to the presence of impurities which can both contribute to the scattering and affect collection efficiency, it is necessary to thoroughly outgas the apparatus by baking.

In the early stages of the experiment, the whole UHV system of tank, traps and upper halves of the UHVM2 pumps was baked for 48 hrs. at 400°C. A thorough bakeout of this nature was used to clean up the tank before fitting the electrode assembly. The best vacuum reached in this preparation stage was 5×10^{-9} torr. During the gun development stage bakeout was usually at temperatures between 250° and 350°C with bakeout most often restricted to the tank only.

After fitting the analyser, bakeout is limited to 250°C because some P.T.F.E. components were used. The spectrometer potential supply and cathode heater supply are left switched on and connected via. P.T.F.E.

insulated screened leads during bakeout below 200°C. A routine overnight bake of the tank to 100° - 150°C is now possible by simply throwing a switch due to two copper-clad heating elements which are clamped to the outside of the tank, surrounded by "Viceroy" multi layer insulation which is then surrounded by the magnetic shielding. As they lie inside the magnetic shielding, the heating elements had to free from magnetism. This was checked using a Hall-effect gaussmeter and no field could be detected at the surface of the elements with the instrument on 100 m.gauss full scale.

Vacuum Gauges

The pressure in each of the UHV chambers is measured by means of Edwards IG3G ionisation gauge heads. The pressure between the UHVM2 pumps and the 2M4A pump is measured with an Edwards M6A pirani gauge. These gauge heads are connected to Vacuum Generators IGP2 combined ionisation and pirani control units. Pressure between the 2M4A and the backing volumes is measured by two Edwards capsule dial gauges, one 0 - 760 torr and one 0 - 40 torr. It was hoped to be able to use a MKS Baratron series 90 capacitance manometer for pressure measurement in the collision chamber. However, the zero drift of 2×10^{-5} torr in 20 minutes of the instrument made its use impracticable for continuous monitoring of gas pressures of around 10^{-4} torr.

Differential Pumping

The limiting aperture for the purposes of differential pumping between the two chambers is the 0.9 mm dia. one at the collision chamber end of tube T3. Although the angle stop in tube T1 is only 0.6 mm dia., the region between T1 and T2 has pumping channels which allow the bulk of the gas to be pumped away before reaching this aperture.

For a typical gas pressure of 10^{-4} torr, the corresponding pressure in the gun chamber is only 10^{-7} torr, i.e. only one thousandth of the gas pressure. This compares favourably with previous versions of this type of spectrometer(29,32,35) where the pressure in the gun chamber was about one fiftieth of the gas pressure.

Control Circuits

Two control circuits are employed in connection with the vacuum

system : an automatic filling system for the diffusion pump traps; and an interlock or fail-safe circuit to protect the vacuum system against failure of certain essential supplies. These were designed by Mr.A.H. Young.

The automatic filling system consists of two solenoid valves, one for each trap, connected to compressed air line and two circuits for liquid level detection and control of filling duration. A germanium diode(OC 81) used as a level sensor is immersed at a suitable depth in the trap and when the liquid nitrogen level falls below the level of the diode, it warms up, the voltage developed across it falls below a pre-set limit and a relay circuit switches on the solenoid valve, thus pressurising the liquid nitrogen container and driving liquid along a lagged transfer tube to the trap. As the level rises and the diode is again cooled, the voltage developed across it increases and is used to start an electronic timer which allows the liquid to flow for a predetermined time before the solenoid valve is again closed thus cutting off the air supply.

The interlock protects the system against failure of vacuum, mains electricity, cooling water and liquid nitrogen. An Edwards M6A pirani head in front of the 2M4A diffusion pump is used for pressure sensing, an Edwards Flotrol flow meter , used to measure water flow, has a preset switch which can be set to the minimum safe flow rate for the pumps, and lack of liquid nitrogen is detected by two OC 81 diodes positioned $\frac{1}{2}$" from the bottom of the traps.

Pressure failure can be overriden to allow operation of the 2M4A between pressures of 30 torr and 0.1 torr. Liquid nitrogen and water failure can be overriden for bakeout of the traps and upper halves of the UHVM2 pumps.

Gas Inlet Line

The sample gas inlet line is mainly constructed of glass, although metal valves with neoprene diaphragms are used. It consists of a 3 litre storage flask, a mercury manometer and a cold trap for freezing out any condensible impurities in the sample gas. Gas is bled into the collision chamber via. a Granville Phillips servo-controlled needle valve fitted with .25" bore stainless steel tubulation. The line is fitted with ionisation and pirani gauges and is pumped by a trapped

mercury diffusion pump, which may be backed by any of the main vacuum system roughing pumps. The line is pumped to below 10^{-4} torr before valving off the pumps and admitting sample gas to a pressure of around 1 atmosphere.

3.3 Magnetic Field Cancellation

In low energy electron scattering experiments the presence of a magnetic field causes both the incident and scattered electrons to deviate from straight line paths.

For the incident electrons, too high a residual field can place severe restrictions on the distances over which a low energy beam may be transmitted. Curvature in the paths of the scattered electrons can upset angular distribution measurements and , in the case of retarding field analysers, can also reduce the energy resolution. It is therefore necessary to consider methods of reducing the magnetic field in the experimental region to acceptable proportions, i.e. a few milligauss.

Helmholtz Coils

A commonly used method of magnetic field cancellation is to use a pair of current carrying coils, symmetric about the central plane of the system and normal to the axis. Parry(63) has described the theory of these coils.

For circular coils of radius a cm, carrying I amps through n turns of wire, the field on the (z) axis is

$$H_z = 2\pi n I a^2 /[10(a^2 + z^2)^{3/2}] \qquad (3.0)$$

and the Helmholtz condition,

$$\partial^2 H_z / \partial z^2 = 0$$

is satisfied when $z = a/2$. Hence the correct separation for the pair of coils is the coil radius, a . A similar relation may be derived for square coils and expressions are also available which permit calculation of the field component parallel to the axis, H_z, and the radial component, H_r, at points off-axis and near the centre.

One pair of coils is sufficient to cancel the Earth's field if it can be adjusted in azimuth, inclination and field strength. However normal practice is to use one pair to cancel the vertical component and two pairs to cancel the horizontal component of the Earth's field.

Magnetic Shielding

A magnetic shield is an enclosure of high permeability material which provides a very low reluctance path for the magnetic flux, thus preventing its entry into the experimental region(64). The higher the permeability of the material, the better the attenuation of the field. The permeability increases with the field strength up to a limit at which saturation occurs and little additional shielding is obtained with increasing field strength. If the field to be minimised has a field strength which would saturate a high permeability material, then double shielding must be used. An outer shield of moderate permeability material reduces the field to a value below the point at which the inner shield would saturate. The outer shield should be made of the highest permeability material which will not saturate in the field involved.

For the case of a uniform d.c. field perpendicular to the axis of an infinitely long cylindrical shield, the attenuation, g, is given by

$$g = H_{(out)}/H_{(in)} = \mu t/2d \qquad (3.1)$$

where t is the material thickness, μ is its permeability and d is the o.d. of the cylinder. In practice this relation holds for cylinders with a length to diameter ratio of 4 or greater. For ratios less than this, maximum shielding is obtained at the centre and the shielding efficiency falls off towards the ends of the cylinder.

For an axial field, the attenuation for a cylindrical shield may be only 65% of that for a perpendicular field. Maximum shielding again occurs at the centre but just outside the ends of the cylinder, the axial field is stronger than the field it is desired to cancel. This is known as the "overshoot effect" and if the interfering field has a sizeable axial component, it is advisable to cap the ends of the cylinder.

A.c. fields are attenuated by reflection of the wave at the surface of the shield, by absorption loss and by eddy currents. In general, any given shield will provide better attenuation for a,c. fields than for d.c. fields.

Chosen Design

Magnetic shield ing appeared preferable for several reasons: it is not so bulky as a system of 3 Helmholtz coils; it operates by attenuation, hence provided the attenuation factor is large enough, it is insensitive

to changes in the ambient field unlike coil systems which often require servo - control(65) and stabilised power supplies; and it provides efficient attenuation of a.c. fields.

A double cylindrical shielding system consisting of an outer shield of Radiometal 50 (50% Ni) of wall thickness .069" and 8" o.d. and an inner shield of mu-metal of .032" wall thickness and 7" o.d. was constructed with an end cap on the top end of the outer shield. Cut-outs were provided to clear the input recepacles of the electrometer head amplifiers, while the diffusion pump attached to the gun chamber prevented the fitting of an end cap at the lower end of the shield.

As the vertical component of the Earth's field is .45 gauss and as this is directed along the axis of the shielding, a significant residual component was quite probable. To overcome this, one pair of Helmholtz coils was constructed. Circular formers of 38 cm radius were made by bending 8' lengths of brass channel by hand and each coil had 10 turns of twin flex wired to give effectively 20 turns. As magnetic shielding is still moderately efficient at attenuating axial fields, we would expect no necessity for accurate positioning of the coils or for high current stability.

Tests using a Hall-effect gaussmeter (zeroed before each measurement) with the shielding in position and the vacuum tank open gave readings of 3 m.gauss or less for the horizontal component over the whole experimental region, this being independent of the coil current and position. Corresponding values for the vertical component were around 10 - 12 m.gauss with the coils switched off and less than 2 m.gauss with the current between .95 and 1.05 amps. The coils could be moved up to 6" off centre and up to 3" out from the Helmholtz spacing and no variation was observed in the gaussmeter readings.

3.4 Measuring Instruments and Power Supplies

A block diagram [fig. 3.3] shows the interconnection of the electronic equipment used in the spectrometer.

The emmision current, i.e. that to the anode is measured with an Anders multi-range microammeter type SM 301. This will measure from 50 microamps full scale to 1 mA full scale.

The electron beam current into BC is measured with an E.I.L. Vibron 33B2 vibrating reed electrometer which can measure currents from 1 pico-

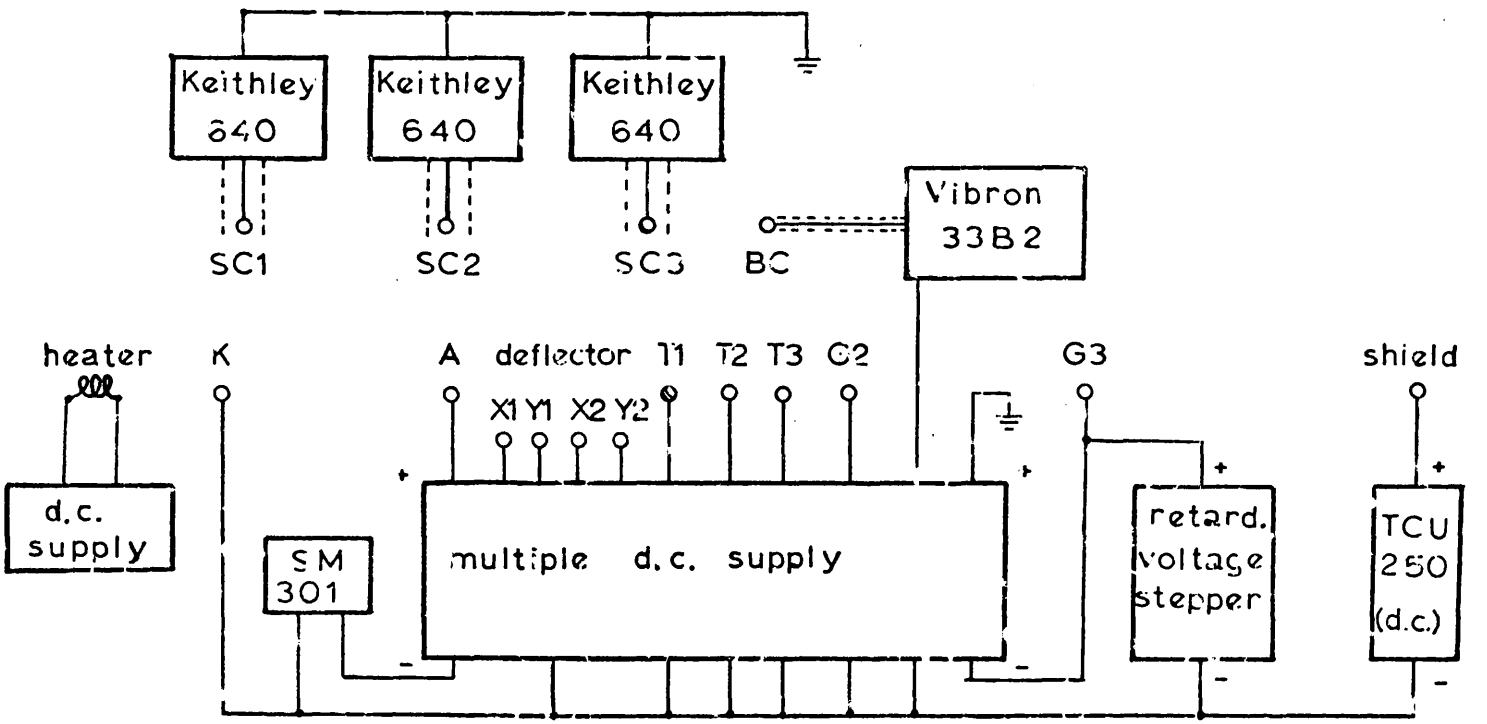

Fig. 3.3 The Circuit Diagram

amp to 1 micro-amp full scale. This instrument was also found useful for monitoring currents to various electrodes during development of the electron gun.

Scattered electron currents to the three collectors may be monitored simultaneously by means of three Keithley 640 vibrating capacitor electrometers, the input connectors of the head amplifiers being mounted directly onto the appropriate feedthroughs on the top flange. These instruments have a maximum sensitivity of 3×10^{-17} amps full scale but this may only be achieved if leakage currents are negligible and the inputs are meticulously shielded. For the present application, the performance is more than adequate however except for the lack of a backing - off control. To provide a backing -off facility the instruments were modified by fitting a simple mercury cell and helipot circuit in series with the zero controls through a changeover switch which provided for normal operation.

Voltage measurements are made with a Solartron LM 1426 digital voltmeter which is fitted to a Solartron Mk II Compact Logger. This voltmeter has a fully floating input, is calibrated against internal standard cells and has a normal display of 4 digits with overranging up to 11000. The maximum sensitivity is 25 mV full scale.

Data recording may be made on any conveniently available X-Y recorder or on punched paper tape using the data logger. In its present form the logger can scan up to 20 channels of information at a rate of up to 2 channels per second, the paper tape output being provided by a Data Dynamics DD 110 punch in a format which can be set up on a patchboard.

Pressure is measured using Vacuum Generators IGP2 ion gauge control units and during a run the output is continuously monitored on a Servoscribe strip chart recorder.

Magnetic fields are measured with a Bell model 620 Hall-effect gaussmeter fitted with a temperature compensated probe. The most sensitive scale is 100 m.gauss full scale and on this scale the zero drift is about 1 m.gauss per minute.

The cathode heater is powered by a current stabilised d.c. supply. It provides an output of 0 - 15 volts, 0 - 1.5 amps.

The potentials on the anode, deflectors, T1, T2, T3, G2, and BC are provided by a multiple d.c. power supply which also provides the holding

voltage between G3 and the scattered collectors, the latter being earthed through the input resistors of the electrometers. This power supply was specially designed and the stability is of the order of 0.01% or better over a six hour period. Jacks are provided which enable voltages to be checked without disconnecting leads. The ranges available are as follows.

anode - - - - - 0-200 volts
deflectors - - - mean potential 0 - 50 volts
bias on each pair ± 0 - 5 volts
T1 - - - - - - - - 0 - 50 volts
T2 - - - - - - - - 0 - 200 volts
T3 - - - - - - - - 0 - 100 volts
G2 - - - - - - - - 0 - 100 volts
holding voltage - - - - - 0 - 50 volts

The potential to the shield is provided by an A.P.T. stabilised d.c. power supply, type TCU 250. The output available is 0 - 50 volts, 0 - 2 amps.

The Helmholtz coils are powered by a TCU 250 supply also.

The potential to G3 may be scanned either continuously by a combination of a TCU 250 power supply and a motor-driven helipot or stepwise in 100 mV steps over a preset range by the retarding voltage stepper shown in fig 3.3. For data logging the stepwise mode is used and the logger is used to control the stepper . The stepper has its own built-in stabilised d.c. supply and operates by means of uniselector circuits and two chains of precision resistors(1%). A scan may be selected over a range of from 1 to 9 volts and the starting position may be from 0 to 20 volts. A counter displays the number of scans completed, from 0 to 100.

The cathode heater supply, the multiple d.c. supply and the potential stepper were designed and built by A.H. Young and W. Stirling of Stirling University Electronics Workshop.

CHAPTER 4 OPERATION AND CHARACTERISTICS

4.1 Cathode Activation

Before the spectrometer can be put into operation, it is necessary to activate the cathode. After a few hours pumping, the pressure is generally below 10^{-6}torr and the oven can be switched on to bake the vacuum tank to 100°-150°C overnight. Next day, the oven is switched off and current can be supplied to the cathode heater. The current is increased slowly over a period of several hours so that the pressure does not rise above 10^{-6}torr until the filament current is at about 1.1 amp. After about another hour, outgassing of the cathode is complete and activation may be begun. This consists of applying a large positive potential to the anode and 300 - 500 volts is generally found to be sufficient. Over a period of up to 14 hours the emmision current to the anode increases to several hundred micro-amps at which point the anode voltage is reduced to about 100 volts and the filament current is reduced to 1.0 amp. The cathode is then 'aged' for 24 hours. For operation, the filament current is reduced to the lowest value which will allow a sufficiently intense beam to be obtained. Typical filament and emmision currents are 0.8 - 0.9 amps and 2 - 25 micro-amps respectively for beam currents in the range 10^{-8}- 10^{-7} amps.

4.2 Optimisation of Electron Gun Potentials

Once the cathode has been activated, the potentials on the electrodes of the gun may be set to obtain a beam of the desired energy, focussed at the centre of the scattering region. A useful criterion for determining when the potentials are optimised is that the ratio of background scattered current to beam collector current should be a minimum. Figs. 4.1, 4.2 and 4.3 show background current ratios as functions of anode voltage, lens voltage ratio and beam collector holding voltage. The subscripts refer to the scattered collectors as numbered in fig.3.1. Optimum anode voltages were found to be in the range 100-150 volts in good agreement with the calculation of chapter 2. Minima in the background current ratios were also found for voltage ratios, V_2/V_3 , in the region of 2 : 1 as predicted. The value of V_1 was not found to be critical and is normally set at 25 volts as is the mean potential of the quadrupole deflector. The background current ratios for the pseudo-spherical

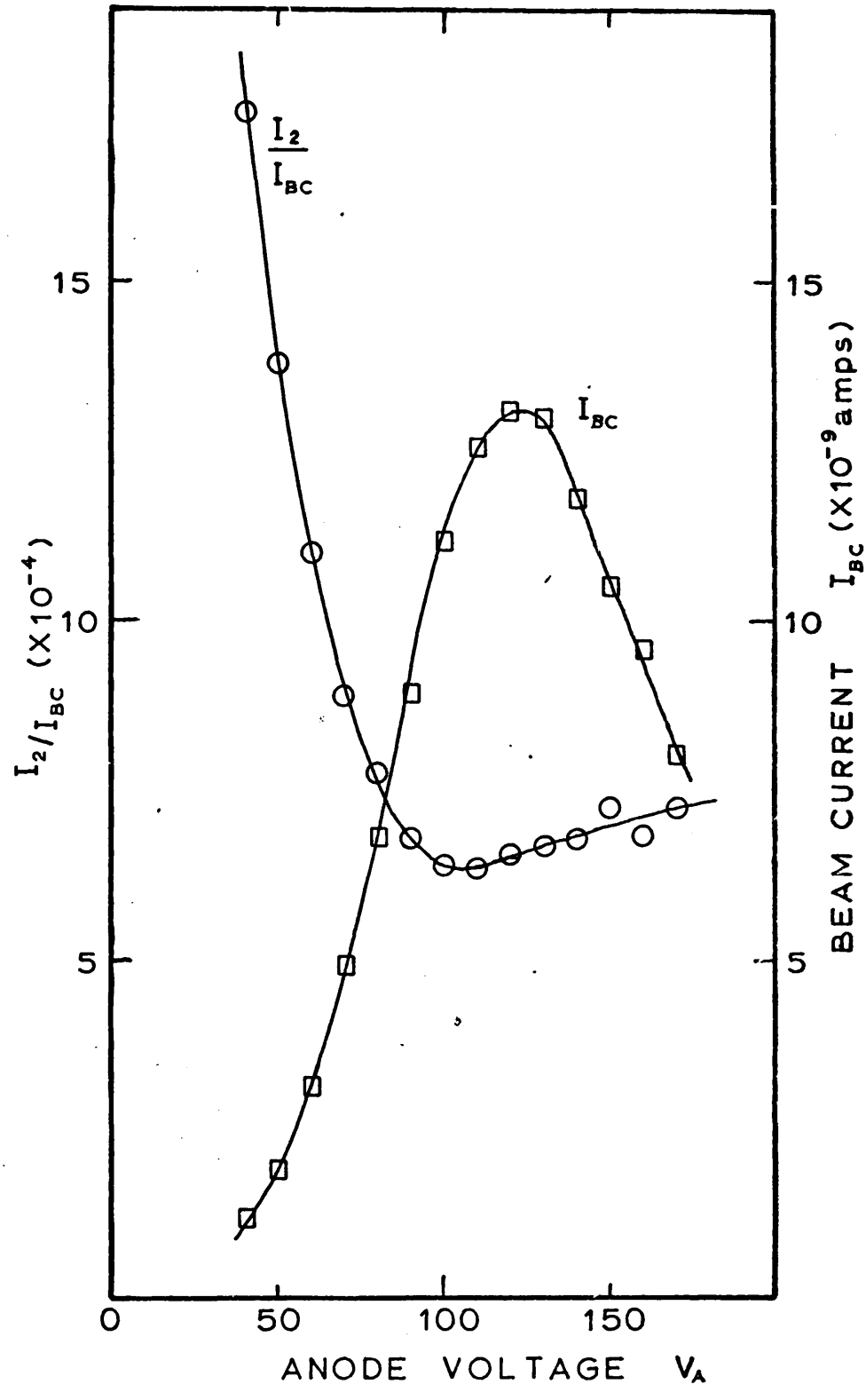

Fig. 4.1 Background current ratio and beam current as functions of anode voltage for the spherical analyser. Electron energy, 13 eV. Pressure = 1.5 x 10^{-8} torr, $V_{G3} = V_{T3}$ = 15 volts, V_{T2} = 31.5 volts

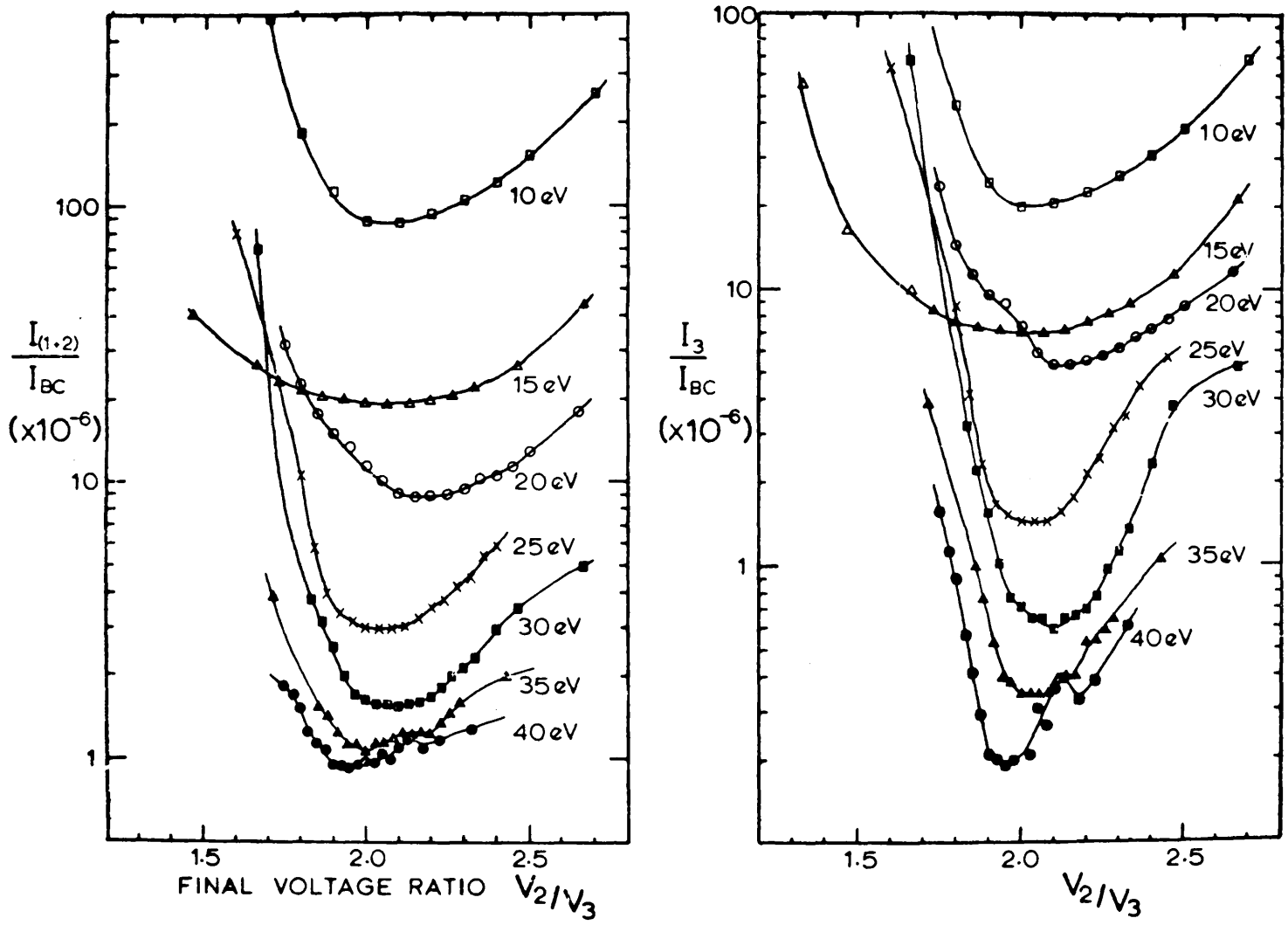

Fig. 4.2 Background current ratios as a function of the final voltage ratio of the three - tube lens, V_2/V_3, for the pseudo-spherical analyser. Subtract 2.25 $\pm$ .25 eV to calibrate electron energies shown. Beam currents $\propto 10^{-8}$ amps, pressure = 10^{-8} torr, V_{G3} = 10 volts, $V_{G2} = V_{T3} + 3$ volts.

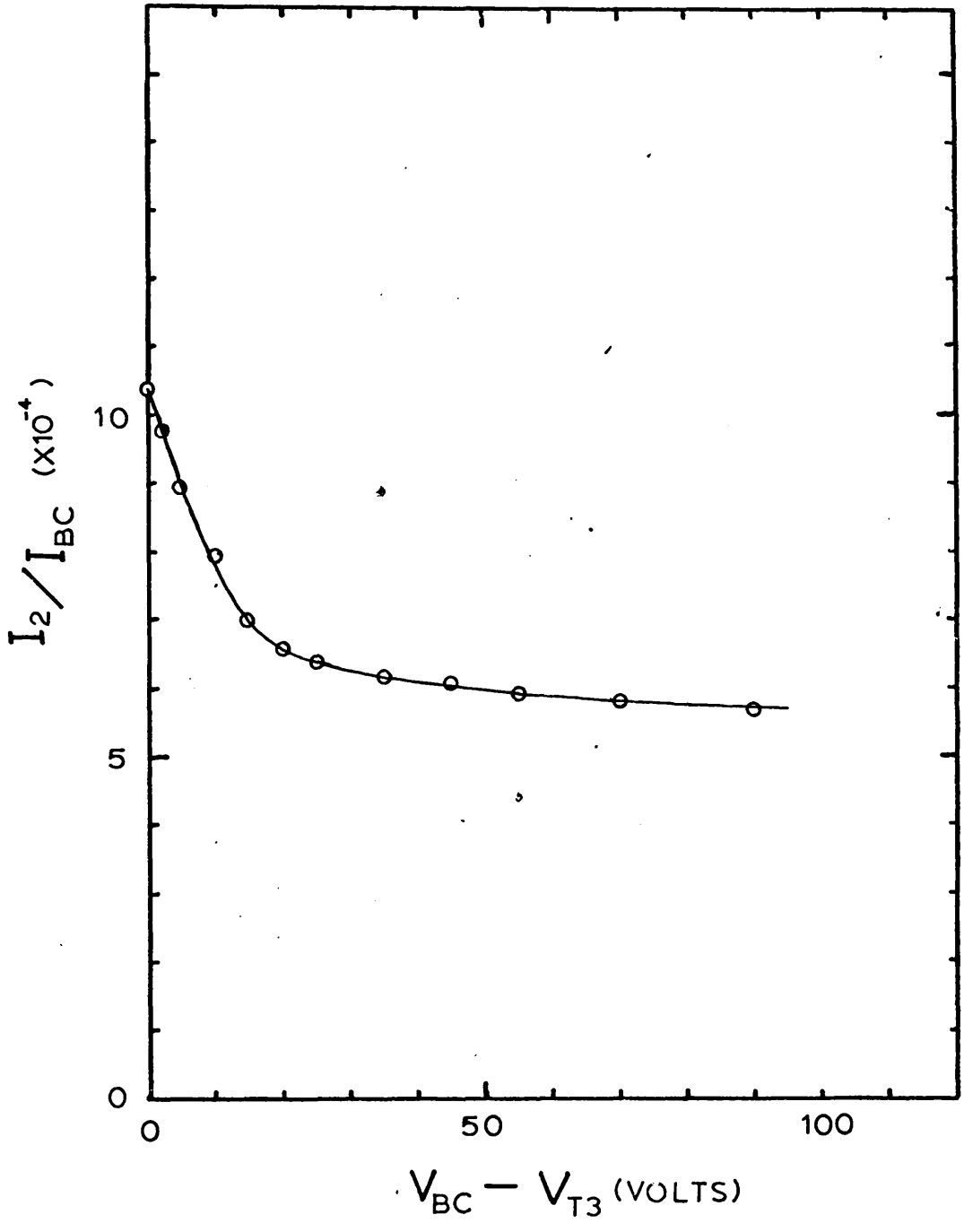

Fig. 4.3 Background current ratio as a function of beam collector holding voltage for the spherical analyser. Electron energy 13 eV. V_A = 110 volts, $V_{G3} = V_{T3}$ = 15 volts, V_{T2} = 31.5 volts.

analyser [see fig. 4.2] are significantly lower than those for previous R.F.E.A. electron impact spectrometers which were of similar analyser transmission(32). Beam collector holding voltages of 30 - 40 volts are normally applied to ensure efficient collection.

4.3 Energy Analysis of Electron Beam

During testing of the electron gun the analyser was not fitted and the tube T4 [see fig. 3.1] was insulated from plate C by a 0.4 mm thick mica disc. A temporary scattered collector was fitted to permit optimisation of the gun electrode potentials. Once a suitable beam was obtained the potential on T4 could be varied and the current to the beam collector measured as a function of this potential using an X - Y recorder. Differentiation of this curve then provides an estimate of the energy spread of the electron beam as shown in fig. 4.4. When these measurements were made, the cathode in use did not activate particularly well and it was necessary to use a filament current of around 1.1 amps to obtain adequate beam current. The energy spreads obtained may therefore be taken as upper limits. It should be noted that during energy analysis by retardation at T4, the beam no longer passes through a field-free region on its way to BC and this may introduce an additional error into the measurements.

4.4 Current to T4

While T4 was insulated from plate C, the currents to T4 and BC were measured for different beam energies. This provided a check on the alignment and angular divergence of the electron beam. Potentials to the electrodes were supplied from 90 volt radio batteries and the current to any of the electrodes could be measured using a switching circuit and a Vibron 33B2 electrometer. The current to T4 relative to that on the beam collector is shown in fig. 4.5 over the range of beam energies employed in the spectrometer. The current to T4 is always less than 10% of the beam collector current over this energy range.

4.5 Adjustment of Analyser Potentials

The first grid,G1, is in electrical contact with T3 and T4 and thus provides a field-free scattering region.

When operating at beam energies greater than the ionisation potential of the sample gas, G2 is set 3 volts positive with respect to G1 to

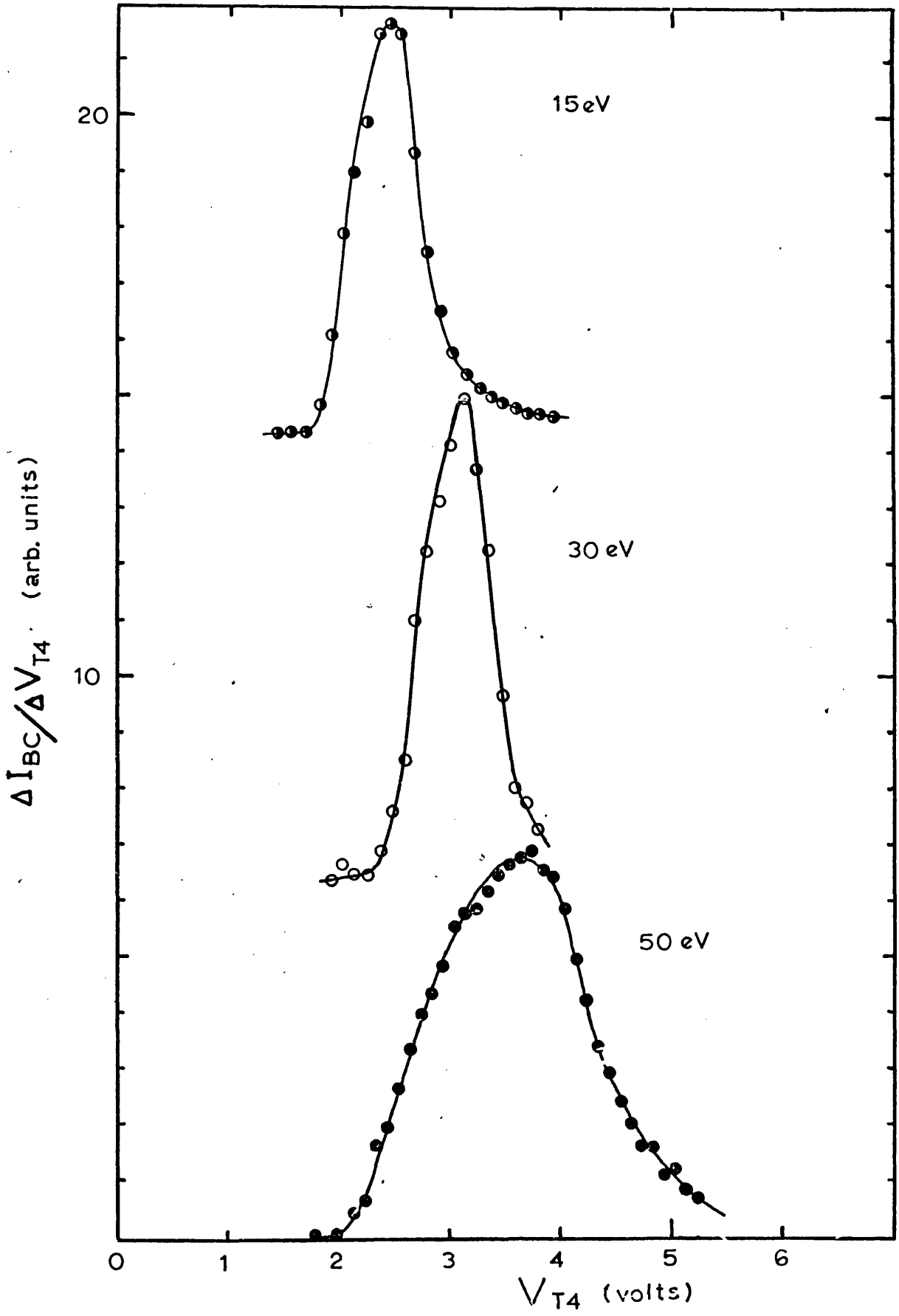

Fig. 4.4 Estimate of electron beam energy spread by retardation at T4. cathode heater current 1.1 amps , pressure = 1 x 10^{-8} torr.

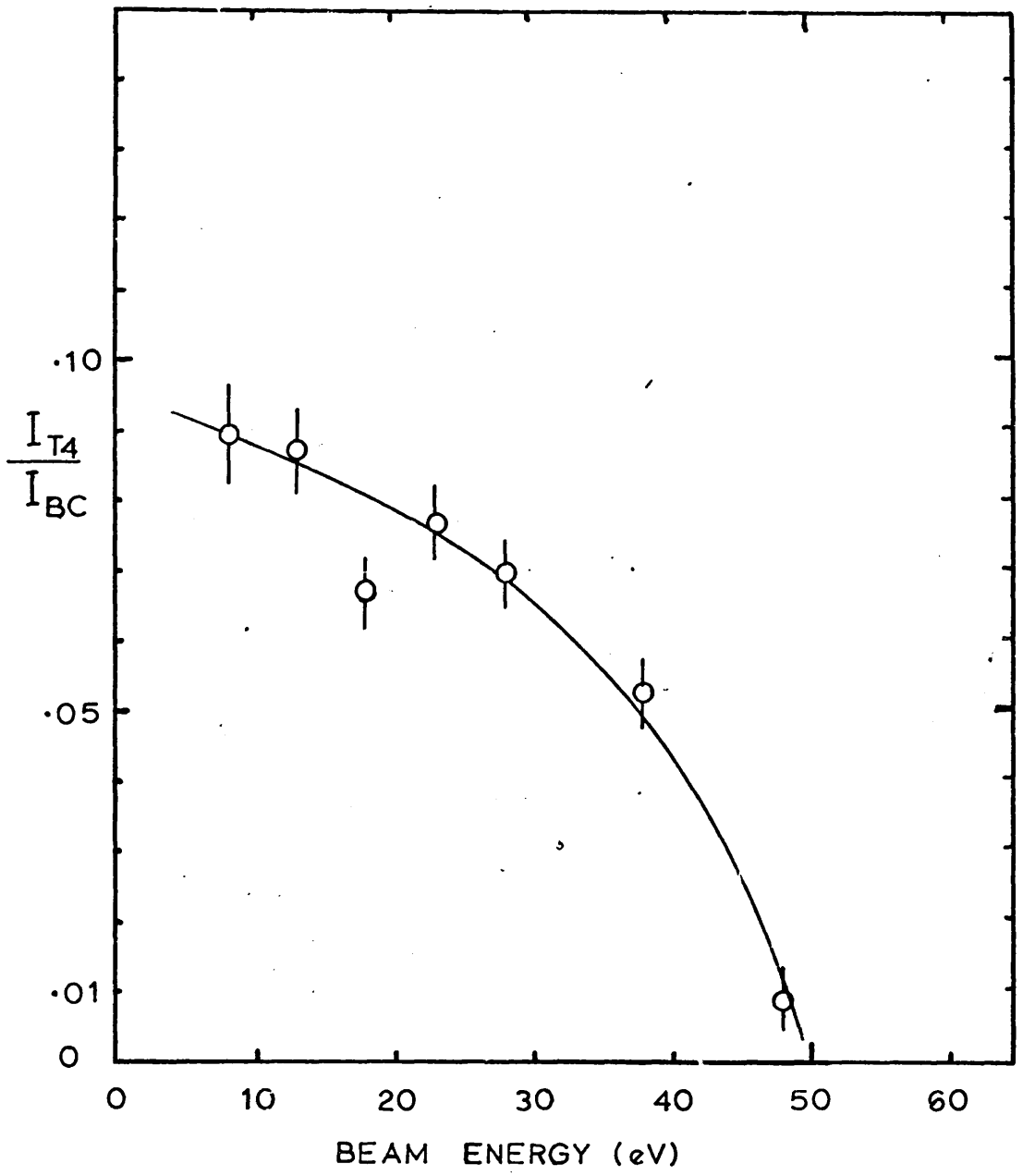

Fig. 4.5 Currents to T4 relative to beam collector current for various electron beam energies. Pressure $\simeq 10^{-8}$ torr.
$V_{T4} = V_{T3} + 2$ volts, $V_{BC} = V_{T3} + 20$ volts.

prevent positive ions from reaching the scattered collectors, while at beam energies below the ionisation potential, G2 is set to the same potential as G1.

The holding voltage between G3 and the scattered collectors is set to the minimum value consistent with efficient collection of electrons to minimise field penetration through G3. For the clean tantalum surfaces used in the pseudo-spherical analyser, values of 15 - 20 volts were necessary while for the "black gold" treated collectors in the spherical analyser, values of 2.5 - 5.0 volts were adequate.

4.6 Pressure Regulation

Pressure regulation was attempted using a Granville-Phillips servo-controlled leak valve with an ion gauge as the pressure transducer. This arrangement controlled the average pressure well but fluctuations occurred each time an adjustment for drift was made by the controller. A more suitable method was to use the leak valve manually to set the approximate pressure and then leave the system to reach equilibrium. After about 5 hours the pressure would generally be very steady as shown by continuous monitoring on a strip chart recorder. The ethylene pressure was found to fluctuate in a characteristic manner each time the automatic liquid nitrogen filling system operated. The traps were therefore topped up manually about half an hour before commencing measurements on ethylene and this resulted in a very steady pressure recording for at least an hour of continuous running time.

4.7 Data Collection

With an electron beam current of 5×10^{-8} to 10^{-7} amps and a sample gas pressure between 10^{-4} and 10^{-3} torr, the total scattered current to each collector is of the order of 10^{-12} to 10^{-10} amps depending on the beam energy. To obtain an energy loss spectrum, it is necessary to energy analyse these scattered electrons. This may be accomplished in several ways, each of which has its advantages and disadvantages.

Integral Spectrum

An integral spectrum such as that shown in fig. 4.6 may be readily obtained after pressure stabilisation has been achieved by displaying the output from one of the Keithley 640 electrometers on the Y-axis of an X-Y recorder as the potential between G3 and the cathode is

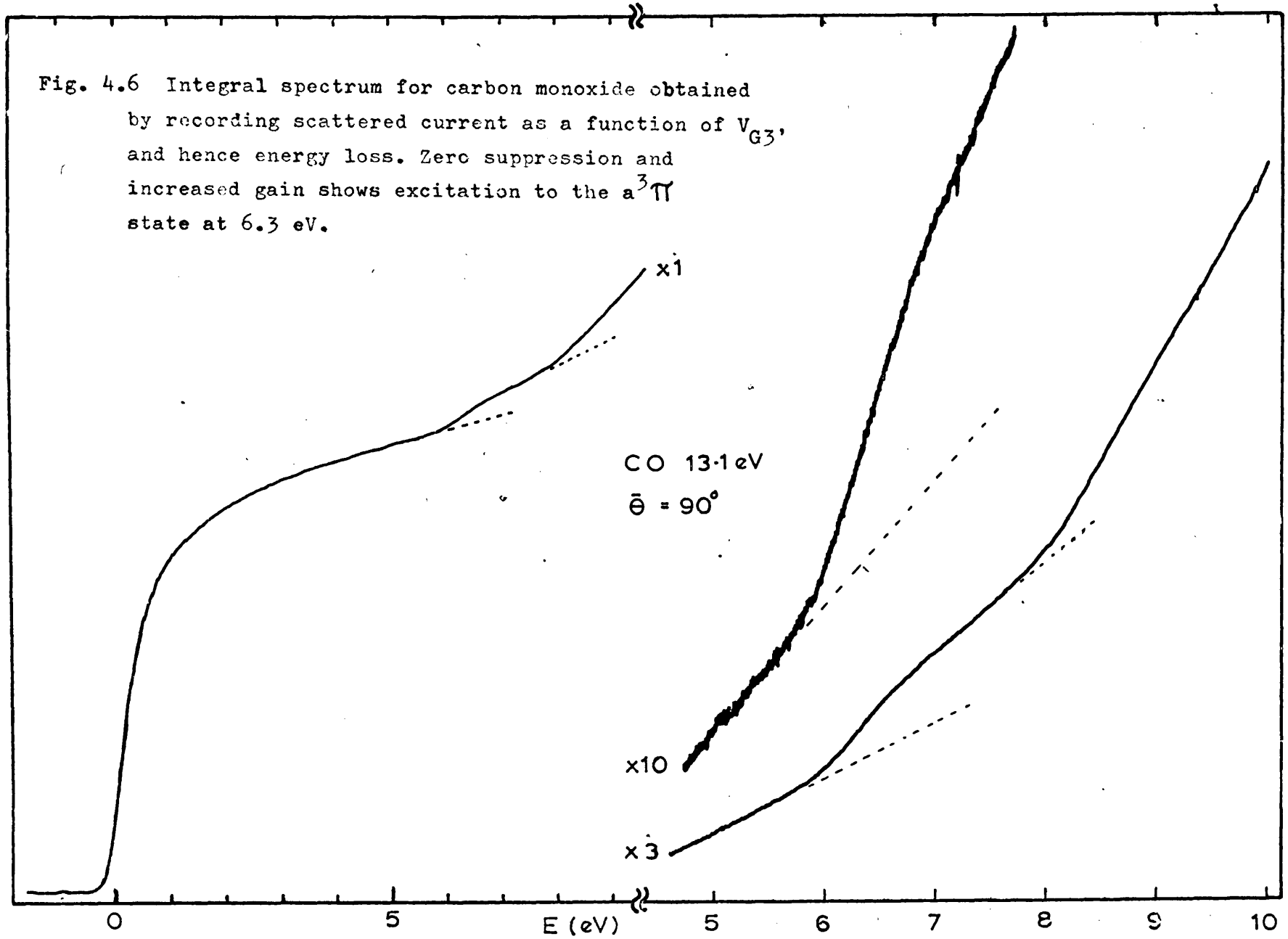

Fig. 4.6 Integral spectrum for carbon monoxide obtained by recording scattered current as a function of V_{G3}, and hence energy loss. Zero suppression and increased gain shows excitation to the $a^3\Pi$ state at 6.3 eV.

continuously scanned and displayed on the X-axis using a motor-driven helipot and a stabilised power supply. A contact potential exists between the dispenser cathode and the apparatus which may be between 1.9 and 2.5 volts and this must be subtracted from V_{G3} to give the energy loss. This is determined and the energy scale calibrated, by differentiation to obtain the elastic peak position which is then defined as zero energy loss. Inelastic transitions appear as steps in the integral spectrum and the step heights are proportional to the differential cross-sections over the angular range involved.

Integral spectra at various energies and a fixed scattering angle may thus be used to determine the energy dependence of the differential cross-section of a transition of interest relative to another transition which is chosen as a reference (usually an optically-allowed transition). A quick scan through the complete spectrum can be made initially by this method and any regions in which weak transitions may be indicated can be investigated by using zero suppression and increased sensitivity on the electrometer as shown in fig. 4.6.

The main advantage of this method is that it is fast and gives immediate feedback of information regarding the quality of the measurements. Unfortunately, these curves become difficult to interpret if superimposed on a rising background such as that which occurs at low energies in the present instrument. It is also sensitive to pressure fluctuations which appear as a sharp discontinuity in the trace.

Electrical Differentiation

Differentiation of the collected current with respect to the retarding voltage gives the energy distribution of the scattered electrons and thus provides calibration of the energy scale via. the elastic peak and facilitates comparison with spectra obtained in instruments using deflection analysers.

Differentiation may be achieved electrically(66,67) by superimposing a small a.c. signal on the retarding voltage and using a lock-in amplifier to detect the a.c. component which is induced in the signal current and which is proportional in magnitude to the slope of the integral curve.

This mode of operation was investigated using a Princeton Applied Research HR-8 lock-in amplifier which also provided the a.c. signal. The

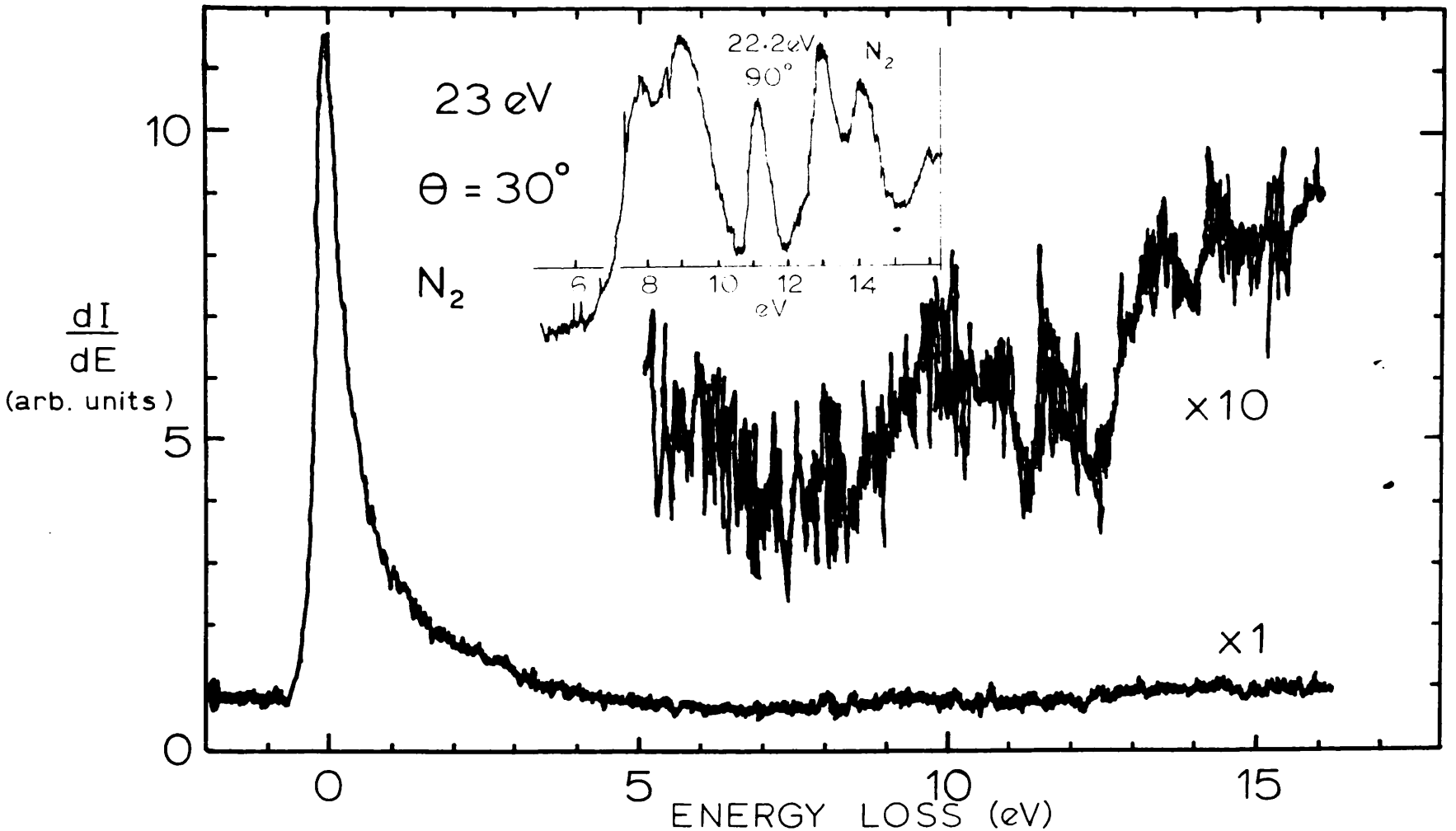

Fig.4.7 Spectrum of nitrogen obtained by electrical differentiation of the scattered current with a.c. modulation at 1.5 Hz, 90mV peak-to-peak amplitude, 1 sec. time constant. Inset shows spectrum by Doering and Williams(34).

a.c. signal was connected in series with the retarding voltage via. a transistor driver transformer since one side of the output from the lock-in was earthed. One of the Keithley 640 electrometers was used as a preamplifier and this necessitated using low frequency modulation. The unity gain output of the electrometer was used to feed the signal into the lock-in amplifier.

This arrangement was satisfactory for displaying the elastic peak but when the zero was suppressed and the sensitivity increased to show the inelastic structure, the noise became excessive. Nevertheless, the spectrum obtained [fig. 4.7] using the pseudo-spherical analyser was consistent with the known spectrum of nitrogen at the energy and scattering angle used.

In Auger electron spectrometers using retarding field analysis and electrical differentiation, it has been found(68) that increasing the modulation frequency from 250 Hz to 2.5 kHz results in both a decrease in noise and an increase in signal. Noise can also be reduced by neutralising the capacitance between the retarding grid and the scattered collector. Replacement of the electrometer by a high input impedance a.c. amplifier and the use of capacitance neutralisation should therefore enable differentiated spectra to be plotted directly (and quickly) on a X-Y recorder. Pressure fluctuations are less serious using this method since they show up as sharp spikes leaving the general trend of the curve unaffected.

Data Logging Combined with Numerical Differentiation

Spectra may be obtained using the automated data-logging system described on pages 39 and 40. Once the general features of the spectrum have been determined from an X-Y plot of an integral spectrum, a suitable starting voltage and scan range may be set up on the retarding potential stepper and the logger scan initiated. The logger then scans V_{T3}, V_{G3}, pressure, beam current and the three scattered currents at its maximum rate of 2 channels/sec. after which V_{G3} is increased by 100 mV and, after a 2 second delay for electrometer stabilisation, the above parameters are again scanned. This pattern is repeated until V_{G3} reaches the upper limit of the pre-set scan range, when the stepper resets V_{G3} to the starting point and actuates the scan counter. After a 4 second delay, the stepper

initiates the second scan. This procedure is then repeated until the required number of scans have been recorded, when the system is switched off manually and the punched tape taken away for off-line processing on a digital computer.

The data processing program normalises the three scattered currents to constant pressure and beam current, averages them over the number of scans and prints out the mean values along with the corresponding mean values of V_{G3}, the potential between G3 and the cathode. The same program then numerically differentiates the integral spectrum using the method of Rutledge(46). In the form used here this consists of fitting a sixth degree polynomial to seven successive points and calculating the derivative at the midpoint, then moving the polynomial along the curve and calculating the derivative at the next point and so on until the complete curve has been covered. The derivatives of the three scattered currents are then printed out along with the values of V_{G3}.

This is the most reliable method of data collection used and it enables structure to be picked out against a rising background and hence is especially useful at very low incident energies. The arrangement used gives a simultaneous measurement of the energy loss spectra on three collectors at a fixed incident energy and thus enables a study to be made of the angular dependence of the cross-section of a particular transition of interest relative to a reference transition. Unfortunately, the data logging equipment itself was not as reliable as the results obtained by this method as both the Solartron logger and the Data Dynamics punch were subject to almost routine breakdown and malfunctioning.

The main disadvantages of this method are its slow speed and the delay between performing the experiment and knowing the quality of the results. For elastic peaks, 5 scans are adequate while between 10 and 30 scans are used for inelastic regions of the spectrum, 10 scans over a 5 volt range requiring 1 hour of running time. Off-line computation means that at least a day has elapsed before the results of a run are known. A modification to the logger which would increase the maximum scanning speed from 2 channels/sec. to 12 channels/sec. is available from the manufacturer as a plug-in board at moderate cost and this would cut down the running time necessary.

4.8 Instumental Effects

Instumental effects in the Kuppermann and Raff spectrometer have been suggested(30) as a possible explanation for the discrepancy between their results and those of Simpson and Mielczarek for ethylene.

Wei and Kuppermann have recently made a study(36) of instrumental effects occurring in a modified version of the Kuppermann and Raff spectrometer which is fitted with a baffle to restrict scattering to $90^{\circ} \pm 6^{\circ}$. They have found two effects which can occur : an undulating background which gives rise to spurious peaks; and a rising background which occurs in the region of large energy loss. They suggest insulating films on grids as a possible cause of the undulating background, while the rising background is attributed to the combined effects of field penetration from the scattered collector into the collision region and scattering from grids which gives rise to reflected and secondary electrons.

In their instrument, they find that the undulating background is small when the holding voltage between G3 and the scattered collector is maintained at $V_{SC \text{ to } G3} + V_{incident} \geqslant 65$ volts. For a 30 eV beam this corresponds to a holding voltage of at least 35 volts and this results in field penetration which contributes to the rising background at large energy loss when V_{G3} approaches V_{G1}. The general shape of their energy loss spectrum corresponds to a typical secondary electron energy distribution(68) as does their vacuum background spectrum. They find that the background is pressure dependent but no simple relation is found with either pressure or the elastic peak.

Our instrument does not suffer from undulating backgrounds and this may be due to the use of a mercury pumped UHV system. It is common in X-ray photoelectron spectroscopy(69) to find peaks due to deposition of pump oil on surfaces which increase with the time of pumping and this could be responsible for the effect observed by Wei and Kuppermann as their diffusion pumps use a silicone oil.

Spectra obtained using the pseudo-spherical analyser do not show much evidence of a secondary electron energy distribution although there is a slight rise in background at large energy loss which may be attributable to field penetration since holding voltages of around 15 volts were necessary for efficient collection with the untreated surfaces used in

this analyser. We would expect field penetration to be less pronounced in this analyser than in that of Wei and Kuppermann since the G3 - SC spacing is 7 mm as opposed to 4.5 mm and 100 mesh gauze is used as opposed to 50 mesh gauze of the same transparency.

When the spherical analyser is used, field penetration may be assumed to be negligible as 100 mesh gauze is used and the G3 - SC spacing is increased to 15 mm at SC2 and 11 mm at SC1 and SC3 while evaporation of "black gold" on the collectors permits holding voltages of only 2 to 5 volts to be used. However the spectra are superimposed on a pressure dependent secondary electron distribution. A vacuum background spectrum such as that in fig. 4.8, shows the same energy distribution but at reduced intensity. Fig. 4.8 was actually obtained using a faulty cathode which had a blemish at its centre which resulted in a defocussed beam being obtained. Under these conditions beam electrons would be expected to strike the cone fitted to T4 which defines the scattering region and the spherical grid support ring of G1 which is clamped around this cone. As the cone is constructed of .005" thick Ta sheet and as it presents only a small area to electrons emerging from the scattering region it is not thought to be the main source of secondary electrons. Rather, the spherical grid support ring is thought to be responsible since it presents a 1½ mm thick annulus to electrons scattered from the beam. As elastic differential cross-sections are large in the angular range subtended by the support ring(70), the secondary electron emmision would appear to be due to electrons scattered elastically from the gas striking this support ring as this would account for the pressure dependence.

A secondary electron energy distribution such as that shown in fig. 4.8 is generally smoothly varying with two peaks : a broad peak at low electron energy[shown as large "energy loss" in fig. 4.8] corresponding to true secondary electrons; and a sharp peak close to the primary beam energy due to what are usually termed "reflected" electrons. The broad secondary peak gives rise to the rising background discussed by Wei and Kuppermann while the "sharp" peak turns out to be broader than the elastic peak observed from gas scattering and results in an increased base width for the elastic peak during operation with sample gas. The position of the "reflected" electron peak is also shifted thus increasing the base width of the elastic peak even more. From fig. 4.8, we see that the reflected

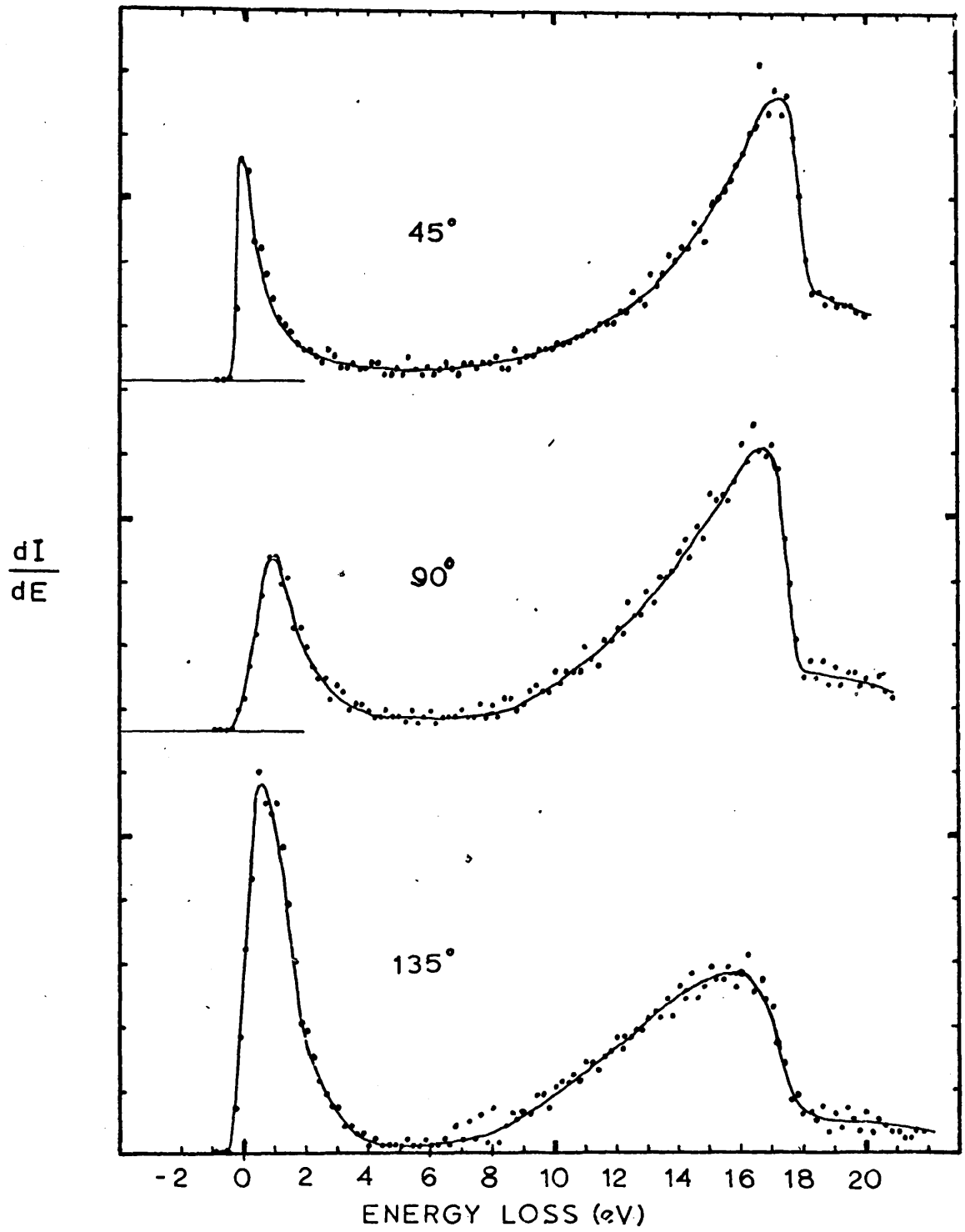

Fig. 4.8 Energy analysis of background scattered current at 18.1 eV beam energy. The energy scale is calibrated by the elastic peak obtained when gas is present in the collision chamber. These curves are obtained by differentiation of three retarding curves normalised to the scattered current at 18 eV energy loss.

electron peaks have a F.W.H.M. of 1.7 eV and the maximum is shifted by around 0.8 volts with respect to the elastic peak position determined with gas in the collision chamber when a F.W.H.M. of only 0.5 eV was obtained. The peak obtained at 45^{o} mean scattering angle is sharper because under the conditions used some primary beam electrons could reach SC 1 directly without striking metal surfaces. This effect of "reflected" electron production places a limitation on the performance of the spectrometer in the low energy loss region below 4 eV, a region in which some low-lying triplet states of organic molecules are expected(7,8).

Of the effects encountered by Wei and Kuppermann, the undulating background can apparently be avoided by use of a UHV system, the field penetration contribution to the rising background can be made negligible by using a large collector - retarding grid spacing and large mesh number gauze for grid construction and the remaining problems are associated with production of secondary and reflected electrons by electrons elastically scattered from the gas. Graphite is known to have low backscattering and secondary emmision coefficients(68) and evaporation of graphite onto all the metal components of the analyser should result in a significant reduction of the rising background and anomalous elastic peak base width effects. The situation could be further improved by removing G1 and operating the present G2 grid at the T3/G1 potential. The only disadvantage would be the necessity of adjusting the electrometer zero to allow for positive ions when operating with beam energies above the ionisation potential of the gas under investigation.

CHAPTER 5 RESULTS AND DISCUSSION

Spectra have been obtained for N_2 , CO and C_2H_4 at different scattering angles (total range 15°- 165°) and incident beam energies between 10 and 50 eV.

In obtaining spectra, the electron beam current is maintained at 5×10^{-8} to 1×10^{-7} amps as this generally results in sufficient scattered current when sample gas is admitted at a pressure in the range 10^{-4} to 10^{-3} torr without increasing the electron energy spread unduly. Two methods are used to obtain spectra and these have been described in detail in chapter 4, pp 43 - 46. Spectra at a fixed scattering angle and various beam energies are obtained conveniently by displaying the appropriate scattered current as a function of energy loss on a X-Y recorder. This method gives an integral (step) spectrum but is adequate for displaying the general features of the energy loss spectrum. Reproducibility of spectra is achieved by allowing adequate time for pressure stabilisation which is determined by continuously displaying the pressure on a chart recorder. More detailed spectra may be obtained using the data logging system with numerical differentiation and this method gives three spectra simultaneously at different scattering angles for a chosen incident energy. Spectra may therefore be studied as a function of incident energy and scattering angle.

Differential cross-sections for elastic and inelastic processes are known to fall off rapidly with increasing scattering angle at medium and high energies but as the incident energy is lowered, the scattering becomes more isotropic and we might reasonably expect to obtain a larger signal at large angles at, say, 20 eV rather than at 50 eV. This is in fact found to be so and it is considerably more difficult to obtain a 90° spectrum at 50 eV than at 30 eV and lower incident energies because of decreased signal-to-noise.

As 90° spectra have been obtained by both Doering(33) and Wei(35) in the

30 - 50 eV energy range and as the spectra obtained with the present instrument are in general agreement with theirs over the same energy range, attention has been directed to obtaining detailed spectra at incident energies below 30 eV. This range is inaccessible to Wei because of instrumental problems not shared by the present instrument and it is the region in which singlet-triplet transitions are expected to be most pronounced, i.e. where the incident energy is close to the threshold energy of these processes.

5.1 Nitrogen

The energy loss spectrum of N_2 has been extensively studied at high and medium energies (9d,12) in forward scattering. Spectra obtained under these conditions are very similar to optical spectra with forbidden transitions either absent or extremely weak. With the scattering angle fixed at zero and incident energy close to threshold, Heidemann et.al.(17) have shown significant singlet-triplet excitation with the $C^3\pi_u$ state approximately the same intensity as the $b^1\pi_u$ for 15.7 eV incident energy. Using an incident energy of 48 eV and small scattering angles in the range 0 - 15°, Skerbele et.al.(13) were able to detect excitation to the $A^3\Sigma_u^+$, $B^3\pi_g$ and $C^3\pi_u$ states but the intensity of the spin-forbidden $C^3\pi_u$ transition was only about 0.5% of that of the allowed $b^1\pi_u/p'^1\Sigma_u^+$ peak at 12.93 eV while the electric quadrupole allowed $a^1\pi_g$ transition was about 10% of the 12.93 eV peak. Lassettre (71) has remarked that in forward scattering the 30 - 100 eV region is not a favourable one for the detection of singlet-triplet transitions because they tend to be obscured by more intense electric quadrupole transitions and the $a^1\pi_g$ state of N_2, lying as it does between the $B^3\pi_g$ and $C^3\pi_u$ states, provides an example of this.

Threshold excitation spectra for nitrogen have been obtained by a number

of investigators using both the trapped-electron technique(18,19,20,21a) and the SF_6^- 'scavenger' technique (22,24,25). Schulz(18) assigned the main peaks in his low resolution spectrum to the $A^3\Sigma_u^+$ and $C^3\pi_u$ states but in later, high resolution (~100 meV), work by Brongersma and Oosterhoff(20) partially resolved vibrational structure in the first peak showed it to be due to excitation of the $B^3\pi_g$ state while the second major peak at 11.82 eV was assigned to the $E^3\Sigma_g^+$ state.

In a recent threshold spectrum by Hall et.al.(21a) at higher resolution (70meV), using a parallel plate electron trap, the $B^3\pi_g$ state is resolved into 11 vibrational levels while 3 vibrational levels of the $E^3\Sigma_g^+$ can be observed as well as less intense structure corresponding to the $A^3\Sigma_u^+$ and $C^3\pi_u$ states. What is particularly interesting, however, is the existence of an unusually shaped peak at 9.75 eV which does not correspond to any observed state in optical spectroscopy but which these authors suggest could be due to a $^5\Sigma_g^+$ state. A peak of similar shape at 9.7 eV had been previously reported in an SF_6^- experiment by O'Malley and Jennings(25) at lower resolution(500 meV) but they assigned it to the $a^1\pi_g$ state.

Although Kuppermann and Raff made some of the early studies of large angle energy loss spectra, they did not investigate nitrogen.

Experiments by Doering and Williams(34) in which the scattering angle was fixed at 90° and in which the best resolution was 200 meV using a 180° monochromator and a 127° analyser, showed that singlet-triplet transitions dominate the 90° spectrum of N_2 at incident energies below 20 eV.

Trajmar, Rice and Kuppermann(37) using a variable angle spectrometer with hemispherical deflectors for both monochromator and analyser have found that the energy loss spectrum of N_2 changes significantly as the scattering angle is increased for a fixed impact energy. A spectrum at 40 eV and 20° scattering angle shows the main peak to be due to excitation of the dipole-allowed $b^1\pi_u$ with the

quadrupole-allowed $a^1\pi_g$ the second strongest at about 1/3 the intensity. The singlet-triplet transitions are almost masked by the wings of the $a^1\pi_g$ peak, the $B^3\pi_g$ and $E^3\Sigma_g^+$ peaks being observed at about 1/30 and the $C^3\pi_u$ at about 1/15 the intensity of the $a^1\pi_g$ peak. When the scattering angle is changed to 80°, however, the $B^3\pi_g$, $a^1\pi_g$, $C^3\pi_u$ and $b^1\pi_u$ peaks all appear at approximately equal intensity while the $E^3\Sigma_g^+$ is now only 1/10 of the $C^3\pi_u$ peak. Identification of the $B^3\pi_g$ and $a^1\pi_g$ is possible because the resolution (~100 meV) is sufficient to partially resolve vibrational structure in these states.

Williams and Doering(3) have investigated the scattering of electrons with energies close to threshold from N_2 at angles of up to 30° using a variable angle instrument with hemispherical deflectors for monochromator and analyser and lenses which minimise chromatic aberation and thus enable relative peak heights to be accurately determined. In a spectrum at 15 eV incident energy and 20° scattering angle, they find that the $a^1\pi_g$ and the $C^3\pi_u$ are the most intense peaks and that they are excited equally, while the $b^1\pi_u$ is only about ½ as intense as these. The peaks corresponding to excitation of the $A^3\Sigma_u^+$ and $B^3\pi_g$ are of about equal intensity and only 1/16 of the $a^1\pi_g(v=2)$ peak, while the $E^3\Sigma_g^+$ state is not observed. If we compare this spectrum with that of Trajmar et.al.(37) at 40 eV and 20° scattering angle, we see that the reduction of incident energy at this angle causes excitation of the $b^1\pi_u$ to fall off sharply relative to the $a^1\pi_g$ while the $C^3\pi_u$ increases rapidly relative to the $a^1\pi_g$. The $A^3\Sigma_u^+$ and $B^3\pi_g$ intensity ratios, relative to the $a^1\pi_g$, only increase by a factor of two on reducing the incident energy from 40 eV to 15 eV. However, on reducing the incident energy further to 10 eV and 9 eV, Williams and Doering find that, for the angular range 10° to 30°, the transitions from the ground state to the $A^3\Sigma_u^+$ and $B^3\pi_g$ are equiprobable while peaks corresponding to the $a^1\pi_g$ state cannot be identified with certainty from the noise.

Williams and Doering (41) have also found a peak at 13.2 eV in N_2 the intensity of which increased relative to the $b^1\pi_u$ bands as the scattering angle was varied from 1° to 40° at an incident energy of 19.2 eV, suggesting the possibility of a singlet-triplet transition at this energy.

Wei (35) has studied the electron impact spectrum of N_2 at energies of 30 - 50 eV and a fixed scattering angle of 90° using a modified Kuppermann and Raff apparatus in which a stack of discs placed in front of the retarding grid serves to provide angle selection. The resolution is ~1 eV and the spectra show three bands below the ionisation potential. The lowest band between 6.5 and 10.3 eV is assigned to the unresolved $A^3\Sigma_u^+$, $B^3\pi_g$ and $a^1\pi_g$ states. The second, smaller, band at 11.1 eV is partially resolved and assigned to transitions to the $C^3\pi_u$. The third band peaks at 13.2 eV and is assigned to transitions to both optically allowed and spin forbidden states in this region. The relative intensities of the three peaks did not change significantly as the incident energy was reduced from 50 eV to 30 eV with the first and third peaks at about equal intensity and the second peak about 1/3 as intense.

In the present work the energy loss spectrum of N_2 has been investigated in the energy range 12.4 eV to 48 eV over the three angular ranges available.

As the incident energy is lowered from 48 eV to 18 eV at a mean scattering angle of 45° the most noticable effect is the increase in intensity of the $a^1\pi_g$ transition relative to the $b^1\pi_u$ (fig. 5.1). This is in agreement with Lassettre's work at energies of 30 - 100 eV and scattering angles 0 - 15°. At 45° and 18 eV, the $a^1\pi_g$ transition is the strongest feature in the spectrum, while scattering may now be observed in the regions associated with excitation of the triplet states $A^3\Sigma_u^+$, $B^3\pi_g$ and $C^3\pi_u$.

If a scattering angle of 90° is used, however, excitation of the $C^3\pi_u$ and of

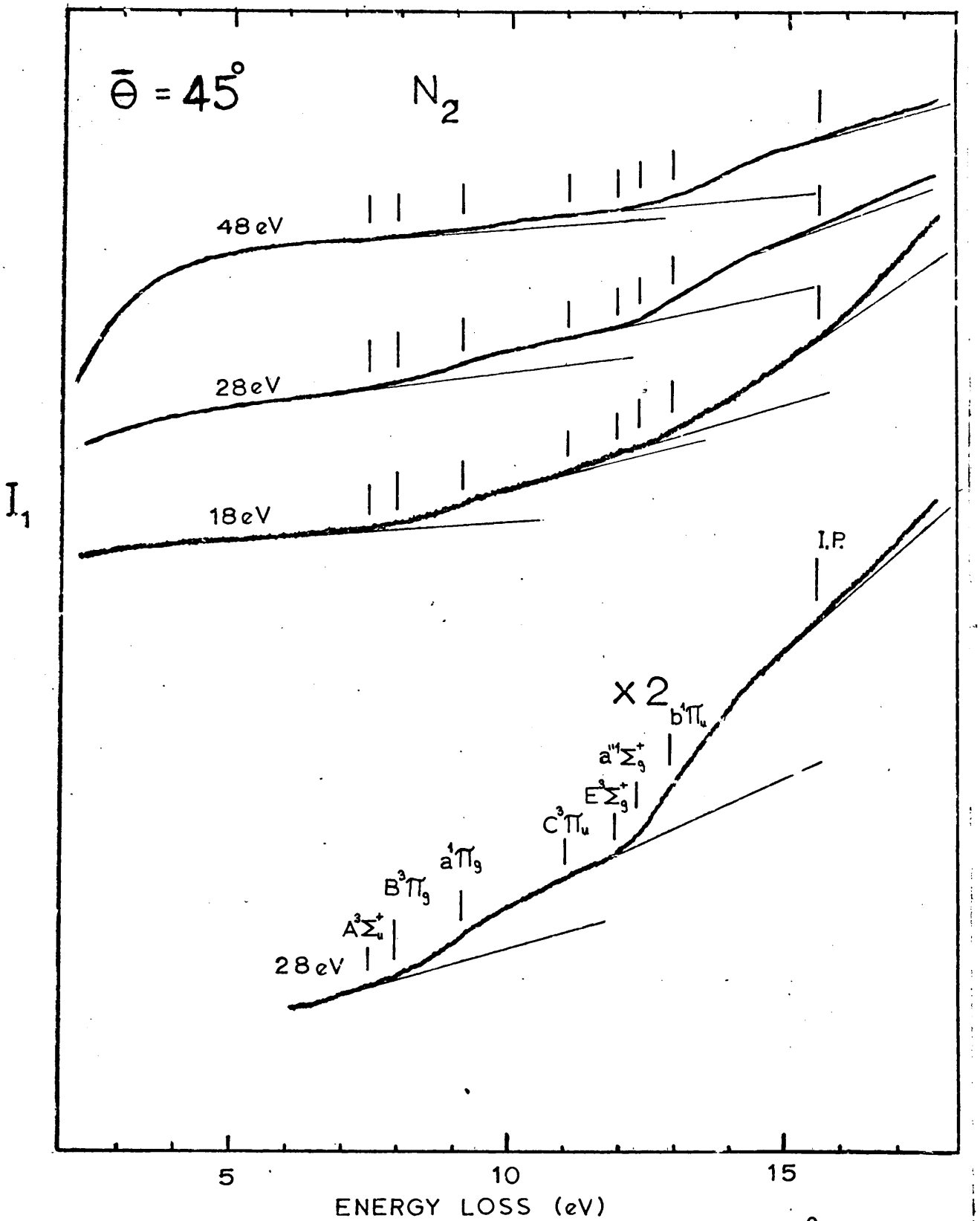

Fig. 5.1 Integral spectra of N_2 at a mean scattering angle of 45° for various incident energies, using the spherical analyser. The positions at which peak maxima are expected for known states are indicated by vertical bars.

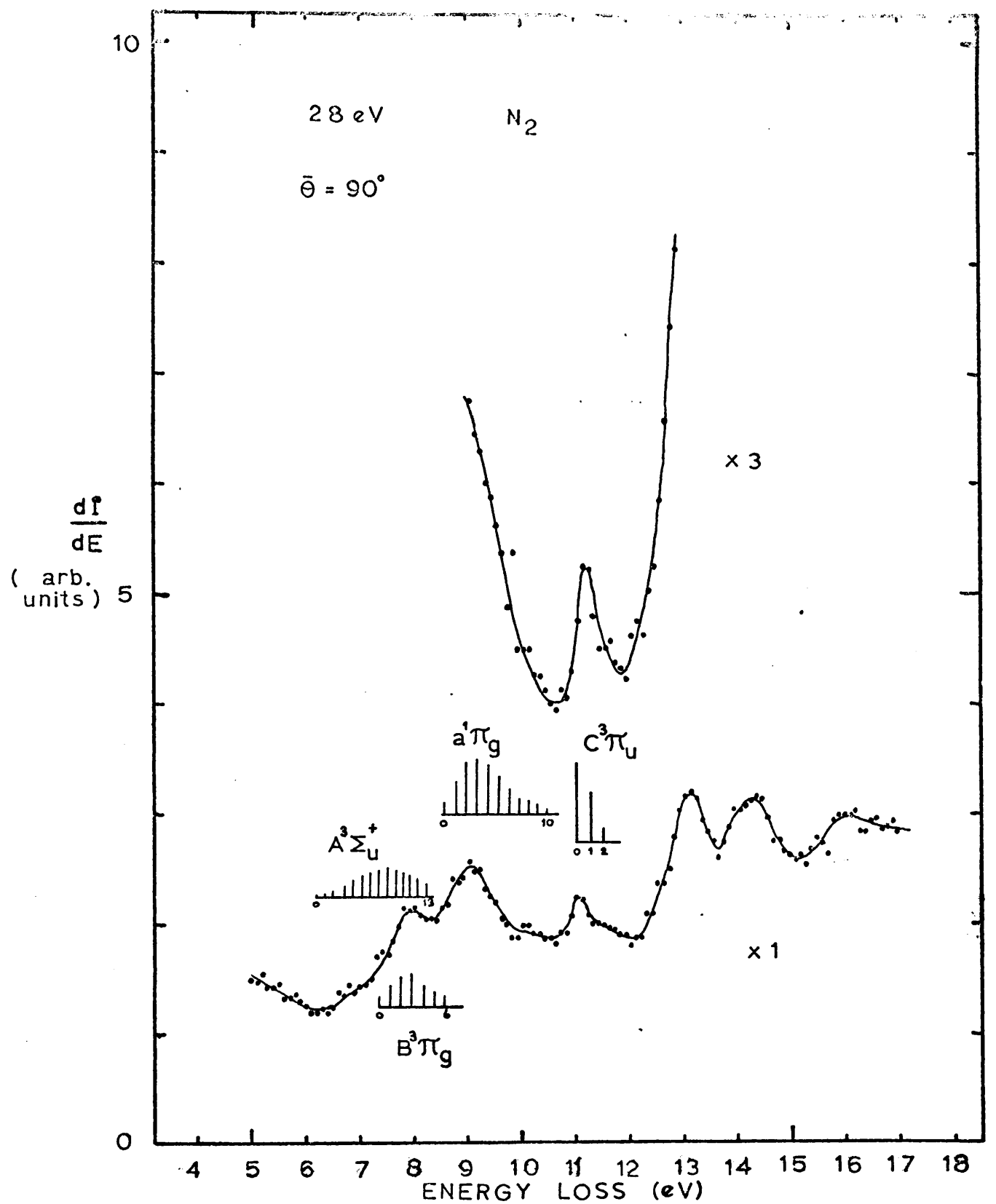

Fig. 5.2 Energy loss spectrum of N_2 obtained by differentiation of a recorder tracing of scattered current v. retarding potential. The upper curve was obtained from a re-run at higher sensitivity and clearly shows excitation of the $C^3\pi_u$.

states of lower energy than the $a^1\pi_g$ may be observed using higher incident energies of 28 - 48 eV. One such example is shown in fig. 5.2 and from the relative Franck-Condon factors given by Williams and Doering (3) and shown in fig. 5.3, we can say that the scattering below 8.5 eV is mainly due to excitation of the $B^3\pi_g$ state which peaks at 7.9 eV although the weak shoulder from 6.2 eV to 7.3 eV may be attributed to the $A^3\Sigma_u^+$. Other peaks are observed at 13.2 eV, 14.25eV and 16.1 eV in agreement with spectra by Doering and Williams(34). The peak at 14.25 eV has been observed by a number of investigators and is normally assigned to several Rydberg states, while the 13.2 eV peak at this resolution (~500 meV) would be due to a combination of singlet states which lie in this region, the strongest, in forward scattering, being the $b^1\pi_u$ (12.84 eV) and $p'^1\Sigma_u^+$(12.93 eV). As Williams and Doering (41) have obtained evidence suggesting a triplet state at 13.2 eV, however, it is possible that this triplet may be making a significant contribution to the 13.2 eV in fig. 5.2.

Spectra taken at a mean scattering angle of 135° over the same range of incident energies show the $B^3\pi_g$ and $a^1\pi_g$ states and the 14.25 eV peak at intensities similar to those at 90°, but the $C^3\pi_u$ state cannot be detected even with zero suppression and increased sensitivity, while the 13.2 eV peak is reduced by about a factor of two. The reduction in the 13.2 eV peak may be due to the singlet states which contribute to it having a more forward peaked differential cross-section than those singlet states which contribute to the 14.25 eV peak. On the other hand, it has been suggested(41) that a probable triplet state corresponding to the "singlet-triplet" peak observed by Williams and Doering at 13.2 eV would be the $^3\pi_u$ state associated with the $o^1\pi_u$ Rydberg state. As this state and the $C^3\pi_u$ have identical terms, it would be reasonable to expect scattering from both states to have a similar angular dependence and thus the triplet contribution

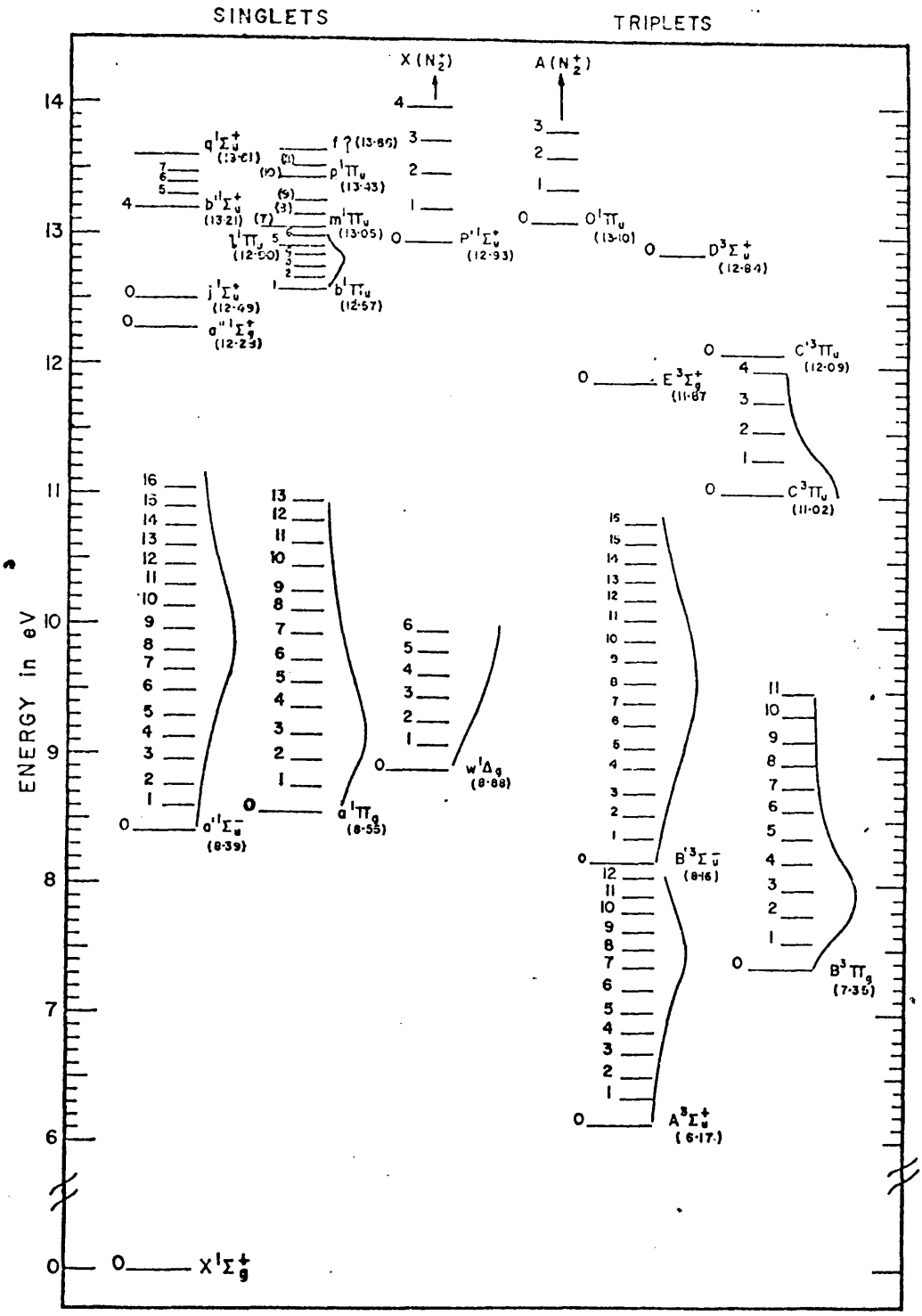

Fig. 5.3 Energy level diagram of N_2. The relative Franck-Condon factors for the overlap of the various vibrational states with the v = 0 level of the ground state are shown increasing to the right, next to the levels. Taken from ref.(3).

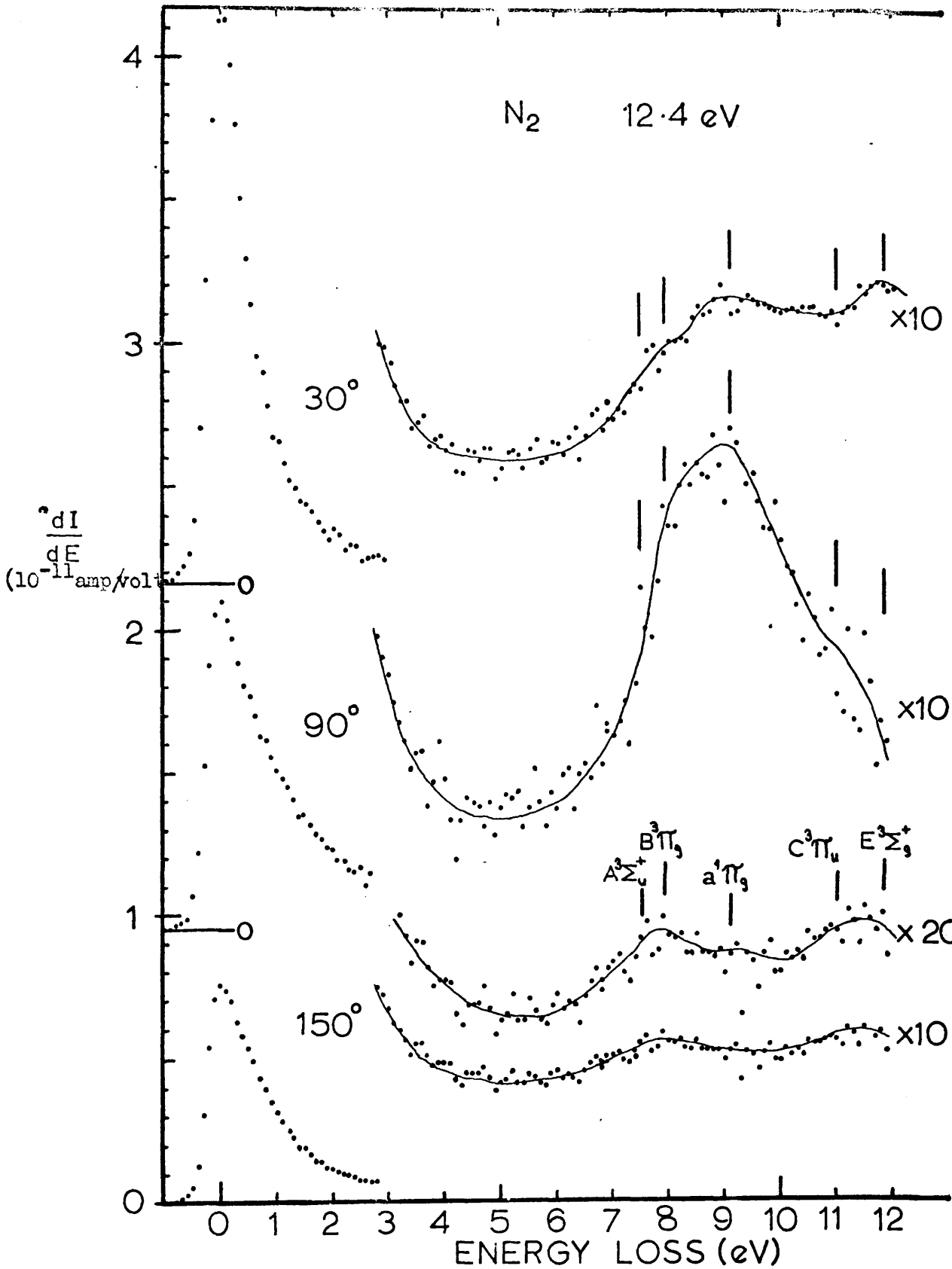

Fig. 5.4 Energy loss spectra of N_2 at 12.4 eV incident energy, using pseudo-spherical analyser with each data point normalised to a beam current of 10^{-7} amp and a pressure of 10^{-4} torr.

to the 13.2 eV peak at 135° would be reduced in the same way as the intensity of the $C^3\pi_u$ peak is.

A major difference between large angle energy loss spectra and threshold excitation spectra is in the magnitude of the peaks corresponding to the $a^1\pi_g$ state. This state is absent from threshold spectra of N_2 (21a) as the $a^1\pi_g$ has a very small cross-section at threshold, but is usually more strongly excited than neighbouring triplet states in energy loss spectra, thus tending to mask the triplets. However, if we use an incident energy close to threshold, then we can obtain an energy loss spectrum in which triplet states are more strongly excited than the $a^1\pi_g$. Such a spectrum is shown in fig. 5.4 for 12.4 eV incident energy and 150° scattering angle. The spectra in fig. 5.4 were taken at lower resolution using the pseudo-spherical analyser but although the $B^3\pi_g$ and $a^1\pi_g$ states are not resolved, the maximum of the composite peak is observed to shift from 9.1 eV to 7.9 eV as the scattering angle is increased from 30° to 150°, showing that the $B^3\pi_g$ gains intensity relative to the $a^1\pi_g$ as the scattering angle is increased. Excitation of the $C^3\pi_u$ and $E^3\Sigma_g^+$ states is also indicated, excitation of the latter being feasible at this energy (17). Higher resolution to permit observation of vibrational structure is necessary before more definite assignments can be made.

5.2 Carbon Monoxide

Carbon monoxide has been less extensively studied than N_2 in electron impact spectroscopy. Early work by Lassettre and co-workers(10e,10g,11) at several hundred eV and angles of 0° - 15° was directed at investigating the angular dependence of the scattering from singlet states and no singlet-triplet transitions were observed. However, in later work by Skerbele, Dillon and Lassettre(72) at 48 eV incident energy and zero scattering angle, transitions from the ground state, $X^1\Sigma^+$, to the $a^3\pi$ and $b^3\Sigma^+$ states were observed. Four vibrational levels of the $a^3\pi$ were

resolved, the strongest (v=1) being about 0.05% of the intensity of the $A^1\Pi$ (v=2) peak, while the $b^3\Sigma^+$ (v=0) peak was about 0.2% of the $A^1\Pi$.

Threshold excitation spectra of CO have been obtained at low resolution by Schulz(73) in which the most prominent transition is that from the ground state to the $a^3\Pi$, while transitions to the $A^1\Pi$ and $b^3\Sigma^+$ appear at lower intensity. A threshold spectrum at higher resolution (~100 meV) has been obtained by Brongersma and Oosterhoff(20) in which 5 vibrational levels of the $a^3\Pi$ can be identified, while the $b^3\Sigma^+$ is observed at 10.4 eV with about 0.4 of the intensity of the strongest $a^3\Pi$ peaks (v=0 and v=1). A peak is also observed at 10.75 eV at half the intensity of the $b^3\Sigma^+$ which may be due to the $B^1\Sigma^+$ state.

Wei (35) has obtained energy loss spectra for CO at ~1eV resolution using 90° scattering angle and incident energies of 30 - 50 eV. Three bands are observed at 6.2 eV, 8.5 eV and 13.5 eV. The first two are assigned to the $a^3\Pi$ and $A^1\Pi$ states while the 13.5 eV band, which has a long shoulder starting at about 11 eV is assigned to the unresolved B,C,E,F,G and higher singlet states and other triplet states. Wei finds that as the incident energy is lowered, the intensity ratio of the $a^3\Pi$ relative to the $A^1\Pi$ stays approximately constant but a weak shoulder gains intensity relative to the $A^1\Pi$ peak in the region of 10.6 eV and this he assigns to the $b^3\Sigma^+$ state. Wei suggests that the stronger energy dependence of the $b^3\Sigma^+$ indicates that it is more strongly forbidden than the $a^3\Pi$.

Trajmar, Rice and Kuppermann(39) have obtained energy loss spectra of CO at energies of 25 eV and 35 eV in the angular range 10° to 80°. In a high resolution (~100 meV) spectrum at 25 eV and 75° scattering angle, they find that the intensity of the $a^3\Pi$ relative to the $A^1\Pi$ (v=2) peak is about 0.5 while those of the $b^3\Sigma^+$, $B^1\Sigma^+$ and $C^1\Sigma^+$ are around 0.1, 0.35 and 0.25 respectively. At 35 eV curves have been obtained showing the intensity ratio relative to the $A^1\Pi$ as a function of

scattering angle for the $a^3\Pi$, $b^3\Sigma^+$, $B^1\Sigma^+$ and $C^1\Sigma^+$ states. The intensity ratio of the $a^3\Pi$ increases by a factor of 100 and that of the $b^3\Sigma^+$ by a factor of 30 over the 10^o - 80^o range, while the trend with angle for the $B^1\Sigma^+$ and $C^1\Sigma^+$ states is not so marked.

Spectra obtained with our instrument are consistent with previous large angle work by Wei(35) and Trajmar et.al.(39). Fig. 5.5 shows integral spectra at 90^o mean scattering angle and incident energies from 18.1 eV to 48.1 eV. Three intensity maxima are observed at 6.2 eV, 8.4 eV and 13.5 eV in agreement with Wei. Also, in agreement with Wei, it is found that the $a^3\Pi$ intensity only increases very slowly with respect to the $A^1\Pi$ as the incident energy is lowered at 90^o scattering angle, this behaviour being confirmed down to 18.1 eV, and at the lower energies weak scattering is also observed in the 10 - 11 eV energy loss region. Relative step heights in the integral spectra give intensity ratios integrated over all the vibrational levels in each electronic state and , for the energy range 48 eV to 18 eV and 90^o scattering angle, this intensity ratio for the $a^3\Pi$ relative to the $A^1\Pi$ is between 0.3 and 0.4. This compares well with the value of 0.4 given by Trajmar et.al.(39) for 35 ev incident energy and 80^o scattering angle where the intensities of both states are integrated over the first three vibrational levels only.

The energy loss spectrum of CO has also been studied as a function of angle using an incident energy close to threshold. About the lowest energy which can be used before the secondary electron background interferes with intensities in the 10 - 11 eV energy loss region is 13 eV. This is only 2.5 eV above the threshold of the $b^3\Sigma^+$ state which is observed readily in threshold excitation spectrometers (20). Spectra at the three scattering angles are shown in fig. 5.6 for an incident energy of 13.1 eV. The $a^3\Pi$ peak is observed to gain intensity relative to the

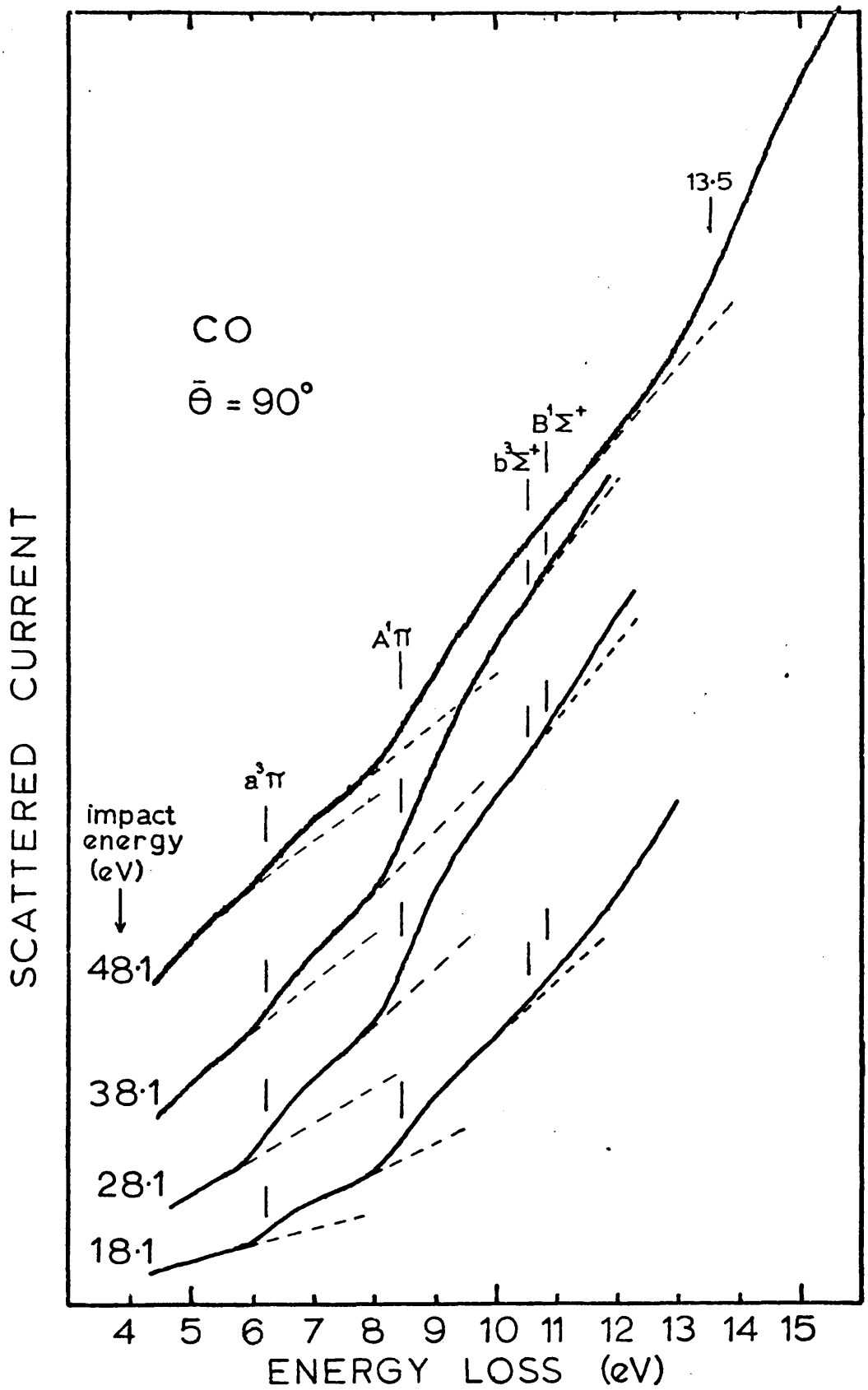

Fig. 5.5 Integral spectra of CO obtained at a mean scattering angle of 90° for various incident energies using the spherical analyser.

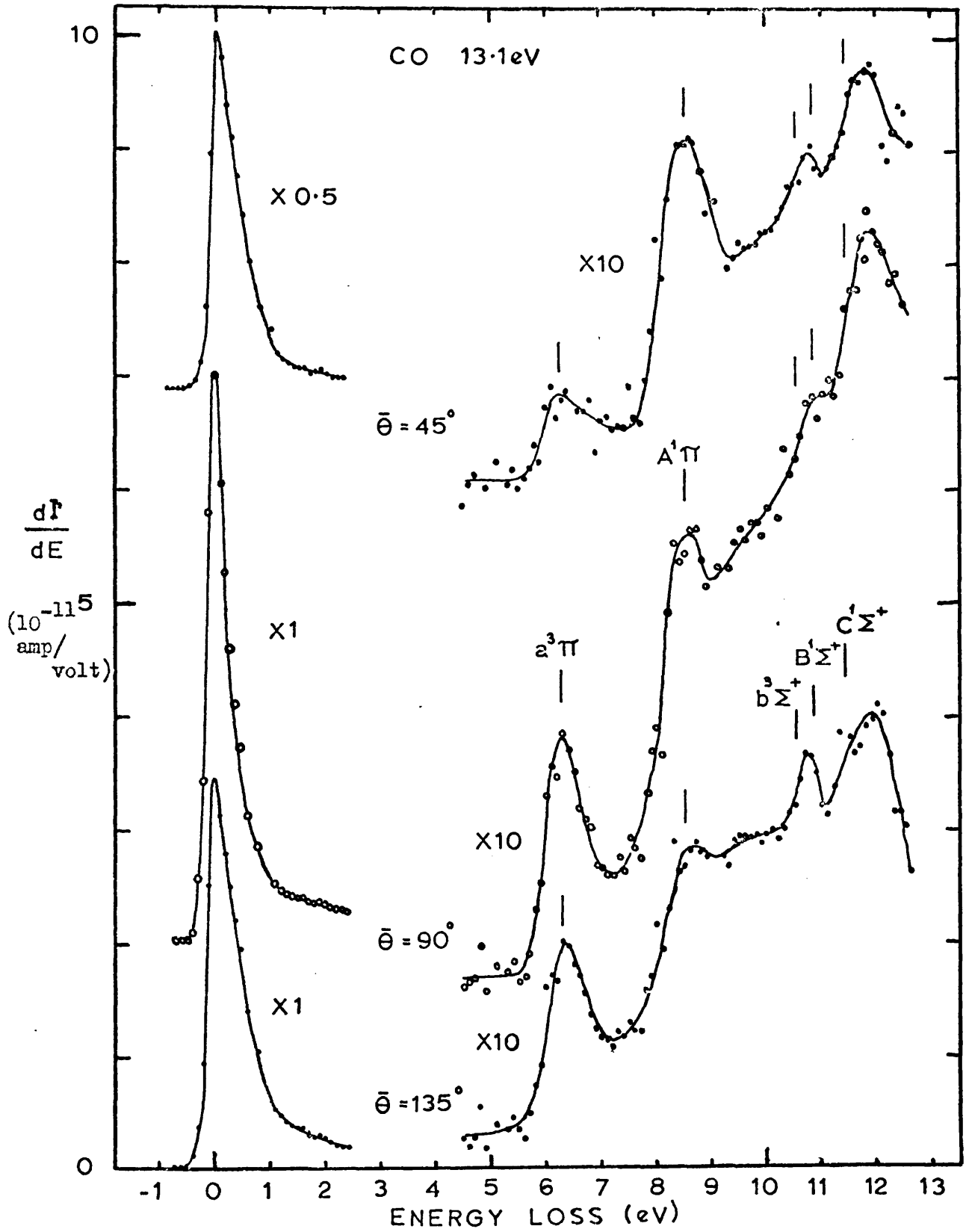

Fig. 5.6 Energy loss spectra of CO at 13.1 eV incident energy, using the spherical analyser with each data point normalised to a beam current of 10^{-7} amp and an ion gauge reading of 10^{-4} torr.

$A^1\pi$ with increasing scattering angle as does a smaller peak at 10.7 eV. However, if we make allowances for the backgrounds on which the spectra are superimposed, we find that whereas the $a^3\pi$ intensity ratio (relative to the $A^1\pi$) increases by a factor of 4.5 between 45° and 135°, that for the 10.7 eV peak only increases by a factor of about 3. It therefore seems probable that the $b^3\Sigma^+$ state is being excited under these conditions but the location of the peak maximum, lying as it does between the $b^3\Sigma^+$ (10.5 eV) and $B^1\Sigma^+$ (10.8 eV) states, suggests that both states are contributing to the 10.7 eV peak and that resolution higher than the 400 meV employed here will be necessary before further studies can be made on the $b^3\Sigma^+$ state.

5.3 Ethylene

The electron impact spectrum of ethylene has been a subject of considerable interest as a result of the controversy which followed the publication of large angle, low energy spectra by Kuppermann and Raff (28,29). In fact, this was one of the main reasons for the initiation of the present research. Ethylene has now been studied over a wide range of incident energies by a number of investigators.

At high incident energies (33 keV) and zero scattering angle, Geiger and Wittmaack (74) have obtained energy loss spectra which agree well with u.v. absorption spectra (76) of ethylene in the gas phase with no indication of singlet-triplet transitions. Forward scattering experiments by Lassettre and Francis (10a) at 390 eV gave spectra similar to the u.v. spectra (and ref. 74) with three peaks at 7.66 eV, 9.03 eV and 9.95 eV. A similar spectrum was obtained by Ross and Lassettre (75) at 150 eV and 0° scattering angle but the resolution was high enough (~25 meV) to determine relative peak intensities for the vibrational structure in the first (and strongest) Rydberg peak. These relative intensities showed a deviation from the u.v. and high energy, energy loss work as did the position of the peak maximum, this being about 7.5 eV as opposed to 7.3 eV. This discrepancy was

attributed to the presence of a quadrupole transition in the same energy loss region. Simpson and Mielczarek (30) made an early study of forward scattering in ethylene at 50 eV incident energy and 100 meV resolution in which they found reasonable agreement with u.v. spectra, observing three peaks below the ionisation potential at 7.6 eV, 9.1 eV, and 9.8 eV with a shoulder at 8.3 eV. A similar spectrum at the same energy and higher resolution was later obtained by Lassettre et.al. (12) with peak maxima at the same positions. The intensity distribution among vibrational levels of the first Rydberg state was practically the same as in the previous 150 eV spectrum. These authors now feel that their observations do not definitely establish that a quadrupole transition is excited in the region of 7.5 eV. The first Rydberg peak is observed at 7.11 eV but this band overlaps with the first excited singlet state, the $\tilde{A}^1B_{1u}$ or V state, which starts as a progression of diffuse bands at around 6 eV, merges into a continuum at 7.08 eV and then rises to a maximum at 7.65 eV. The superimposition of the Rydberg structure on the $\tilde{A}$ continuum could then result in variations in the relative intensity measurements. These authors looked for singlet-triplet transitions around 4.5 eV energy loss, as did Simpson and Mielczarek, but could find nothing.

Threshold excitation of ethylene has been studied by Bowman and Miller(19) using an electron trap. In addition to a peak at 1.8 eV which is attributable to vibrational excitation of the ground state via temporary negative ion formation, three peaks are found at 4.4 eV, 7.8 eV and 9.2 eV with relative intensities 0.29, 1.00 and 0.71 respectively. The 4.4 eV peak is assigned to excitation of the $\tilde{a}\ ^3B_{1u}$ or T state from the ground $\tilde{X}\ ^1A_{1g}$ or N state. A similar spectrum has also been obtained by Brongersma et.al.(21) with peaks at 4.4 eV, 7.8 eV and 9.3 eV in the ratios 0.27 : 1.00 : 0.65.

Energy loss spectra of ethylene at low energies and large scattering angles

were first obtained by Kuppermann and Raff (28,29). Electrons scattered over the range 22° to 112° could be detected, with 90° preferred, and spectra were obtained for incident energies of 40, 50 and 75 eV. Their calibration procedure was to assign a peak to the ionisation potential at 10.5 eV and for the 40 eV and 50 eV spectra, six peaks were obtained at similar intensities at 2.1, 4.4 , 6.5 , 7.8 , 8.8 , and 10.5 eV. The peak at 2.1 eV was assigned to the elastic peak, that at 4.4 eV to the triplet T state and those at 7.8 eV and 8.8 eV to the V state and one of the Rydberg states, respectively. On the basis of its energy dependence, the 6.5 eV peak was felt to be optically forbidden but not to correspond to a singlet-triplet transition. The two new peaks which had been observed at 4.4 eV and 6.5 eV were consistent with some optical experiments. Evans (77) had studied the u.v. spectrum of ethylene using the oxygen intensification technique to increase the probability of singlet-triplet excitation of C_2H_4 mixed with O_2 at high pressure and had obtained an intensity maximum for the T ← N transition at 4.6 eV. Potts (78) had investigated u.v. spectra of substituted ethylenes and had found T ← N transitions around 5 - 6 eV. Extrapolation of these results indicated that the corresponding value for the C_2H_4 T ← N transition would be 6.4 eV. After Evans' experiments, this was reassigned by Mulliken(79) to a Rydberg triplet state.

Shortly after the publication of Kuppermann and Raff's results, Simpson and Mielczarek(30) published their 50 eV 0° spectrum which was radically different from that of Kuppermann and Raff at 50 eV and 90° scattering angle, showing only peaks at 7.6 eV, 9.1 eV and 9.8 eV. Both were energy loss experiments at 50 eV incident energy, only the scattering angle was different. Simpson and Mielczarek suggested the discrepancy was due to artifacts caused by instrumentation or impurities in the Kuppermann and Raff experiment, while Kuppermann and Raff(31) argued that the two experiments could be compatible if the intensity of scattered

electrons falls very steeply with scattering angle for optically allowed transitions while, for spin forbidden transitions the angular distribution remains more nearly uniform.

In order to test this postulate of a dramatic change in the electron impact spectrum with increasing scattering angle, Doering(33) used an unselected electron beam from a thoriated iridium filament and a 127° deflection analyser fixed at 90° scattering angle to determine the 90° electron impact spectrum of C_2H_4. The major features of this spectrum agreed with the zero angle results of Simpson and Mielczarek with the most prominent peak at 8 eV. However a weak transition was observed at 4.7 eV the intensity of which increased relative to the 8 eV peak as the incident energy was lowered, suggesting a singlet- triplet transition at this energy. No peak was observed at 6.5 eV however, although a weak peak was observed at 10.7 eV which Doering assigned as an allowed transition to a bound state near the ionisation limit. Doering concluded that although the energy loss spectrum of ethylene does not change radically as the scattering angle is increased from 0° to 90°, it does appear that allowed transitions become much weaker relative to the forbidden transitions, thereby permitting forbidden transitions which are masked by allowed transitions at small angles to be observed at 90°.

Later work by Doering and Williams(34) at higher resolution (200-300 meV) gave similar spectra for C_2H_4 with the triplet now being observed at 4.4 eV while the 6.5 eV transition of Kuppermann and Raff was not observed for incident energies as low as 10.9 eV.

More recently, using a modified Kuppermann and Raff spectrometer with angle selecting baffles, Wei (35) has obtained spectra at 90° and incident energies of 30 - 50 eV which are in agreement with those of Doering (33) when the energy scale is defined by the elastic peak at zero energy loss. However, Wei and Kuppermann(36) have found that, in this instrument, undulating backgrounds can occur unless large

collector holding voltages are applied and it is suggested(35) that this may have been responsible for the 6.5 eV peak in the original experiments by Kuppermann and Raff.

Trajmar, Rice and Kuppermann(39) have recently reported observation of the triplet T state at 4.4 eV in the angular range 10^{o} to 80^{o} for 25 eV incident energy, using their variable angle instrument. They also find the main peak at 7.6 eV with a shoulder at 8.3 eV and two smaller peaks at 9.1 and 9.8 eV in agreement with other work.

It is also worth noting the results of some ion impact spectroscopy by Moore and Doering(80) on ethylene. The H^{+}-excited spectrum shows no inelastic process below 7 eV, only a peak at 8 eV, while the H_2^{+} -excited spectrum shows an intense transition peaking at 4.6 eV with a weaker and broader peak at 8 eV. As only the H_2^{+} ion contains an electron which is available for spin exchange, the 4.6 eV peak is attributed to the triplet T state, its intensity ratio relative to the 8 eV peak being 1.7 in contrast with electron trap values of 0.29 and 18.1 eV, 90^{o} electron energy loss(34) values of 0.14.

In the present research, ethylene spectra have been studied both as a function of incident energy and scattering angle. The existence of an energy-loss process centred at 4.4 eV is clearly demonstrated in fig. 5.7 which shows integral spectra in the 3 - 7 eV region for selected incident energies with zero suppression and increased electrometer sensitivity. Integral spectra obtained at a fixed angle of 90^{o} and incident energies between 13.1 eV and 48.1 eV show the presence of three bands below the ionisation potential with slope maxima around 4.4 eV, 8 eV and 9.5 eV and are shown in fig. 5.8. Although quantitative intensity determinations are hampered by the incomplete resolution of the 8 eV and 9.5 eV peaks, as the incident energy is lowered the weak process at 4.4 eV is observed to slowly gain

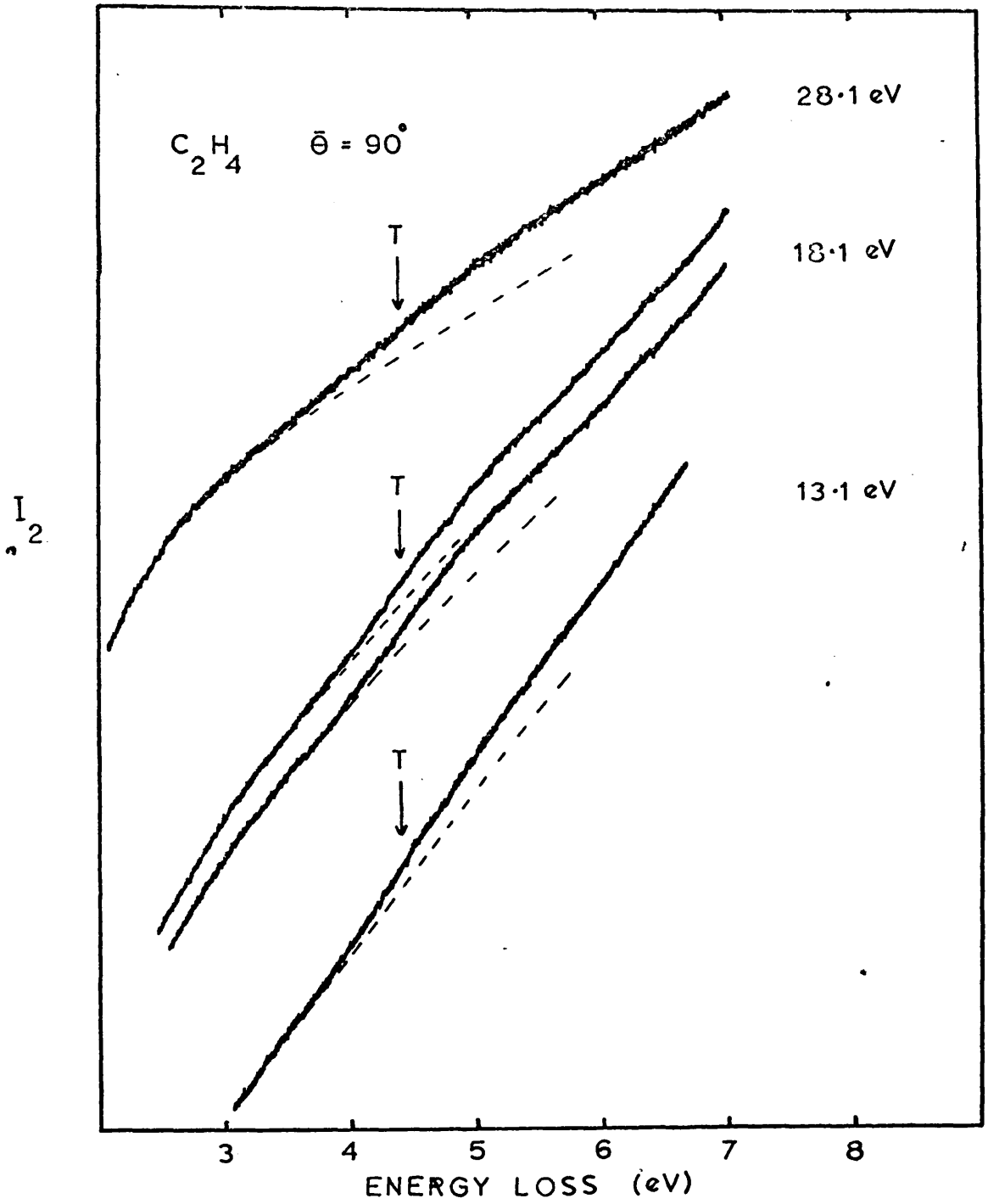

Fig. 5.7 Scattered currents in the 3 - 7 eV energy loss region at 90° mean scattering angle for the incident energies shown. An inelastic process shows up at 4.4 eV and is attributed to a transition to the T state. The lower curve at 18.1 eV was obtained immediately after the upper one by scanning the retarding potential in the reverse direction and illustrates the reproducibility of the instrument.

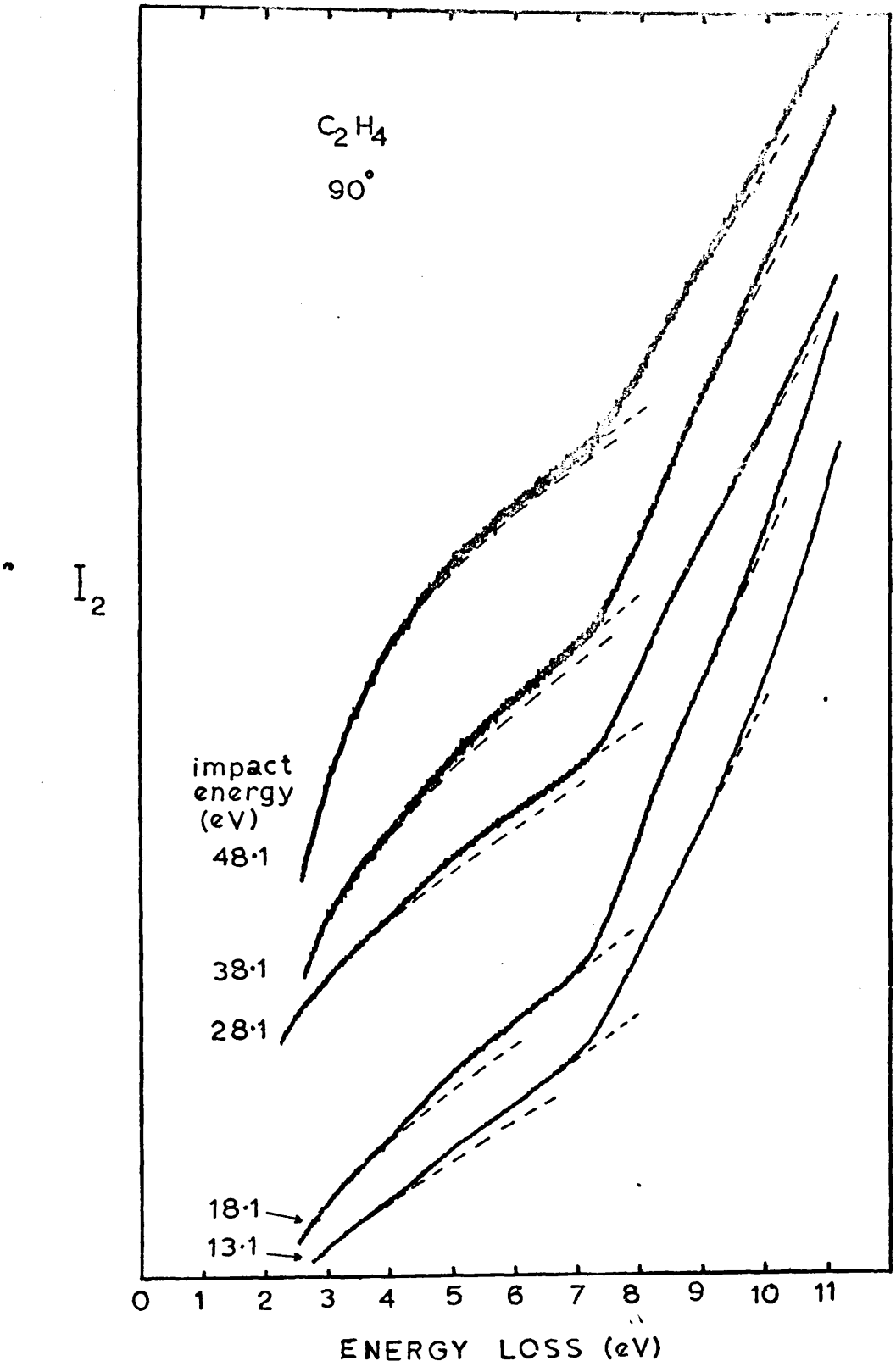

Fig. 5.8 Integral spectra of ethylene obtained at a mean scattering angle of 90° for various incident energies using the spherical analyser.

intensity relative to that at 8 eV, while the relative intensity of the process around 9.5 eV to that at 8 eV remains approximately constant. This energy dependence is consistent with the presence of a triplet state at 4.4 eV. The 9.5 eV peak may be assigned to the unresolved peaks observed in high resolution experiments(30,75,12) at 9.1 eV and 9.8 eV.

When we examine the energy loss spectrum of ethylene as a function of scattering angle at a fixed energy of 28.1 eV (fig. 5.9), we see that the 4.4 eV peak increases rapidly relative to the 8 eV peak as the scattering angle is increased from 45° through 90° to 135°, the intensity ratio reaching that observed in threshold excitation experiments (19,21) at 135°. This observation provides strong evidence for the assignment of the 4.4 eV peak to the triplet T state.

As a final check on the possibility of a forbidden transition at 6.5 eV, as suggested by Kuppermann and Raff, spectra were obtained for 9.1 eV incident energy, i.e. only 2.6 eV above the threshold of the postulated transition. These spectra are shown in fig. 5.10 and, in contrast with the spectra at 28.1 eV, we observe strong excitation of the triplet T state at all angles, although because the secondary electron background interferes with the intensity of the 8 eV peak relative intensities cannot be determined. There is, however, no indication of an inelastic process at 6.5 eV.

In summary then, our spectra compare well with other recent large angle energy loss spectra and disagree with those of Kuppermann and Raff, both in terms of peak maxima and relative intensities. Fig. 5.11 shows our 28.1 eV, 90° spectrum together with spectra by Wei(35) and Doering(33), while fig. 5.12 shows other typical spectra obtained by other workers; forward scattering, electron trap and the Kuppermann and Raff C_2H_4 spectrum. We may conclude that our instrument gives results for ethylene which are consistent with other techniques and shows both the energy and angular dependence expected of the triplet T state.

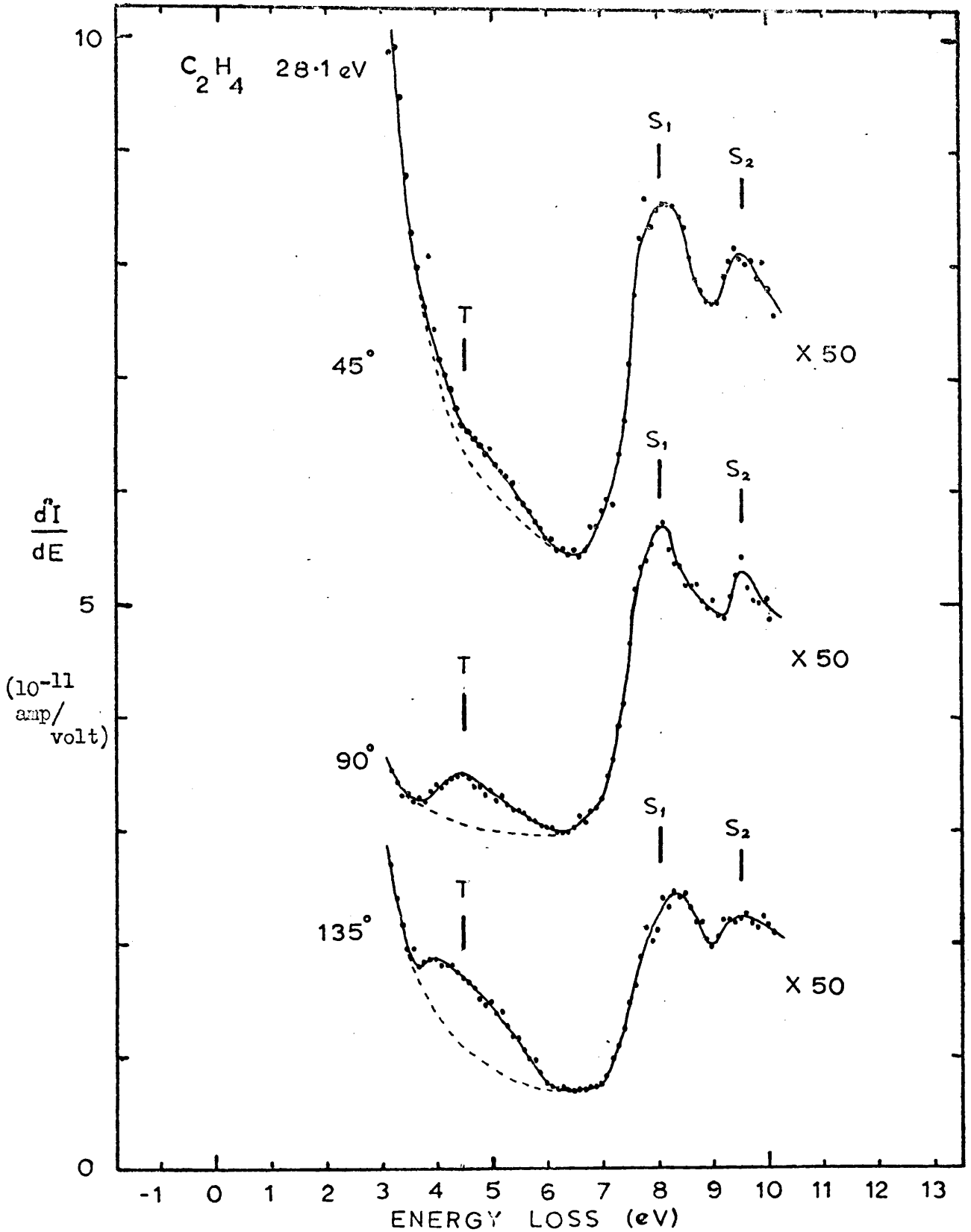

Fig. 5.9 Energy loss spectra of ethylene at 28.1 eV incident energy, using the spherical analyser with each data point normalised to a beam current of 10^{-7} amp and an ion gauge reading of 10^{-4} torr.

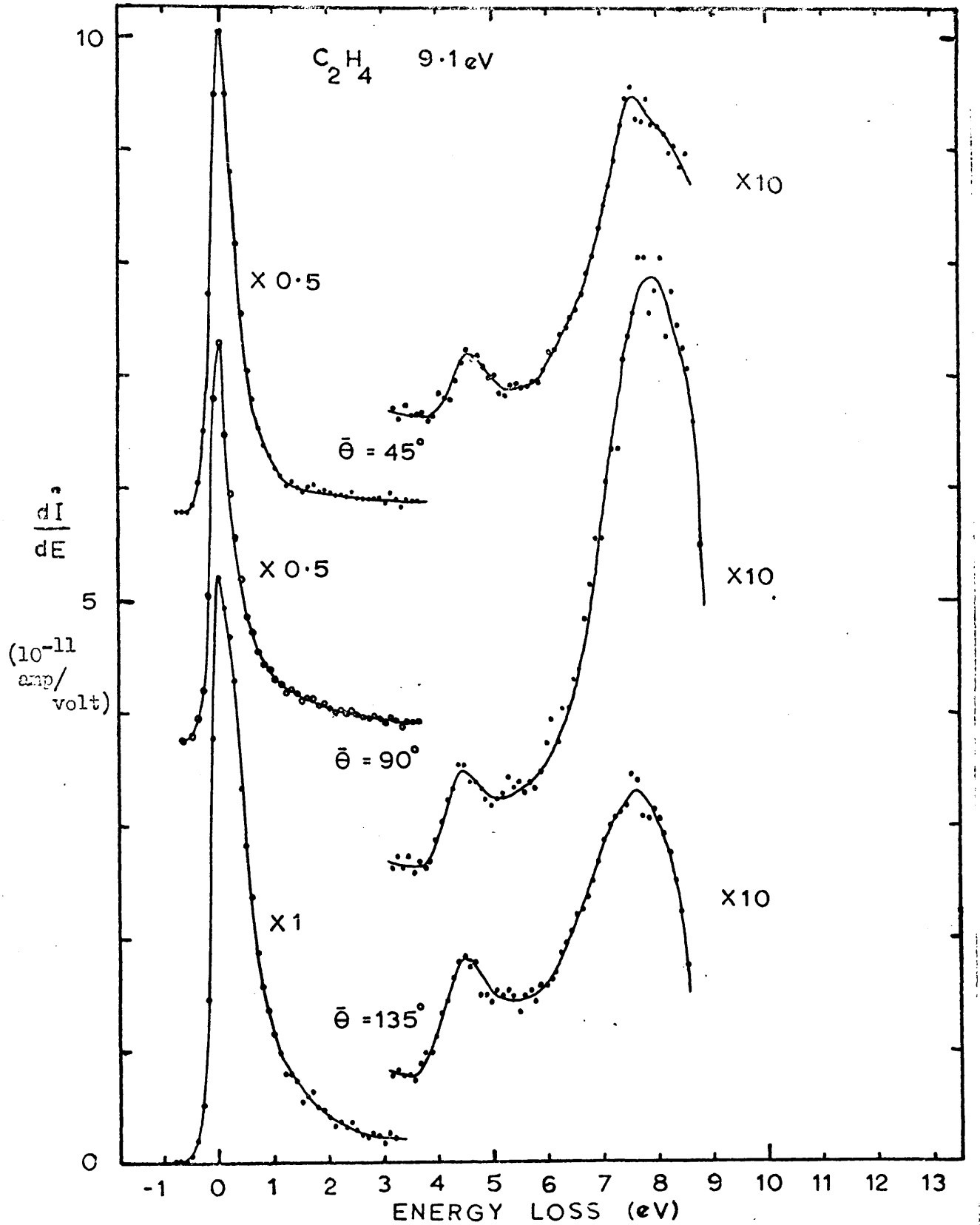

Fig. 5.10 Energy loss spectra at 9.1 eV incident energy using spherical analyser with normalisation as in fig. 5.9. Although the triplet T state is strongly excited at all angles there is no sign of any transition around 6.5 eV, while the singlet-singlet transitions in the 7 - 8 eV region are masked by the secondary electron background.

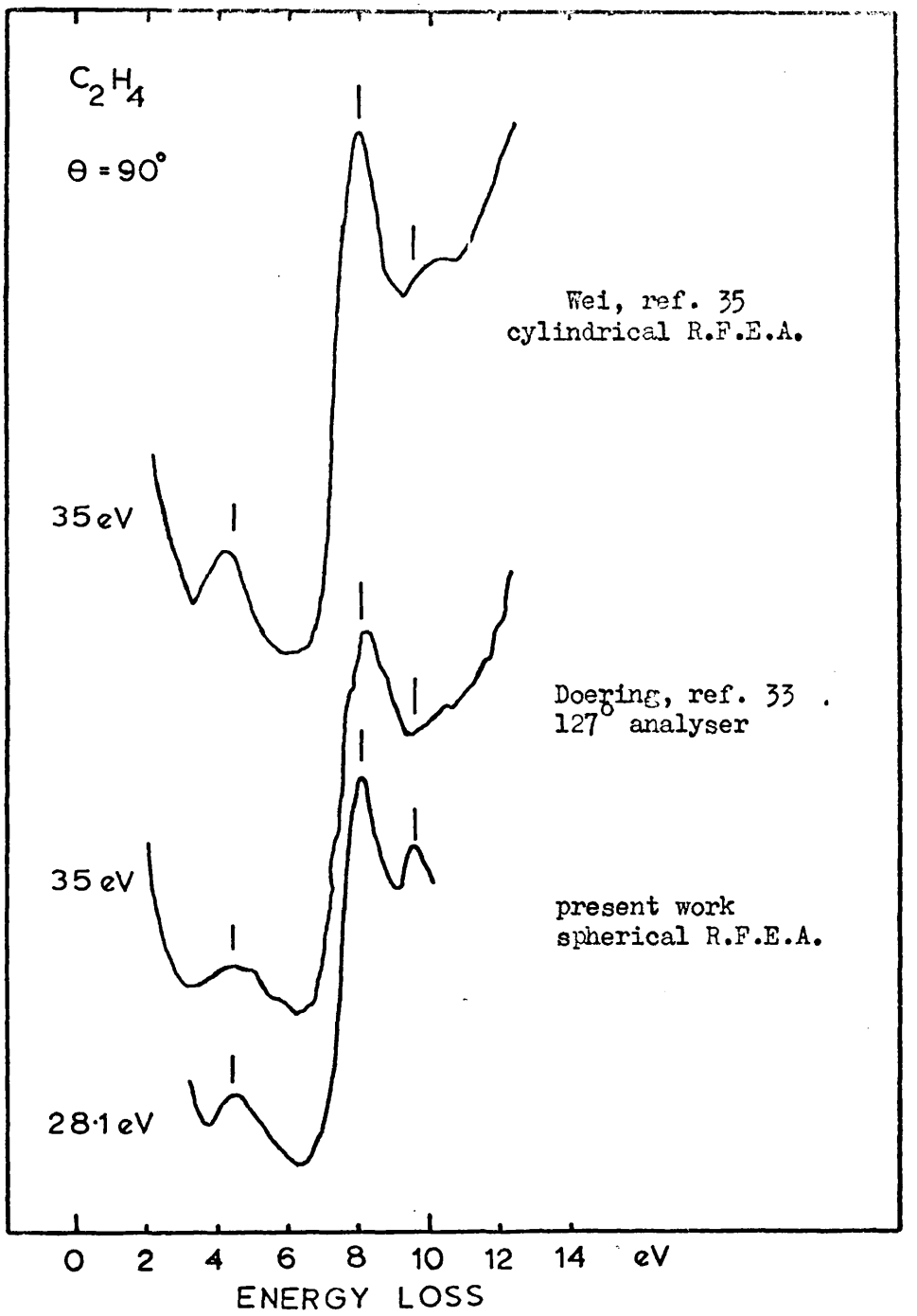

Fig. 5.11 Comparison of ethylene spectrum at 28.1 eV incident energy and 90° mean scattering angle with other work. Top spectrum at 1 eV resolution, middle spectrum at 1.2 eV resolution and bottom spectrum taken with the spherical analyser at 0.5 eV resolution.

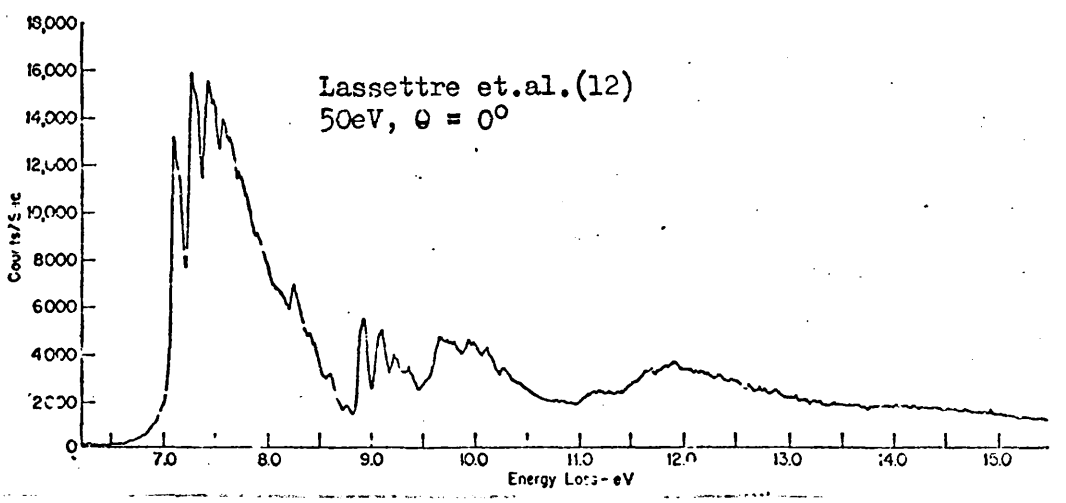

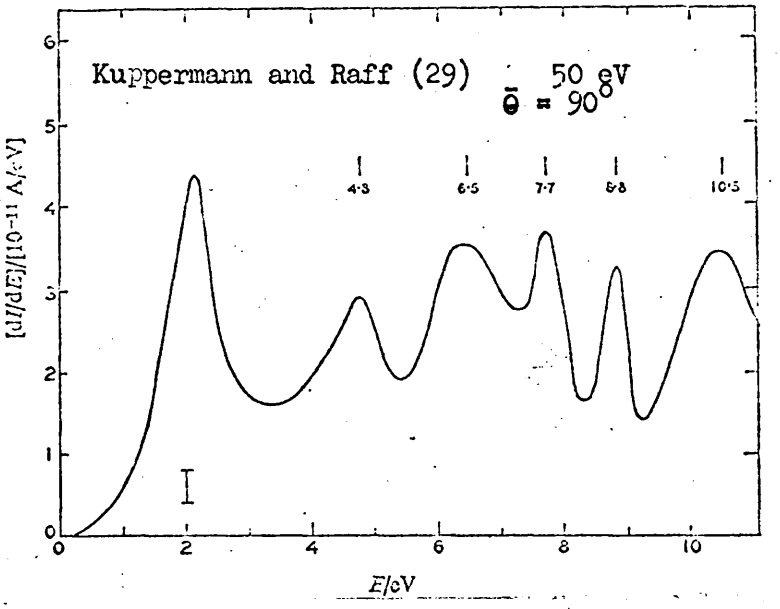

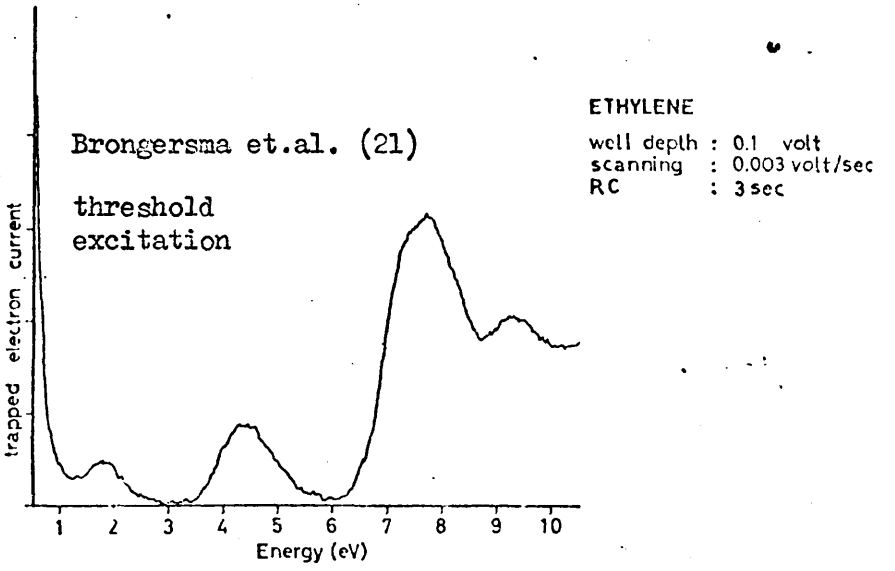

Fig. 5.12 Ethylene spectra obtained by other workers.

5.4 General Trends

On the basis of the limited data available from the three gases studied, we do observe certain general trends in the intensity ratios for triplet states relative to singlet states. In general, the angular dependence of the intensity ratio is found to be a much more sensitive test for the identification of a triplet state than is its energy dependence.

The triplet/singlet intensity ratio at a fixed angle is not very dependent on incident energy in the 20 - 50 eV range, the incident energy having to be reduced to within around 10 eV of threshold before a significant increase is observed.

However, when the incident energy is fixed and spectra are obtained simultaneously on the three collectors, a more dramatic change in the spectrum is generally observed. Fig. 5.13 shows intensity ratios for several states or unresolved pairs of states as a function of scattering angle for various fixed incident energies. These intensity ratios are obtained from peak maxima in differentiated spectra after allowing for backgrounds, where necessary. The maximum errors inherent in this method are indicated in the curves. In all cases we observe triplet state ratios (relative to a reference singlet state) to increase significantly with scattering angle. As a comparison, we may consider the peaks in the ethylene spectra at 8 eV and 9.5 eV, designated S_1 and S_2 respectively. Both correspond to more than one singlet state but these are not resolved. However the intensity ratio, S_2/S_1 , is constant within experimental error over the total angular range, indicating that the angular distributions involved are very similar for these singlet states.

Trajmar, Rice and Kuppermann(39) have studied intensity ratios as a function of scattering angle at 10^o intervals over the 10 - 80^o range and have drawn up a set of rules for the identification of triplet states. They find that triplet state

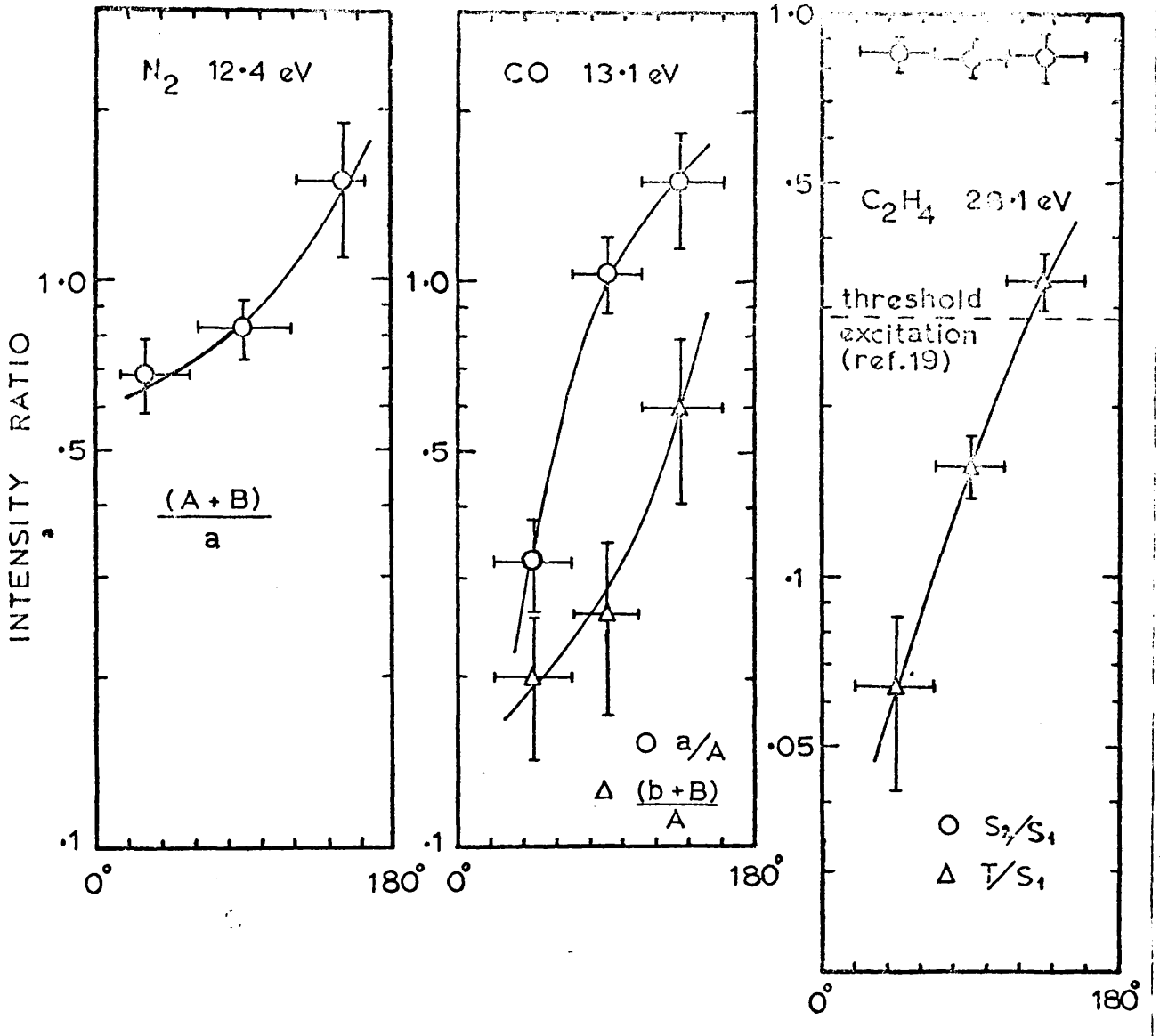

Fig. 5.13 Angular dependence of intensity ratios.

N_2 : The unresolved peak at 7.9 eV is assigned to the $A^3\Sigma_u^+$ and $B^3\pi_g$ states and compared to the $a^1\pi_g$ which peaks at 9.1 eV. Ground state is $X^1\Sigma_g^+$.

CO : The $a^3\pi$ peak at 6.2 eV (upper curve) is compared to the $A^1\pi$ at 8.4 eV as is the 10.7 eV peak which is attributed to the unresolved $b^3\Sigma^+$ and $B^1\Sigma^+$ states. Ground state is $X^1\Sigma^+$.

C_2H_4 : The T state at 4.4 eV is compared to the first unresolved singlet peak, S_1, at 8 eV as is the second singlet peak, S_2, at 9.5 eV. The broken line shows the T/S_1 ratio obtained in threshold excitation experiments by Bowman and Miller (19).

ratios increase markedly with increasing scattering angle in the range 10 - 80° for incident energies 20 - 30 eV above threshold, behaviour which distinguishes them from singlet state ratios. Also they note that the magnitude of the triplet state ratio increase over this angular range is sensitive to the value of $\Delta\Lambda$, the change in angular momentum quantum number for the transition. They find that ratios for which $\Delta\Lambda = 1$ (e.g. $a^3\Pi$ in CO) increase sharply by about two orders of magnitude while those for which $\Delta\Lambda = 0$ (e.g. $b^3\Sigma^+$ in CO) increase by about one order of magnitude. Singlet state ratios are observed to be less sensitive to angle with some ratios constant while others increase or decrease slightly at small scattering angles.

Our results are consistent with the work of Trajmar et.al. within the limits set by the angular resolution available with three collectors and in addition, show that triplet state ratios continue to increase as the scattering angle is increased beyond 80°, the mechanical limit of the instrument used by Trajmar et.al. Clearly, valuable information regarding the detailed shape of these intensity ratio curves could be obtained by using more collectors, possibly twelve, to give higher angular resolution.

5.5 Conclusion

The results obtained with the present instrument using retarding field analysis are comparable with those obtained in instruments which employ electrostatic deflection analysers. The instrument used by Kuppermann and Raff(29) was subject to a number of instrumental effects which prevented such a comparison. These effects have since been systematically studied by Wei and Kuppermann(36), as discussed in Chapter 4, and they were able to minimise the undulating background (which gave rise to spurious peaks) at the expense of using large collector holding voltages with the resultant increase in rising background at large energy

loss due to field penetration. This also restricted the energy resolution to about 1 eV and the incident energy to above 30 eV.

The present work has extended the R.F.E.A. electron impact technique from one of fixed angle, 1 eV resolution and a limited energy range to one in which spectra may be obtained as a function of angle at a resolution of 0.4 - 0.5 eV for incident energies as low as 2.5 eV above the threshold of transitions of interest. Of the background problems previously encountered, we do not observe undulating backgrounds even for a holding voltage of only 2 volts, possibly due to the use of an organic-free U.H.V. system , while low holding voltages and large grid - collector spacings minimise field penetration, leaving only the background effect due to reflected and secondary electrons from metal parts of the analyser. Consequently, future development should be directed towards minimising the area of metal surfaces presented to elastically scattered electrons. Other, more obvious, developments are the increasing of the number of collectors to give higher angular resolution and the fitting of an electron monochromator, combined with larger diameter spherical grids, to give higher energy resolution. Angular resolution of around 15° should be adequate to describe intensity ratio curves as a function of angle at low incident energies. If the "blind angle" at each end of the range can be reduced to $7\frac{1}{2}^{\circ}$, then a system of eleven collectors with the first centred at 15° and the last at 165° would be suitable. It should be possible to accomodate a large radius hemispherical deflection monochromator with the injection optics level with the analyser but outside the analyser chamber. The use of electrical differentiation would simplify the operation of the spectrometer and this may well be worth investigating further.

The R.F.E.A. electron impact spectrometer is competitive with the monochromator - analyser instruments developed by Trajmar et.al.(39) and Williams

and Doering(41) and enables triplet states to be identified by the behaviour of their intensity ratios as a function of scattering angle. However, mechanical limitations in these instruments permit maximum angles of only 80° and 100° respectively to be used, while the R.F.E.A. can be used up to 165°. On the other hand, the background in the R.F.E.A. is unlikely to be completely eradicated by future development. Other techniques for detection of triplet states involve excitation at threshold, i.e. the trapped - electron method and the SF_6^- scavenger technique, but these do not provide a means for positive identification of triplets, although singlet - triplet transitions often dominate threshold spectra.

Of available electron impact methods, the low energy, variable angle energy loss method appears to be superior for identification of triplet states, although the competitive technique of ion impact spectroscopy(70) is possibly even more useful, giving larger triplet/singlet intensity ratios for H_2^+ impact and only exciting singlet - singlet transitions for H^+ impact.

REFERENCES

1) C. Reid "Excited States in Chemistry and Biology" Butterworths, 1957.

2) L.G. Christophorou and R.N. Compton Health Physics 13, 1277, (1967).

3) A.J. Williams and J.P. Doering Planet. Space Sci. 14 1527 (1969)

4) Massey and Burhop "Electronic and Ionic Impact Phenomena" Oxford Univ. Press (1952)

5) V.I. Ochkur Soviet Phys. J.E.T.P. 18 503 (1964)

6) J.K. Rice, A. Kuppermann and S. Trajmar J.C.P. 48 945 (1968)

7) N.J. Turro J. Chem. Educ. 46 2 (1969)

8) J.S. Swenton J. Chem. Educ. 46 7 (1969)

9a) H. Boersch, J. Geiger and H. Hellwig Phys. Lett. 3,64 (1962)

b) " " and W. Stickel Z. Physik 180, 415 (1964)

c) " " and M. Topchowsky Phys. Lett. 17, 266 (1965)

d) J. Geiger and B. Schröder J.C.P. 50, 7 (1969)

10a) E.N. Lassettre and S.A. Francis J.C.P. 40, 1208 (1964)

b) " and E.N. Jones J.C.P. 40, 1218 (1964)

c) " " " J.C.P. 40, 1222 (1964)

d) " ,A.S. Berman,S.M. Silverman and M.E. Krasnow J.C.P. 40, 1232 (1964)

e) " , M.E. Krasnow and S.M. Silvermann, J.C.P. 40, 1242,(1964)

f) " and M.E. Krasnow J.C.P. 40, 1248 (1964)

g) " and S.M. Silverman J.C.P. 40, 1256 (1964)

h) " , S.M. Silverman and M.E. Krasnow J.C.P. 40, 1261 (1964)

i) " and S.M. Silverman J.C.P. 40, 1265 (1964)

j) " and A.M. Skerbele J.C.P. 40, 1271 (1964)

11) V.D. Meyer, A. Skerbele, E.N. Lassettre J.C.P. 43, 805 (1965)

12) E.N. Lassettre, A. Skerbele, M.A. Dillon, K.J. Ross J.C.P. 48 5066 (1968)

13) A. Skerbele, M.A. Dillon, E.N. Lassettre J.C.P. 46, 4161 (1967)

14) A. Skerbele, M.A. Dillon, E.N. Lassettre J.C.P. 49 5042 (1968)

15) J.A. Simpson Rev. Sci. Instr. 35, 1698 (1964)

16) C.E. Kuyatt and J.A. Simpson Rev. Sci. Instr. 38, 103 (1967)

17) H.G.M. Heideman, C.E. Kuyatt, G.E. Chamberlain J.C.P. 44, 355 (1966)

18) G.J Schulz Phys. Rev. 112, 150 (1958)

19) C.R. Bowman and W.D. Miller J.C.P. 42, 681 (1965)

20) H.H. Brongersma and L.J. Oosterhoff Chem. Phys. Lett. 1, 169 (1967)

21) " , J.A.v.d. Hart and L.J. Oosterhoff. Nobel Symposium 5,211(1967)

21a) R.I. Hall, J. Mazeau, J. Reinhardt and C. Schumann J.Phys.(B) 3, 991 (1970)

22) R.K. Curran J.C.P. 38, 780 (1963)

23) A. Stamatovic and G.J. Schulz Rev. Sci. Instr. 39, 1752 (1968)

24) R.N. Compton, R.H. Huebner, P.W. Reinhardt and L.G. Christophorou. J.C.P. 48, 901 (1968)

25) R.M. O'Malley and K.R. Jennings J. Mass Spect. Ion Phys. 2, App.1 (1969)

26a(C.E. Brion and C.R. Eaton J. Mass Spect. Ion Phys. 1, 102 (1968)

b) " and G.E. Thomas J. Mass Spect. Ion.Phys. 1, 25 (1968)

c) " and L.A.R. Olsen J.C.P. 52, 2163 (1970)

27) A. Stamatovic - personal communication

28) A. Kuppermann and L.M. Raff J.C.P. 37, 2497 (1962)

29) " " Disc. Farad. Soc. 35, 30 (1963)

30) J.A. Simpson and S.R. Mielczarek J.C.P. 39, 1606 (1963)

31) A. Kuppermann and L.M. Raff J.C.P. 39, 1607 (1963)

32) M.G. Ferguson Ph. D. Thesis, University of Edinburgh (1967)

33) J.P. Doering J.C.P. 44, 1194 (1967)

34) J.P. Doering and A.J. Williams J.C.P. 47, 4180 (1967)

35) P.S.P. Wei Ph.D. Thesis, California Institute of Technology (1968)

36) P.S.P. Wei and A. Kuppermann Rev. Sci. Instr. 40, 783 (1969)

37) S. Trajmar, J.K. Rice and A. Kuppermann Tech.Memo. 33-373 Jet Propulsion Lab. Pasadena (1968)

38) " " " J. Phys. Chem. 72, 3894 (1968)

39) " " " Advances in Chemical Physics XVIII page 15 Interscience Publishers (1970)

40) C. E. Kuyatt and J. A. Simpson Rev. Sci. Instr. 38, 103 (1967)

41) A.J. Williams and J.P. Doering J.C.P. 51, 2859 (1969)

42) J.P. Doering J.C.P. 51, 2866 (1969)

43) C. Ramsauer and R. Kollath Ann. der Phys. 12, 539 (1932)

44) J.A. Simpson Rev. Sci. Instr. 32, 1283 (1961)

45) J.B. Hasted "The Physics of Atomic Collisions" Butterworths

46) G. Rutledge Phys. Rev. 40, 262 (1932)

47) Mott and Massey "Theory of Atomic Collisions" Oxford Univ. Press

48) D.C. Frost, C.A. McDowell, D.A. Vroom Proc. Roy. Soc. 296, 566 (1967)

49) J.W. McGowan, D.A. Vroom and A.R. Comeaux VI I.C.P.E.A.C., Boston (1969)

50) D.A. Huchital and J.D. Rigden Appl. Phys. Lett. 16, 348 (1970)

51a) K.R. Spangenberg "Vacuum Tubes" McGraw-Hill, New York,(1948) page 296

b) ibid. pp 291-297 and 215-216

c) ibid p 292

d) ibid pp 377-387

e) ibid pp 369-374

f) ibid p 392

g) ibid p 393

52) D.C. Frost, J.S. Sandhu, D.A. Vroom Nature 212, 604 (1966)

53) D.A. Huchital personal communication

54) J.A. Simpson and C.E. Kuyatt J.Res.Nat. Bur.Standards 67C, 279 (1963)

55) " " Rev. Sci. Instr. 34, 265 (1963)

56) E. Harting and K.M. Burrows Rev. Sci. Instr. 41, 97 (1970)

57) W.E. Danielson, J.L. Rosenfeld and J.A. Saloom Bell System Tech. J. 35, 375 (1956)

58) J.R. Pierce "Theory and Design of Electron Beams" Van Nostrand Co.(1954)

59) D.W.O. Heddle J. Sci. Instr.(J.Phys. E.) 2(Ser.2), 1046 (1969)

60) C.E. Kuyatt "Notes on Electron Optics" (unpublished)

61) R.E. Imhof and F.H. Read J. Sci. Instr.(J. Phys. E) 1(Ser.2), 859 (1958)

62) F. Rosebury "Handbook of Electron Tube and Vacuum Techniques" Addison-Wesley Publishing Co. (1965)

63) J.H. Parry "Helmholtz Coils and Coil Design" pp 551-567 in "Methods in Paleomagnetism" edited by Collinson, Crier and Runcorn. Elsevier Publishing Co.

64) " Low Frequency Magnetic Shielding" Parts I and II, Design Electronics, Jan. and Feb. 1969

65) Ross and Garment J. Sci. Instr.(J. Phys. E) 2(Ser.2),(1969)

66) L.B. Leder and J.A. Simpson Rev. Sci. Instr. 29, 571 (1958)

67) P. Harmet, P. Natalis and A. Dumont Rev. Sci. Instr. 39, 686 (1968)

68) J.C. Tracy and C.K. Bohn preprint "Auger Electron Spectrometer Preamplifier" from authors at North American Rockwell Corp., Thousand Oaks, California 91360.

68a) P.R. Thornton "Scanning Electron Microscopy" published by Chapman, Hall.

69) K. Siegbahn et. al. " ESCA, Atomic Molecular and Solid State Structure Studied By Means Of Electron Spectroscopy" Almqvist and Wiksells Boktryckeri A.B. Uppsala 1967.

70) P. Bromberg VI I.C.P.E.A. Boston 1969

71) E.N. Lassettre Canadian J. Chem. 47, 1733 (1969)

72) A. Skerbele, M.A. Dillon and E.N. Lassettre J.C.P. 46, 4162 (1967)

73)G.J. Schulz Phys. Rev. 116, 1141 (1959)

74) J. Geiger and K. Wittmaack Z. Naturforsch. 20A, 628 (1965)

75) K.J. Ross and E.N. Lassettre J.C.P. 44, 4633 (1966)

76) G. Herzberg " Molecular Spectra and Molecular Structure" Vol. 3 "Polyatomic Molecules"

77) D.F. Evans J. Chem. Soc. 1735 (1960)

78) W.J. Potts J.C.P. 23, 65 (1955)

79) R.S. Mulliken J.C.P. 33, 1596 (1960)

80) J.H. Moore Jr. and J.P. Doering J.C.P. 52, 1692 (1970-

APPENDIX A Relations for Analyser Function Calculation

A.1. Transmission Functions

If we consider an electron scattered from the axis of a cylindrical grid at a scattering angle of θ and if the grid is composed of wires of radius, r, separated by a distance, d, then, referring to fig. A.1. we see that the transmission function is

$$T(\theta) = \text{free area/total area} = s\,d\,/(d+2r)^2 \qquad (A.1)$$

Also from fig. A.1 we see that

$$s = d + 2r - 2r/\sin\theta \qquad (A.2)$$

The transmission function for normal incidence is

$$T(\pi/2) = d^2/(d + 2r)^2 \qquad (A.3)$$

and this is the value quoted by the wire gauze manufacturer.

Combination of these expressions gives

$$T(\theta) = T(\pi/2)^{\frac{1}{2}}\,[(\,T(\pi/2)^{\frac{1}{2}} + \sin\theta - 1)/\sin\theta\,] \qquad (A.4)$$

The corresponding expression for scattering into the forward cone is

$$T(\theta) = T(\pi/2)^{\frac{1}{2}}\,[(\,T(\pi/2)^{\frac{1}{2}} + \sin(\theta + B) - 1)/\sin(\theta + B)] \qquad (A.5)$$

while that for the backward cone is

$$T(\theta) = T(\pi/2)^{\frac{1}{2}}\,[(\,T(\pi/2)^{\frac{1}{2}} + \sin(\theta - B) - 1)/\sin(\theta - B)] \qquad (A.6)$$

where B refers to the angle the cones make with the beam axis. In our experiment, $B = 57^{\circ}$.

For the case of a spherical grid, it is convenient to work in terms of β, the angle the electron path makes with the tangent to the grid at the point of intersection [fig. A.3]. The appropriate transmission function is

$$T(\beta) = T(\pi/2)^{\frac{1}{2}}\,[(T(\pi/2)^{\frac{1}{2}} + \sin\beta - 1)/\sin\beta] \qquad (A.7)$$

A.2 Geometric Limiting Angles

For the pseudo-spherical analyser, the obstructions which give rise to these angles are the beam entrance and exit tubes and the grid support rings at the joins of the cones and the cylinder. These angles may be calculated as a function of the position along the path length. In the computor program, the path length, L, is divided into a number (NL) of equal segments from which scattering may be considered. The operator used in the path length cycle is I and this may be varied in steps of one from -J to +J, where

$$J = (NL - 1)/2 \qquad (A.8)$$

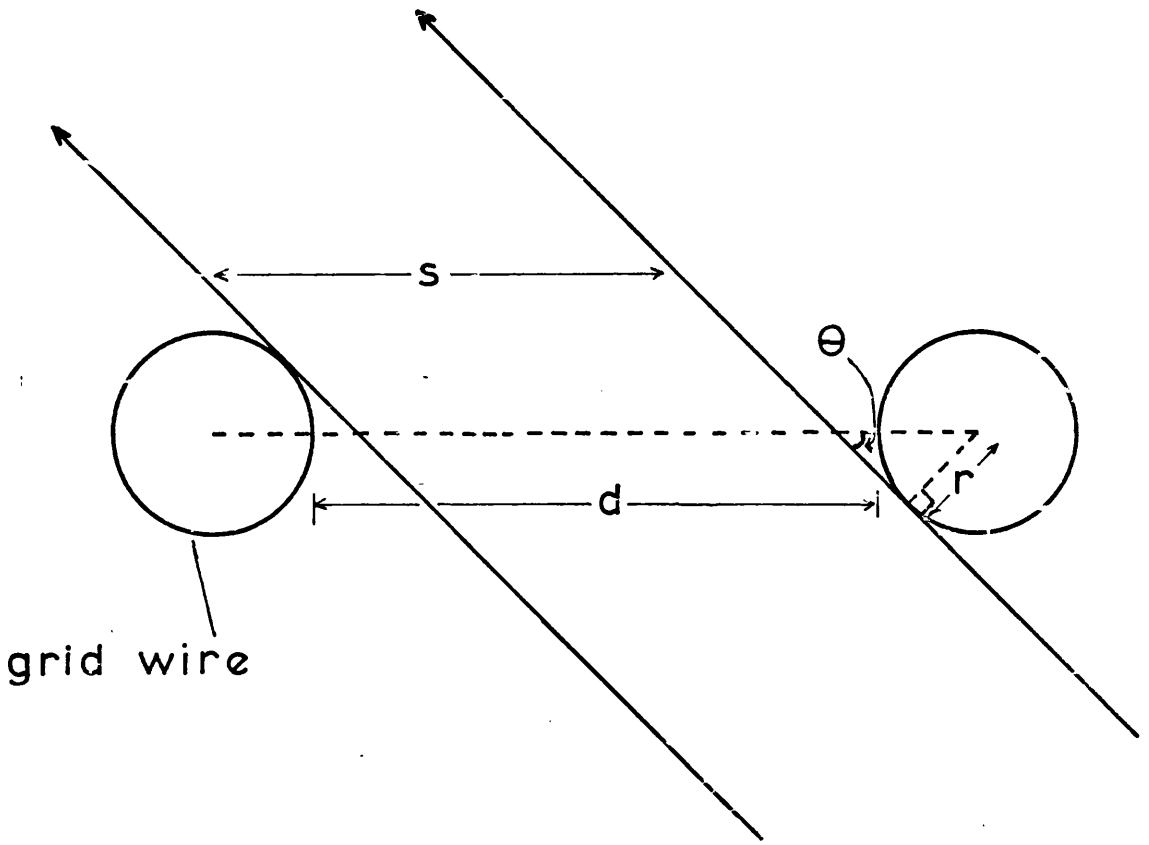

Fig. A.1.

and I is zero at the scattering centre.

For the analyser of fig. 3.1 where RC is the radius of the first grid and LC is the length of its cylindrical section, we obtain

CYLINDER $$p_{min} = \tan^{-1}\left[\frac{RC}{(LC/2) - I(L/NL)}\right] \quad (A.9)$$

$$p_{max} = \pi - \tan^{-1}\left[\frac{RC}{(LC/2) + I(L/NL)}\right] \quad (A.10)$$

FORWARD CONE $$p_{min} = \tan^{-1}\left[\frac{A}{(L/2) - I(L/NL)}\right] \quad (A.11)$$

$$p_{max} = \tan^{-1}\left[\frac{RC}{(LC/2) - I(L/NL)}\right] \quad (A.12)$$

A is the radius at the narrow end of the small cones which define the path length.

BACKWARD CONE $$p_{min} = \pi - \tan^{-1}\left[\frac{RC}{(LC/2) + I(L/NL)}\right] \quad (A.13)$$

$$p_{max} = \pi - \tan^{-1}\left[\frac{A}{(L/2) + I(L/NL)}\right] \quad (A.14)$$

For the case of the spherical analyser, the geometric limiting angles may be determined either by the edges of the small cones or the edges of the support ring for the first grid, depending on the position along the path length, i.e. on the value of I. From fig. A.2 we find that, <u>for the particular case where NL = 15</u>,

if $I > 2$ p_{min} is given by eqn. A.11

$I \leq 2$ $$p_{min} = \tan^{-1}\left[\frac{F}{H + (L/2) - I(L/NL)}\right] \quad (A.15)$$

if $I \geq -2$ $$p_{max} = \pi - \tan^{-1}\left[\frac{F}{H + (L/2) + I(L/NL)}\right] \quad (A.16)$$

$I < -2$ p_{max} is given by eqn. A.14

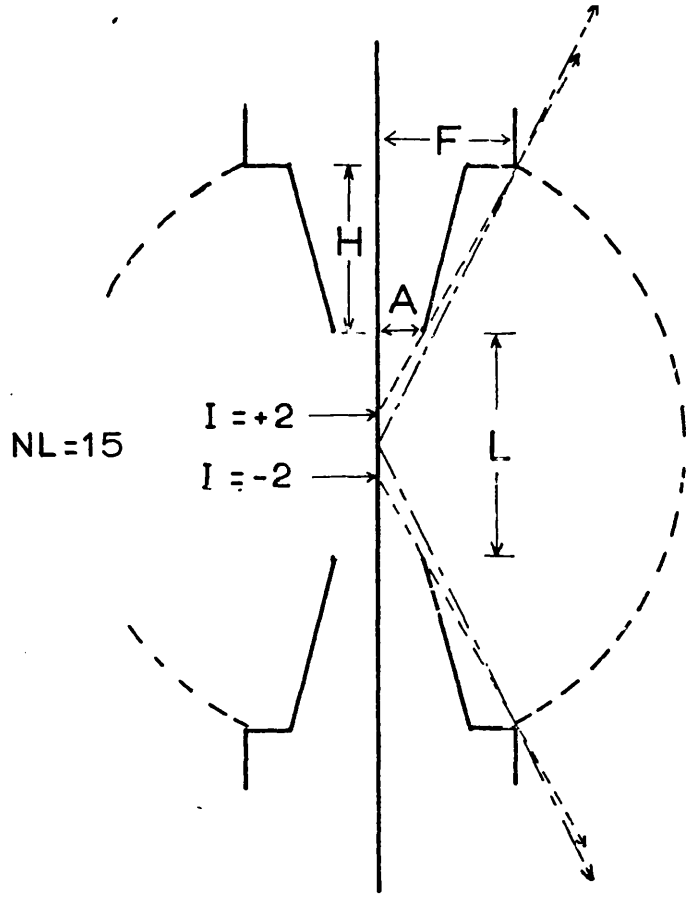

Fig. A.2.

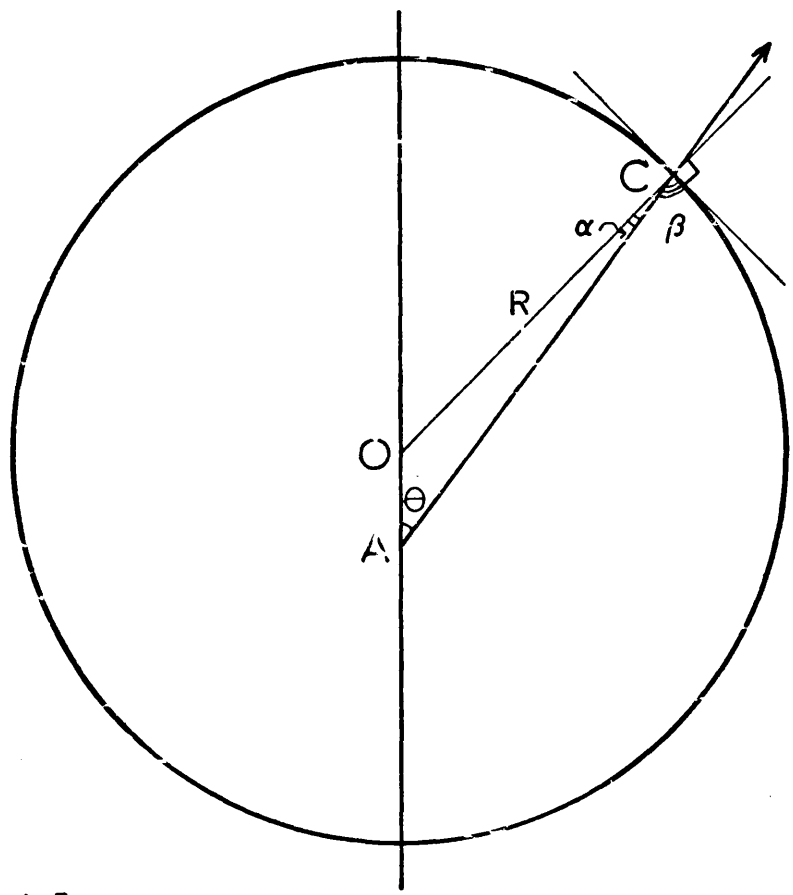

Fig. A.3.

A.3 Physical Limiting Angles

These are determined by the ratio of retarding voltage to electron energy as discussed in Chapter 2.

For the pseudo-spherical analyser, we obtain

CYLINDER $$T_{min} = \sin^{-1}(V/E)^{\frac{1}{2}} \quad (A.17)$$

$$T_{max} = \pi - T_{min} \quad (A.18)$$

When $V/E = 1$, $T_{min} = T_{max} = 90^{o}$

FORWARD CONE $$T_{min} = \sin^{-1}(V/E)^{\frac{1}{2}} - B \quad (A.19)$$

$$T_{max} = \pi - \sin^{-1}(V/E)^{\frac{1}{2}} - B \quad (A.20)$$

When $V/E = 1$, $T_{min} = T_{max} = 33^{o}$

BACKWARD CONE $$T_{min} = \sin^{-1}(V/E)^{\frac{1}{2}} + B \quad (A.21)$$

$$T_{max} = \pi - \sin^{-1}(V/E)^{\frac{1}{2}} + B \quad (A.22)$$

When $V/E = 1$, $T_{min} = T_{max} = 147^{o}$

B is as defined in section A.1.

For the case of the sphere, it is easier to work in terms of β rather than Θ and define the physical angles $[t_{min}, t_{max}]$ as those between the electron path and the tangent to the sphere at the point of intersection. These angles are then

$$t_{min} = \sin^{-1}(V/E)^{\frac{1}{2}} \quad (A23)$$

$$t_{max} = \pi - \sin^{-1}(V/E)^{\frac{1}{2}} \quad (A.24)$$

By application of the Sine Rule in triangle OAC of fig.A.3, we find that we can relate β to Θ by

$$\beta = \cos^{-1}\left[\frac{(L/NL).|I|.\sin\theta}{R}\right] \qquad (A.25)$$

Thus, during the θ cycle, we start with $\theta = p_{min}$ and calculate the corresponding β which is then compared with t_{min} and t_{max} to determine the overall limiting angles.

ACKNOWLEDGEMENTS

I wish to thank Dr. T.L. Cottrell and Dr. I.C. Walker for suggesting the project and for providing funds for equipment and materials and Dr. Walker for her advice and assistance in writing the computer programs. The contribution of Mr. D.F. Dance who introduced me to the modern technology associated with collision physics experiments and who maintained an interest in the project throughout its course is gratefully acknowledged.

I also wish to thank the University of Stirling for provision of excellent laboratory accomodation and specialised facilities necessary for this work, in particular the Special Techniques Laboratory and the Postgraduate Workshop, and to express my gratitude to the members of the Physics department for their readiness to lend equipment on numerous occasions.

My fellow students, C.W. Duncan and H.Q. Porter, must be thanked for many interesting discussions, as must the staff of Shared Technical Services mechanical and electronic engineering sections for their high standard of workmanship which undoubtedly contributed to the success of the project.

I also wish to thank the Science Research Council for providing a studentship during the course of the project.